K-fiber dynamics: a focus on the microtubule minus-ends

Alejandra Laguillo Diego

TESI DOCTORAL UNIVERSITAT POMPEU FABRA / 2020

Department of Experimental and Health Sciences

Thesis supervisor:

Dra. Isabelle Vernos

Cell and Developmental Biology,

Centre for Genomic Regulation

A mi abuelo Nando,

Agradecimientos

Estos cuatro años de tesis han sido un proceso intenso y muy enriquecedor a nivel científico y personal. No podrían haberse desarrollado de la misma manera sin el apoyo y la paciencia de muchas personas a las que les estoy muy agradecida.

En primer lugar me gustaría agradecer a Isabelle haberme dado la oportunidad de unirme a su grupo para llevar a cabo mi tesis doctoral. Gracias por haber tenido la puerta siempre abierta para escuchar y aconsejarme. Valoro mucho que siempre hayas tenido en cuenta mis opiniones y me hayas tranquilizado cuando era necesario. Gracias por tus consejos como mentora a nivel científico y personal.

I would like to acknowledge the tribunal board: Thomas, Jens, Stefannie, Joan and Sebastian for agreeing discussing this work with me in the day of my defense. Thanks also to my thesis committee: Fátima, Sebastian and Thomas M-R for being supportive these four years.

Dresden has being my second host institution during these 4 years. Thanks to Thomas Müller-Reichert for his time and scientific advise and for all the good moments I spent in Dresden during my PhD. It was a pleasure for me to be temporarily part of your group and I enjoyed doing tomography and drinking coffee both. Special thanks to Robert Kiewisz for dedicating a lot of time and effort to move forward our project and to efficiently respond to my requests. Also for the good times in the worm room.

The collaboration with the Müller-Reichert group was possible thanks to the DivIDE training network to which I belonged during these years. Thanks to Natàlia for organizing all the events and also for being so talkative and a good advisor. Thanks to all the PIs and PhD students in the network for the great scientific and personal moments we lived in different european locations in these years. Thanks to Pablo Salaverria for the moments we spent working and arguing together in Barcelona. Thanks to Christel Michel for the patience and technical help in the last moments.

En estos cuatro años no me ha pesado ningún día acudir al CRG gracias al ambiente de trabajo en el centro y sobre todo en el VernosLab. Gracias a Núri y a Georgina por la paciencia para enseñar, escuchar, por los "brunchs" y por los momentos de desconexión entre risas cuando era necesario. Gracias a mis compañeros de tesis Aitor e Ivan, creo que a pesar de lo diferentes que somos hemos tenido muy buen ambiente para disfrutar de los días de ciencia y placer y a la vez nos hemos apoyado mutuamente. Farners gracias por transmitir tanto tu motivación científica como tu optimismo y facilidad para reír, incluso desde tan lejos. Eres un ejemplo para mí. Gracias al resto de miembros pasados y presentes del VernosLab: Krystal, Jacopo, Álvaro, Claudia, Leo, Mónica, Adrián y Miquel por los buenos momentos. Gracias a todos los compañeros del departamento y del CRG que me han ayudado siempre, especialmente a Magüi, Natalia, Raquel.

Gracias a todos los compactos por las conversaciones, los viajes, las cenas y las fiestas. Gracias a Artyom por acompañarme conversando en el recorrido del pasillo del departamento en tantas ocasiones. Danke Tobias, gracias Marcos por haber formado conmigo un reducto de humor, desvarío y consuelo en este proceso. Gracias por contribuir a mi crecimiento personal. Moltes gràcies a Sílvia i Mar per fer-me una immersió completa a la cultura catalano-valenciana. Por todas las vivencias compartidas en estos años en Barcelona y por ser tan guapas por dentro.

Esta tesis no habría sido posible sin el apoyo de mi familia en Barcelona. Muchas gracias a Janire, Isita y Marta por hacerme sentir como en casa y cuidarme tanto. Gracias Isita y Janire por ser políticamente incorrectas y por ser sentimientos. Marta, muchas gracias por plasmar tu arte en mi portada y por tu cariño estos meses. Gracias a Silvia y a Valeria por ayudarme a desconectar de la rutina con tantos momentos de dramas y comedias. Gracias Lourdes por ser tan pura y por estar siempre a 200 km de mí.

Gracias a Yael y Fonso por el continuo apoyo técnico y moral de postdoctores. Muchas gracias por todo Ester. Gracias por llevarme a cualquier otra parte siempre que ha sido necesario. Gracias Víctor por ir contra todos y contra mí. Carlos, gracias por correr conmigo sobre el mismo viejo suelo, por tu paciencia y tu tiempo. Gracias a mis padres y a mi hermana Lara. Gracias por darme la libertad para escoger mis pasos y el apoyo para llevarlos a cabo. Gracias por sembrar en mí la semilla de la curiosidad y por hacerme perseverante. Gracias por formarme como persona.

Abstract

During cell division, microtubules (MTs) organize into a bipolar spindle that drives faithful chromosome segregation through the kinetochore fibers (k-fibers), bundles of parallel MTs that attach the chromosomes through their plus-ends to the spindle poles through their minus-ends. K-fiber MT plus and minus ends dynamics are coordinated to provide stability at the same time as support error correction, chromosome alignment and segregation. However, k-fiber minus-ends have been poorly characterized.

Electron tomography studies showed that the k-fibers MT minus ends have mixed open or close conformations suggesting complex regulatory mechanisms. Consistently, the silencing of MCRS1, currently the only potential regulator, results in k-fibers with less MTs with an increased proportion of open ends morphologies. TIRF based *in vitro* reconstitution assays showed that MCRS1 and KANSL3 associate preferentially with one MT end. Another member of the complex, KANSL1 may mediate their interaction formation of a ternary complex. Altogether, my results suggest that the MCRS1-KANSL-complex could dynamically “cap” some K-fiber MT-minus-ends to regulate their depolymerization rates for proper cell division.

Resum

Durant la divisió cel·lular els microtúbuls (MTs) s'organitzen en el fus mitòtic, que és l'encarregat de la segregació dels cromosomes a través de les anomenades "fibres del cinetocor" (fibres-k). Aquestes fibres son feixos de MTs que connecten a través del seu extrem-(+) els cromosomes amb els pols del fus mitòtic, on tenen el seu extrem-(-). La dinàmica d'aquestes fibres-k en tots dos extrems està coordinada per garantir l'estabilitat del fus mitòtic alhora que permet l'alineament dels cromosomes, la seva segregació i la correcció de posibles errors. Malgrat tot, la dinàmica a l'extrem-(-) gairebé no s'ha caracteritzat.

Els nostres estudis amb tomografia electrònica demostren que els extrems-(-) dels MTs de les fibres-k presenten una barreja en les conformacions dels seus extrems obertes i tancades, el que suggereix que estan subjectes a mecanismes de regulació complexos. D'acord amb això, el silenciament de MCRS1, actualment l'únic regulador potencial de la dinàmica a l'extrem-(-), té com a resultat fibres-k amb menys MTs i amb un increment en la proporció d'extrems amb conformacions obertes. Assaigs de reconstitució *in vitro* basats en microscopia TIRF mostren que MCRS1 i KANSL3 s'uneixen preferentment a un dels extrems del MT. Un altre membre del mateix complex, KANSL1 podria també interaccionar per formar un complex ternari. En conjunt, els meus resultats suggereixen que el complex MCRS1-KANSL podria bloquejar dinàmicament alguns extrems (-) de les fibres-k per tal de regular la seva despolimerizació de manera que la divisió cel.lular sigui adequada.

Abbreviations	**Full name**
ASPM	Abnormal spindle-like microcephaly-associated *protein*
ATP	Adenosine triphosphate
CAMSAP	Calmodulin-regulated spectrin-associated protein
ChIP	Chromatin immunoprecipitation
chTOg	Cytoskeleton-associated protein 5
CLASP	CLIP-associated protein
CPC	Chromosomal passenger complex
Cryo-EM	Cryo-electron microscopy
DMEM	Gibco Dulbecco's Modified Eagle Medium
DOC	Sodium Deoxycholate
DTT	Dithiothreitol
EBs	End-binding proteins
EGTA	Egtazic acid
ET	Electron tomography
FBS	Fetal bovine serum
GDP	Guanosine diphosphate
GEF	Guanosine exchange factor
GFP	Green fluorescent protein
GMPCPP	Guanylyl 5′-α,β-methylenediphosphonate
GTP	Guanosine triphosphate
HCF1	Host cell factor 1
HICE1/ HAUS8	HEC1/NDC80-interacting centrosome-associated protein 1
HURP	Hepatoma up-regulated protein
INCENP	Inner centromere protein
KANSL1	KAT8 regulatory NSL complex subunit 1
KANSL2	KAT8 regulatory NSL complex subunit 2
KANSL3	KAT8 regulatory NSL complex subunit 3
k-fibers	Kinetochore fibers
KMT	Kinetochore microtubule
LB (1)	Laemmli buffer
LB (2)	Luria-Bertani Broth
MAP2	Microtubule-associated protein 2
MCPH	Autosomal recessive primary microcephaly
MCRS1	Microspherule protein 1

MOF/KAT8	Histone acetyltransferase KAT8
MTOC	Microtubule organizing center
MTs	Microtubules
NEBD	Nuclear Envelope Breakdown
NEDD1	Neural precursor cell expressed developmentally down-regulated protein 1
NGS	Next generation sequencing
NLS	Nuclear localization signal
NuMA	Nuclear mitotic apparatus *protein* 1
OGT	UDP-N-acetylglucosamine-peptide N-acetylglucosaminyltransferase
PBS	Phosphate-buffered saline
PCM	Pericentriolar material
PHF20	PHD Finger Protein 20
RIPA	Radioimmunoprecipitation assay
SAC	Spindle Assembly Checkpoint
SAF	Spindle Assembly Factor
SDS	Sodium dodecyl sulfate
SDS-PAGE	Sodium dodecyl sulphate–polyacrylamide gel electrophoresis
SOC	Super Optimal Broth
TACC3	Transforming acidic coiled-coil-containing protein 3
TBS	Tris-*buffered* saline
TIP	Microtubule tracking protein
TPX2	argeting protein for XKLP2
Tx	Taxol
WDR5	WD repeat-containing protein 5
γ-TuRC	γ-tubulin ring complex
γ-TuSC	γ-tubulin small complex

Table of content

1. Introduction 1
   1.1. MT basics 2
      a) Microtubule structure 2
      b) Microtubule dynamics 3
      c) Microtubule nucleation 6
   1.2. Spindle assembly 8
      a) Spindle organization 8
      b) MT assembly pathways 9
      c) Spindle MT dynamics 14
   1.3. Kinetochore fibers 15
      a) Functions 15
      b) Structure 15
      c) Dynamics 17
   1.4. Microtubule minus-end targeting proteins in mitosis 21
   1.5. The KANSL complex 25
      a) The KANSL-complex in interphase 25
      b) The KANSL-complex in mitosis 29
2. Objectives 37
3. Results 41
   3.1. Structure of the k-fiber minus-ends in metaphase 41
      a) Tomographic reconstruction of k-fibers 41
      b) K-fiber minus-ends in metaphase are both, open and closed 44
   3.2. K-fibers and their minus-ends are altered in MCRS1-silenced cells 49
      a) Spindle morphology is altered in MCRS1-silenced cells 49
      b) The MT of K-fibers assembled in MCRS1-silenced cells have their minus-ends further away from the spindle pole 52
      c) K-fibers in MCRS1-silenced spindles have less kinetochore MTs 54
      d) K-fiber MT minus-ends in MCRS1-silenced spindles seem to have a higher proportion of open ends at the spindle poles 55
      e) K-fiber MT plus-ends have an open morphology at the kinetochore 59
   3.3. *In vitro* reconstitution assays to investigate the targeting of the MCRS1-KANSL-complex to the k-fibers MT minus-end 61
      a) MCRS1, KANSL3 and KANSL1 expression and purification for *in vitro* TIRF experiments 61
      b) KANSL3-GFP seems to preferentially bind one of the MT ends *in vitro* 63
      c) MCRS1-cherry seems to preferentially bind one of the MT ends *in vitro* 66
      d) MCRS1-cherry has no obvious MT end tracking *in vitro* 69
   3.4. *In vitro* reconstitution assays to investigate the architecture of the MCRS1-KANSL-complex 71
      a) KANSL1 and MCRS1 directly interact *in vitro* 71
      b) KANSL3 and MCRS1 do not interact *in vitro* 73
      c) KANSL1 and KANSL3 interact *in vitro* 73

4. Discussion.. 77
  4.1. Structure of the k-fiber minus-ends using electron tomography 77
  4.2. The MCRS1-KANSL-complex has moonlighting activity 82
  4.3. How does the MCRS1-KANSL-complex regulate k-fiber minus-end dynamics in mitosis?.. 84
  4.4. Are the k-fiber MT minus-ends the new plus-ends?.................................... 90
5. Conclusions 95
6. Materials and Methods.. 99
7. Bibliography 121
8. Annex.. 133
  8.1. ¼ of a full spindle displays the same characteristics of the full volume of the spindle……………………………………………………………………………..133
  8.2. Proportion of open minus-ends matching for both classifiers..................... 134
  8.3. Analysis of protein levels after silencing MCRS1 135
  8.4. All three control, siScramble and siMCRS1 cells are in metaphase 136
  8.5. Analysis of mitotic transcripts levels after MCRS1-silencing 137

List of figures

Figure 1. Microtubule structure. 2
Figure 2. Microtubule dynamics.. 4
Figure 3. MT end structure… 5
Figure 4. Microtubule nucleation…........ 7
Figure 5. Spindle organization and assembly.…........ 9
Figure 6. Microtubule nucleation pathways…........ 11
Figure 7. K-fiber structure.. 16
Figure 8. K-fibers undergo poleward flux in metaphase... 18
Figure 9. Microtubule minus-end targeting proteins in mitosis… 23
Figure 10. The KANSL-complex in interphase.. 26
Figure 11. The KANSL-complex in mitosis: mammalian cells and Drosophila..........31
Figure 12. Tomographic reconstruction of the k-fibers.. 42
Figure 13. Microtubule end morphology as a readout of dynamics........ 44
Figure 14. Characterization of the K-fiber minus-end distribution and morphology.…... 46
Figure 15. Characterization of spindle morphology in MCRS1-silenced cells.. 50
Figure 16. Tomographic reconstruction of k-fibers assembled in the absence of MCRS1. 53
Figure 17. Characterization of the k-fiber minus-end morphology in MCRS1-silenced cells. 57
Figure 18. Characterization of the k-fiber plus-end morphology. 60
Figure 19. MCRS1-Cherry, KANSL3-GFP and KANSL1-GFP structure and purification from insect cells. 62
Figure 20. Schematic of TIRF setup for the localization assays on Taxol-stabilized MTs. 64
Figure 21. KANSL3-GFP preferentially binds one of the MT ends of Taxol-stabilized MTs.. 65
Figure 22. MCRS1-Cherry preferentially binds one of the MT ends of Taxol-stabilized MTs.. 67
Figure 23. MCRS1-Cherry binds to GMPCPP-seeds and soluble tubulin.…........ 69
Figure 24. MCRS1, KANSL1 and KANSL3 interactions. 72
Figure 25. Open end morphology........ 81
Figure 26. Drosophila spindle and Taxol-MTs.…........ 85
Figure 27. Possible model of minus-end dynamics regulation by the KANSL-complex. 88
Figure 28. Map of pCoofy27-10xHis-zz-tag-TEV-KANSL3-GFP.…........ 102

Figure A. Comparison of the characteristics of a full spindle versus its versus three. 133
Figure B. Proportion of open minus-ends in a ¼ of spindle taking into account only the matching ends for both classifiers. 134
Figure C. Analysis of the protein levels after MCRS1-silencing. 135
Figure D. Determination of the interkinetochore distance for the WT, siControl and siMCRS1……………………………………………………………………………………..133
Figure E. Analysis of the mitotic transcripts levels after MCRS1-silencing in HeLa cells. 138

Introduction

1. Introduction

Life relies on cell division. Cell division aids in the formation of gametes. Following fertilization, the zygote undergoes a series of mitotic cell divisions that are fundamental during all stages of development. The growth of a full organism is only possible thanks to coordinated rounds of divisions. Besides, cell division is required for tissue maintenance during adulthood. On the other hand, abnormal cell divisions are the basis of diseases such as cancer and genetic disorders such as Down's syndrome.

The cell division or mitosis is the process by which a parental cell divides into two or more daughter cells. The main requirement of mitosis is the maintenance of the original cell's genome. Before cell division, the genetic information contained in the parental cell is replicated and then, segregated in the form of chromosomes to the two daughter cells. The mitotic spindle is the machinery in charge of the faithful segregation of the chromosomes.

The mitotic spindle is structurally and functionally defined by its main component, the microtubules (MTs). MTs in the spindle form two antiparallel arrays with their plus ends overlapping at the spindle midzone and their minus ends focused forming the spindle poles. The chromosomes oscillate in the midzone of the spindle and sister chromatids are pulled to the spindle poles thanks to the forces generated by the MTs. The main population of MTs that drives chromosome movement to the spindle poles are kinetochore-fibers (k-fibers). K-fibers are bundles of MTs that connect the chromsomes to the spindle poles. K-fiber MT dynamics both at the plus and minus-ends are crucial for spindle function. Although much is already known about the plus-end dynamics and their function, the mechanisms controlling MT minus-end dynamics are poorly understood. During the next chapters, I will go through the basics of MT structure and dynamics and how individual MTs assemble to form the mitotic spindle. Next, I will describe the structure and dynamics of the k-fibers, specifically those at their MT minus-ends, which are the object of study of this thesis. Finally, I will write about different regulators of the MT minus-end dynamics with a focus on the KANSL-complex, a chromatin regulator that when the cell enter into mitosis locates to the k-fiber minus-ends and regulate their dynamics.

1.1. MT basics

Besides being fundamental during cell division, MTs participate in a wide variety of cellular processes such as development, maintenance of cell shape, intracellular trafficking or cell signaling through cilia[1]. All these functions are supported by their characteristic structure and their dynamic properties, both of which are tightly connected.

a) Microtubule structure

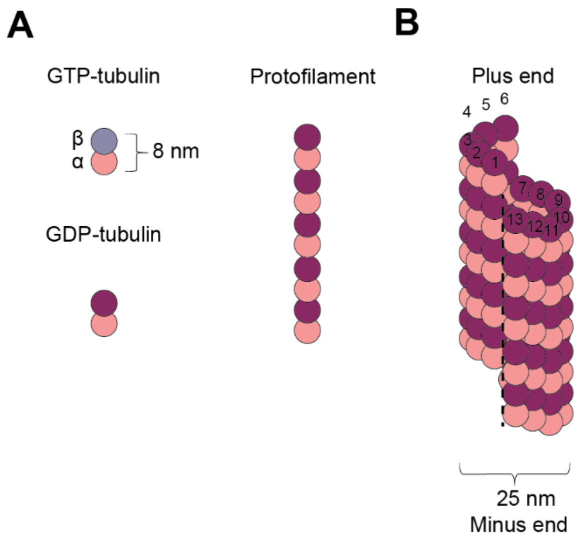

Figure 1. Microtubule structure. A) α and β-tubulin interact non-covalently to form a very stable heterodimer of 8 nm length. β-tubulin can bind GTP (top image) and hydrolize it to GDP (bottom image). α-tubulin binds GTP but does not hydrolize it. The heterodimers associate head-to-tail to form the protofilaments (PFs). B) In a canonical mammalian MT, 13 of these PFs interact laterally to form a sheet that closes into a hollow cylinder with a diameter of 25 nm. The end capped by β-tubulin is defined as the MT plus-end whereas the end capped by α-tubulin is the minus-end.

MTs are hollow filaments composed of subunits of a single type of a globular protein called tubulin. Each tubulin subunit is a heterodimer formed from two closely related 55 kDa polypeptides named α and β-tubulin. The α and β monomers interact non-covalently to form a very stable building block of 8 nm length (Figure 1. Microtubule structure. A) α and β-Figure 1 A, left). These building blocks associate head-to-tail to form the so-called protofilaments (PFs) (Figure 1, right). In mammalian cells, 13 of these PFs interact laterally to form a sheet that closes into a hollow cylinder with a diameter of 25 nm, the MT[1,2] (Figure 1 B). *In vitro* MTs with 14 PFs are the most abundant, but tubulin can actually nucleate to form MTs having from 9 to 16 PFs[3] *in vivo*.

Since the tubulin dimers are aligned in the same orientation in a PFs and all PFs in a microtubule are parallel to each other, the MT is intrinsically polar. The end capped by the β-tubulin monomer is defined as the plus-end whereas the end terminated by the α-tubulin monomer constitutes the minus-end. MT polarity implies different dynamic properties for both MT ends as will be discussed later.

When PFs associate laterally two types of protein-protein contacts form to sustain the MT structure. Along the longitudinal axis of the MT, the “top” of one β-tubulin molecule forms an interface with the “bottom” of the α-tubulin molecule in the adjacent heterodimer (strong interaction). Perpendicular to these interactions, neighboring PFs form lateral contacts (weak interaction) that are parallel to the longitudinal axis when the sheet closes. Both types of contacts, lateral and longitudinal, are important for the maintenance of the tubular structure.

b) Microtubule dynamics

During mitosis, the array of MTs within the cell completely disassembles and reorganizes to form the bipolar spindle structure. The continuous remodeling of the MT length occurs through stochastic length fluctuations at the ends of the MTs. The dynamic behavior at the MTs ends constitutes the so-called dynamic instability[4,5]. The dynamic instability is the stochastic switching between slow growth and rapid shrinkage phases. MTs undergo dynamic instability both *in vivo* and *in vitro*. The dynamic instability has been linked both to the state of the guanosine-5’-triphosphate (GTP) molecules that bind the tubulin and to the structure of the tubulin PFs at MT tips[6].

The tubulin subunits are enzymes that can bind and hydrolyze GTP[7–9]. Each α or β-monomer has a binding site for one molecule of GTP. The GTP binding site at the β-subunit can hydrolyze the GTP to GDP whereas the GTP binding site at the α-monomer is nonexchangeable. GTP is required for MT polymerization but at the same time its hydrolysis releases free energy that destabilizes the MT lattice. The text book model to explain the dynamic instability is “the cap model”. According to this model, shortly after polymerization, the GTP bound to the β-tubulin is hydrolyzed to GDP. The body of the MT is made out of GDP-tubulin subunits that are unstable. However, a layer of tubulin subunits at the ends that retain their GTP, the so-called GTP-caps (Figure 2 A), stabilizes the whole structure of the MT. When this cap is stochastically lost, “catastrophe”, the MT rapidly depolymerizes. Oppositely, when a GTP-cap binds to the shrinking MT, there is a “rescue” and the MT starts to slowly polymerize[5,10](Figure 2 B). Whether a microtubule grows or shrinks is determined by the rate of tubulin addition relative to the rate of GTP hydrolysis[2].

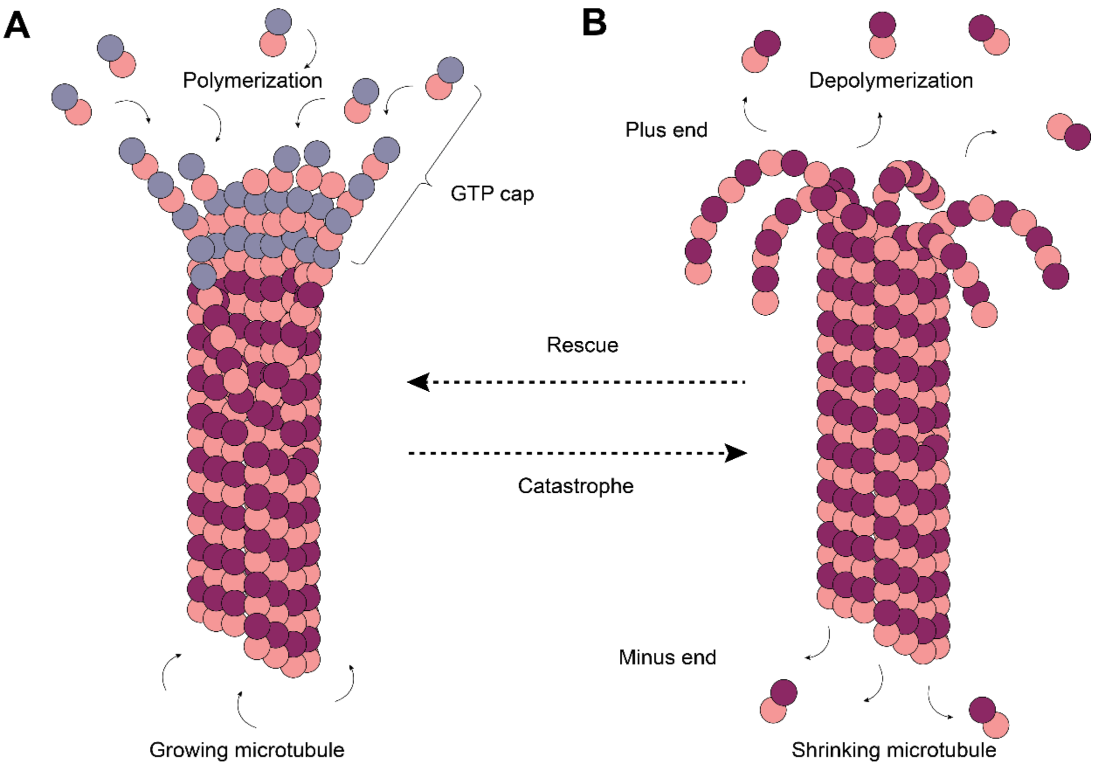

Figure 2. Microtubule dynamics. A) MTs polymerize by incorporation of dimers of GTP-bound tubulin. Shortly after incorporating to the MT lattice, GTP hydrolizes to GDP. This reaction generates free energy that destabilizes the MT structure. However, the MT lattice is protected by a layer of GTP-tubulin at its plus-end, the so-called “GTP-cap”. B) When the “GTP-cap” is stochastically lost, there is a catastrophe and the MT depolymerizes. Oppositely, when a GTP-cap binds to the shrinking MT, there is a “rescue” and the MT starts to slowly polymerize. The stochastic switching between phases of slow growth and rapid shrinkage is termed dynamic instability.

GTP hydrolysis generates mechanical strain in the MT lattice that triggers conformational changes at the MT tips. Initially, it was proposed that the mechanical strain was released by bending the PFs (“peeling-off”) and therefore, disrupting the lateral contacts. However, recently, new structural data suggested that the destabilization of the ends starts at the longitudinal interfaces and then, translates into the bending of the PFs during the catastrophe[11,12]. On the other hand , the process by which a shrinking MT is rescued by converting the outwardly peeling PFs back into a growing MT, “rescue”, is much less understood[9,13].

Since MTs are polar filaments, their plus-ends are capped by β-tubulins that can hydrolyze GTP whereas their minus-ends are capped with α-tubulin. This leads to very distinct dynamics at both ends. The minus-end grows more slowly and undergoes catastrophe less frequently than does the plus end[14].

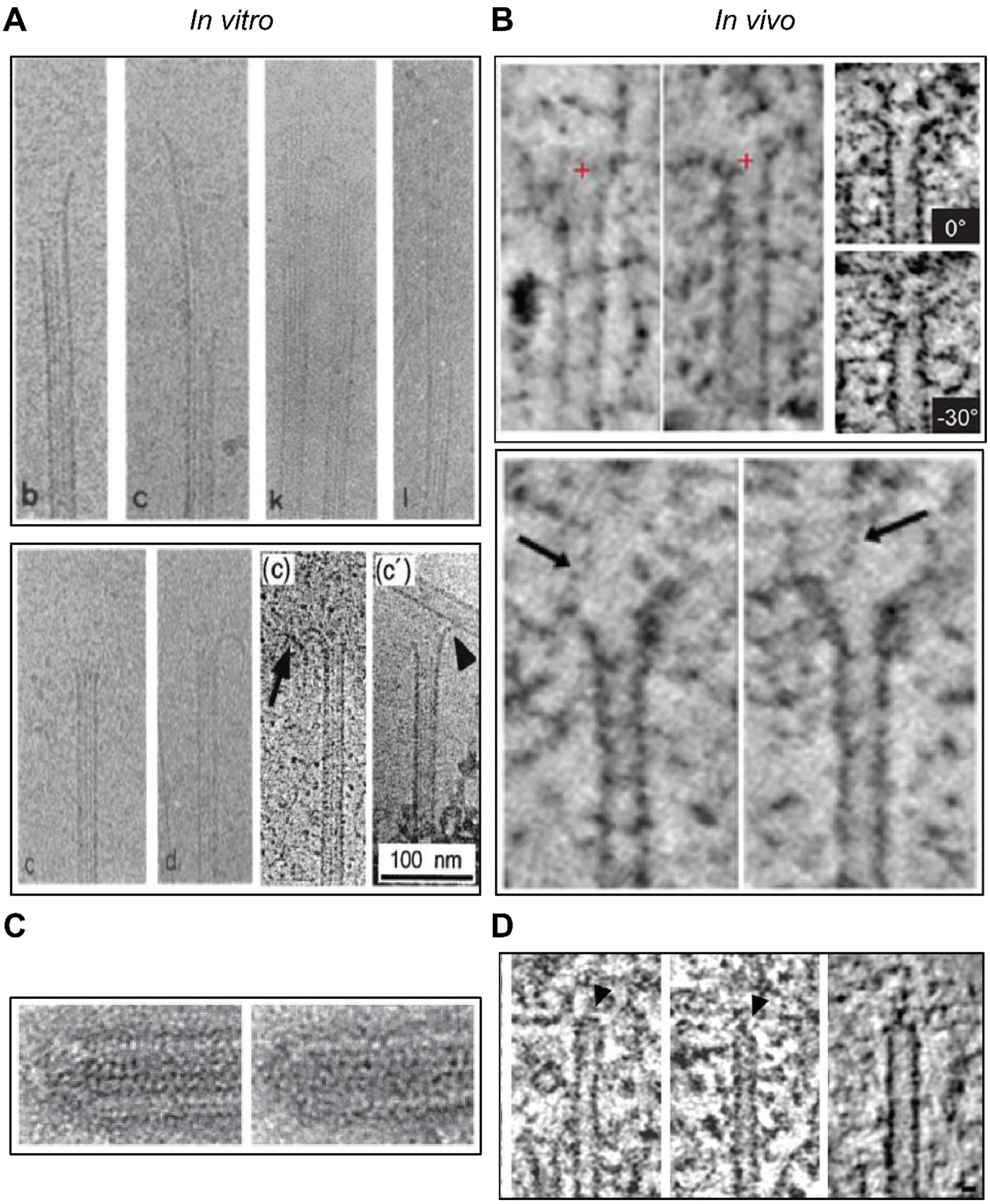

Figure 3. MT end structure. A) Top image: electron micrographs of MTs nucleated from centrosomes *in vitro*. Growing ends have tapered and partially curved sheet-like structures (b, c, k, l) (adapted from [15]). Bottom image: electron micrographs of MTs nucleated from centrosomes *in vitro* (c, d) and of *in vitro* grown GTP or GMPCPP MTs (c, c'). Shriking ends have curled PFs) (adapted from [15,16]). B) Top image: electron tomography reconstructions of MTs showing growing ends with a flared morphology in Ptk1 mitotic spindles (left, middle) and in *S. pombe* (right) (adapted from[6,17]). Bottom image: electron tomography reconstructions of Ptk1 spindle MTs showing shriking ends with a flared morphology (adapted from[18]). C) Electron micrographs showing capped ends as observed after growing MTs in the presence of γ-TuSC rings *in vitro* (*S. cerevisiae*) (adapted from [19]). D) Electron tomography reconstructions of MTs from *C.elegans* spindles (left and middle) and of *S.pombe* MT (right) with a cap-like structure at their ends. This "cap-like" structure is assumed to be the γ-TuRC ring complex (adapted from [17,20]).

In vitro and in cells, the structure of the MT ends serves as a readout of their dynamics. First structural studies on centrosome-nucleated MTs revealed tapered and partially curved sheet-like structures at growing MT ends distinct from more curled PFs on shriking ends[15,21–23] (Figure 3 A, top and bottom). The curled oligomers at the ends of depolymerizing MTs were further observed in different classes of MTs *in vitro*[16] (Figure 3 A, bottom). In cells the situation differs as many MT-associated proteins (MAPs) surround the MT tips. Polymerizing and depolymerizing ends have been sometimes described to have a distinct morphology, similar to that observed *in vitro*[24]. But most recent descriptions show growing end and depolymerizing ends having a similar "flared" morphology after electron tomography, suggesting that polymerizing and depolymerizing MTs in cells display the same structure (Figure 3 B). A most recent and ambitious study aiming to compare *in vitro* with *in vivo* MT ends from six different species reports that indeed the structure of growing and shrinking MT ends is very similar to each other, challenging the field[6,23].

c) Microtubule nucleation

MTs can spontaneously nucleate *in vitro.* They can form from purified tubulin dimers in buffer solutions containing GTP and Mg^{2+}. However, this process is not energetically favourable. This is a consequence of both MT structure and its dynamic properties. The lattice structure sustained by longitudinal and lateral contacts is very complex. Besides, it can be easily destabilized upon incorporation of the new tubulin dimers with GTPase activity. The process is favoured at higher tubulin concentrations (Figure 4 A). *In vivo,* the tubulin concentration is below the critical concentration. The energetic barrier is overcome by the use of nucleation templates. The major nucleation template or nucleator in eukaryotic cells is the γ-tubulin ring complex (γ-TuRC). The γ-TuRC is formed by the lateral association of multiple γ-TuSCs rings, two molecules of γ-tubulin and proteins called γ-tubulin complex proteins (GCPs) 2 and 3, with GCP4, GCP5 and GCP6[25] (Figure 3 C). Additionally, accessory proteins with regulatory functions such as GCP-WD (also known as NEDD1 (Neural Precursor Cell Expressed, Developmentally Down-Regulated), GCP8 (also known as Mozart-2, MZT2) and Mozart-1 are part of the γ-TuRC. All these proteins are arranged into a pseudo-helical conical structure that caps the MT minus-ends. According to the so-called template nucleation model, the helical arrangement of γ-tubulin molecules matches the symmetry of a MT and thereby provides a template for the addition of tubulin heterodimers. In cells, the γ-tubulin ring complex (γ-TuRC) is observed as a cap-like structure with higher electron density by electron tomography (Figure 3 D) [17,20,26,27]. The MTs ends with this structure are the minus-ends. Recent efforts have been devoted to understand how the γ-TuRC is structured, assembled and activated (Figure 4 B)[28,29]. The structures of MT ends grown from reconstituted γ-TuRC rings have yet to be resolved, as the complex was only recently purified[28,29]. In addition, cells control where and when to nucleate new MTs by specific targeting of the γ-TuRC. This is fundamental for the establishment of a functional bipolar spindle as will be discussed in the next section.

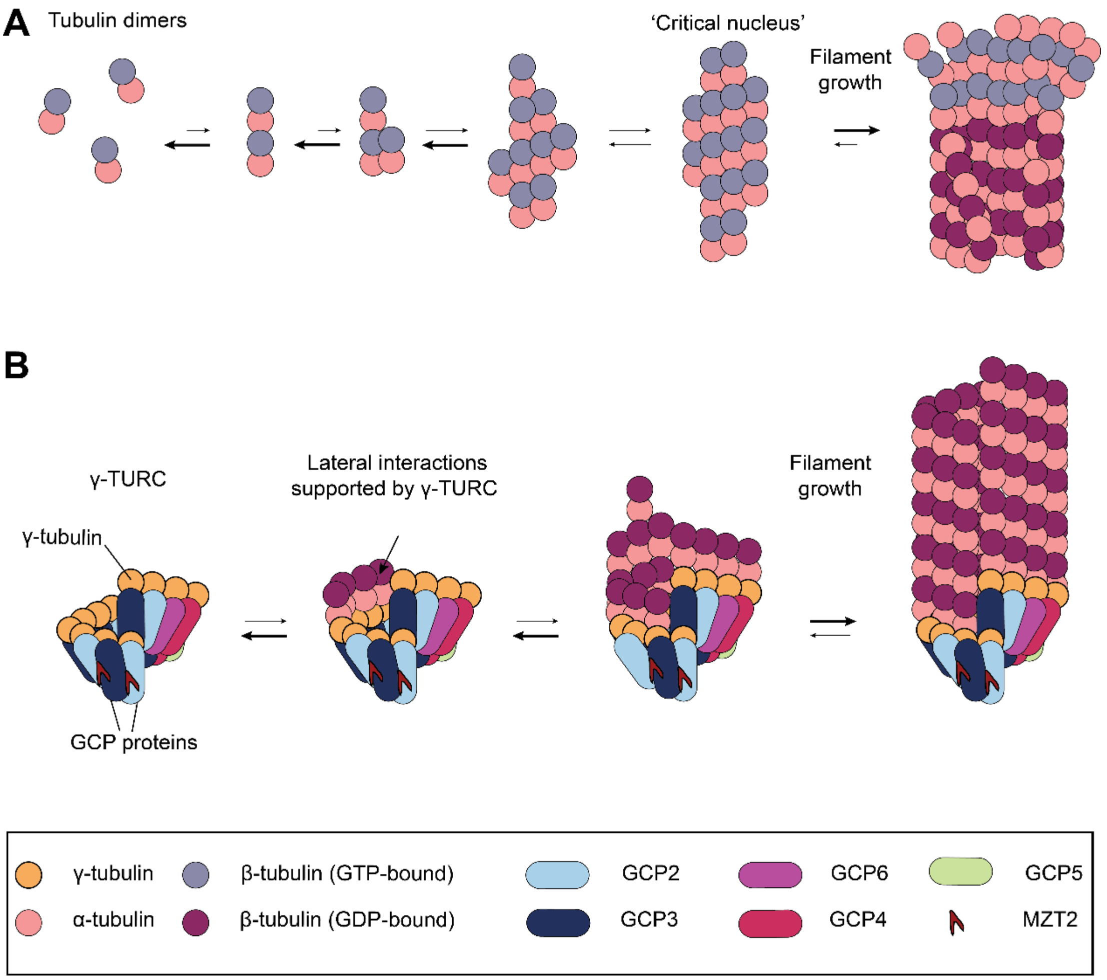
A
Tubulin dimers
'Critical nucleus'
Filament growth
B
γ-TURC
γ-tubulin
GCP proteins
Lateral interactions supported by γ-TURC
Filament growth
γ-tubulin
α-tubulin
β-tubulin (GTP-bound)
β-tubulin (GDP-bound)
GCP2
GCP3
GCP6
GCP4
GCP5
MZT2

Figure 4. Microtubule nucleation. A) Spontaneous microtubule nucleation. Tubulin dimers can spontaneously assemble into PFs and form MTs *in vitro*. However, the intermediate assemblies are highly unstable due to GTP hydrolysis (as indicated by the darker and longer arrows). Upon the formation of a "critical nucleus", the growth of a MT is most favoured (adapted from [30]). B) Templated microtubule nucleation. *In vivo* MT nucleation is favoured by the γ-TuRC ring complex Model of the γ-TuRC ring complex as recently reconstituted[29]. The γ-tubulin molecules within the ring are located in a single turn helix via their binding to GCP proteins. The γ-tubulin molecules bind the tubulin heterodimers which support their lateral interactions as they grow into PFs. MT assembly passes through unstable intermediates in which disassembly is more favoured than polymerization (as indicated by the darker arrows) until a stable "MT seed" forms. Then, MT polymerization progresses rapidly (adapted from [29,31]).

1.2. Spindle assembly

The mitotic spindle self-assembles thanks to the collective activities of multiple proteins that result in localized MT dynamics, organization and nucleation. All the process can be referred as to spindle assembly[32].

a) Spindle organization

The mitotic spindle forms right after nuclear envelope breakdown (NEBD) to segregate the sister chromatids. The spindle captures and aligns the condensed chromosomes at its center, known as the metaphase plate. It presents mirror symmetry with respect to the metaphase plate, referred as to bipolarity. Each sister chromatid faces towards one of the two spindle poles, made up of centrosomes. MTs are also arranged into a bipolar array, such that each half spindle contains uniformly oriented MTs, with their minus-ends laying at the pole and their plus-ends in the metaphase plate area. The chromosomes in the metaphase plate have a pair of specialized structures at its centromeres, the kinetochores. The kinetochores are connected to the spindle pole by MTs[33–35].

According to their location and function, MTs can be classified into three different subclasses in the mature mitotic spindle: astral MTs, interpolar MTs and kinetochore fibers (k-fibers) (Figure 5 A). Astral MTs emanate from the two centrosomes and anchor the spindle to the cell cortex. They play a major role in separating the centrosomes during prophase and in orienting and positioning the spindle within the cell[33,36]. Interpolar MTs are the most abundant class of MTs in the spindle. They also emanate from the centrosome but span towards the midzone of the spindle where they form an antiparallel overlap with other interpolar MTs originated from the opposite pole. These interactions generate a MT array that provides the spindle with mechanical stability. Interpolar MTs are also important for the maintenance of spindle biopolarity and chromosome congression due to their interaction with the chromosomes through the chromokinesins or through lateral interactions with the kinetochores. Nevertheless, they do not participate directly in chromosome segregation[33]. Astral and interpolar MTs are both very dynamic, having a fast turnover (average half-life time below 1 minute)[37]. Kinetochore MTs connect the pole to the kinetochores in the sister chromatids. These connections form parallel bundles known as k-fibers that mediate chromosome segregation. Kinetochore MTs are the less dynamic population of MTs in the spindle (average half-life time 4-8 minutes)[37].

The different MT subclasses originate through different pathways that drive MT assembly in the spindle.

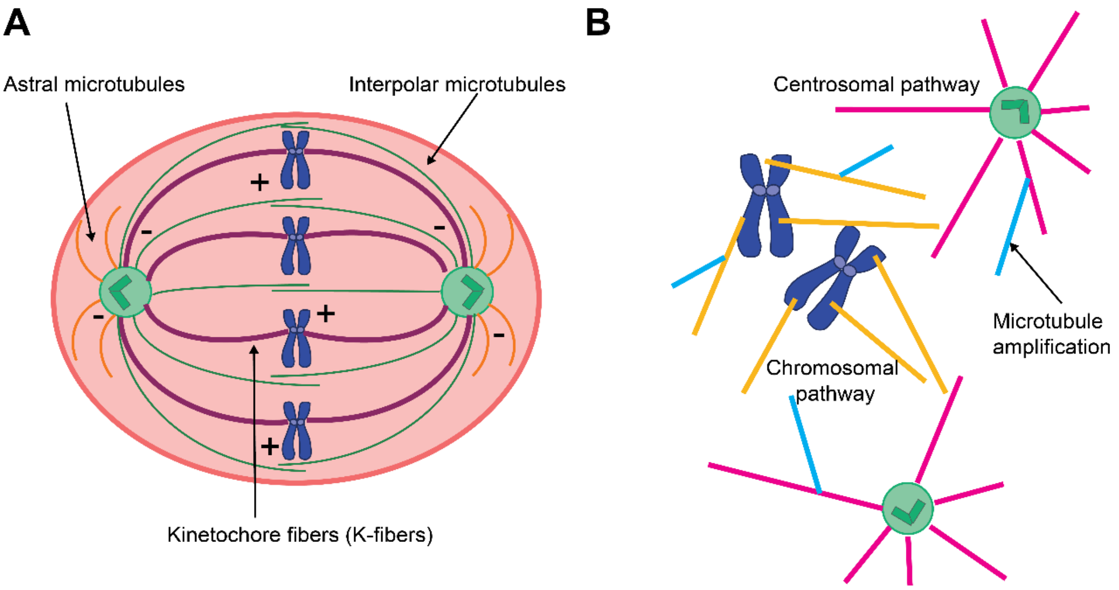

Figure 5. Spindle organization and assembly. A) MTs can be classified into three different populations in the mitotic spindle. Astral MTs emanate from the centrosomes and anchor the spindle to the cortex (orange). Interpolar MTs also emanate from the centrosomes and overlap in the spindle midzone (green). K-fibers are bundles of MTs that connect the kinetochore to the spindle poles (purple). MT plus-ends lay in the midzone whereas MT minus-ends are embedded at the spindle pole. B) MTs can be assembled through three different pathways. MTs can nucleate at the centrosomes (centrosomal pathway), around the chromosomes (chromosomal pathway) and also nucleate from pre-existing MTs (microtubule amplification pathway) to form the mitotic spindle (adapted from [33]).

b) MT assembly pathways

In mitosis, MT nucleation increases through different mechanisms that involve the γ-TuRC ring complex. This, in turn, defines the different MT assembly pathways[30,32,38]. MTs can nucleate through a centrosomal pathway or through non-centrosomal pathways that will be described in the next sections (Figure 5 B).

Centrosomal pathway

The centrosome is the main microtubule-organizing center (MTOC) in animal cells and regulates the nucleation and spatial distribution of MTs wihtin the cell. The centrosome is comprised of a pair of barrel-shaped centrioles displaying a nine-fold radial symmetry, one of which is decorated with distal and subdistal appendages, the so-called mother centriole. The pair of centrioles is surrounded by an electron-dense matrix termed the pericentriolar material (PCM), composed of proteins[25]. The centrosomes are responsible for both, nucleating and anchoring the MTs. In interphase, the centrosome duplicates at the nuclear envelope. After mitotic entry, centrosomes move apart from each other and undergo a “maturation” process. During maturation, the PCM recruits the MT nucleator γ-TuRC and gets thicker by incorporating components that mediate the binding and nucleation of γ-TuRC. NEDD1, CEP192, pericentrin (PCN), CDK5RAP2, and AKAP9 are some of the factors recruited to the PCM. Maturation increases the nucleation activity of the centrosomes which promotes the formation of two asters of dynamic MTs that start to get positioned at the opposite sides of the cells. This was fundamental to the “search-and-capture”[10] model that postulates that dynamic centrosomal MTs emanating from the two centrosomes grow and shrink, thereby exploring the cellular space until their plus-end become captured by the kinetochores[33]. At the same time the newly formed k-fibers exert force that drive centrosomes apart[39]. All together, centrosomal MTs dynamics, centrosome separation and kinetochore attachment would lead to the formation of bipolar spindle[32,33,40]. In the spindle, the minus-ends remain tethered at the centrosomes whereas the plus-ends would be attached to the kinetochores[41]. Nevertheless, centrosomes are not essential for bipolar spindle assembly. Cells naturally occuring without centrosomes such as plant cells and oocytes can assemble spindles and divide. Besides, spindles can also form in cells manipulated to eliminate their centrosomes, although they help with the proper chromosome segregation[42]. Therefore, non-centrosomal MT assembly pathways must be fundamental for spindle assembly.

Non-centrosomal pathways

Two main mechanisms trigger acentrosomal assembly in mitotic cells. The first mechanism is driven by the chromosomes. It can be dependent on the Ran complex and on the chromosomal passenger complex (CPC) (chromosome-dependent pathways). The second mechanism drives MT amplification through a MT-dependent nucleation mechanism (MT amplification). Interestingly, intereferring with both the RanGTP pathway or the augmin pathway prevents spindle assembly in egg extract and in cells[33].

Chromosome-dependent pathway

MTs nucleate near the chromosomes in mitotic cells. The underlying mechanism of nucleation is dependent on Ran. Ran is a small Ras-related GTPase that is key for nuclear import and export, nuclear envelope formation and mitotic assembly.

In interphase, Ran interacts with the karyopherins across the nuclear envelope to control the shuttling of proteins between the nucleus and the cytoplasm. Proteins containing a nuclear localization signal (NLS) are bound by importins and tranported into the nucleus. In the nucleus, RanGTP binds to importin and releases the import cargo. Likewise, proteins that need to be exported from the nucleus bind to exportin and RanGTP. Once outside, the proteins are released upon RanGTP hydrolysis to RanGDP. GTP hydrolysis is favoured by GTPase-activating proteins (RanGAP) and Ran-binding proteins (RanBP1 and RanBP2). These proteins are cytoplasmic and thereby, GDP-bound Ran is predominantly cytoplasmic. On the contrary, RanGDP is converted into RanGTP through the action of its guanosine exchange factor (GEF), RCC1. RCC1 binds to the chromatin making GTP-bound Ran more abundant in the nucleus.

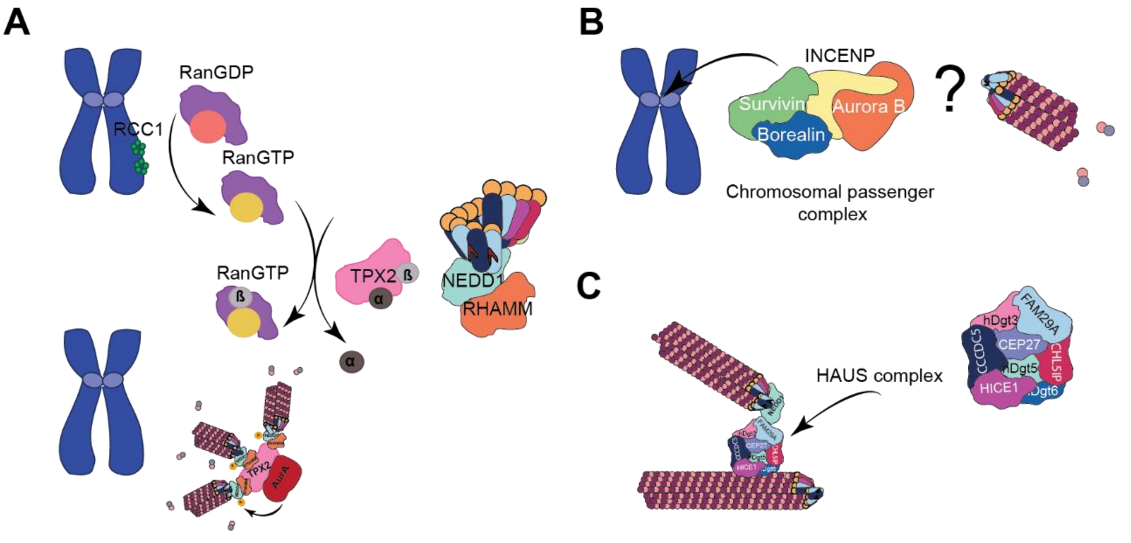

Figure 6. Microtubule nucleation pathways. A) RanGTP-dependent pathway. MTs nucleate in the close proximity of the chromatin through a RanGTP-dependent mechanism. RCC1-bound to the chromatin makes RanGTP to be enriched in the region. RanGTP releases different spindle assembly factors (SAFs) from α-β-importin. One of the targets of RanGTP is TPX2. Upon release, TPX2 interacts with the a MT complex containing the γ-TuRC, NEDD1 and RHAMM, which promotes MT nucleation next to the chromatin. This interaction is regulated by the kinase Aurora A. B) Chromosomal passenger complex (CPC)-dependent pathway. The CPC-complex has been also proposed to nucleate MTs from its location in the inner centromere region of the chromosomes. However, how it recruits the γ-TuRC and promotes nucleation is not clear. It is also likely that the complex helps stabilizing already nucleated MTs. C) Microtubule amplification pathway. MTs can nucleate on pre-existing MTs along the spindle body. Amplification in humans is mediated by the HAUS-complex. The complex targets pre-existing MTs through HICE1, and binds NEDD1 and the γ-TuRC through FAM29A to promote nuclation (adapted from [33]).

In mitosis, RanGTP influences spindle assembly by a mechanism closely related to that of nucleocytoplasmic transport. After NEBD, all components of the cell mix. Proteins with a NLS are trapped by α-importin-β-importin while RCC1 remains bound to the chromatin, in this case chromosomes. RanGTP is enriched in the proximity of the chromosomes and as it diffuses away the RanGAP present in the cytoplasm promotes its hydrolysis into RanGDP, generating a RanGTP gradient around the chromosomes. This RanGTP gradient promotes MT nucleation only wihtin a region close to the chromosomes and also helps to stabilize MTs at greater distances[43]. Close to the chromosomes RanGTP interacts with importin-β and promotes the release of the cargoes, termed spindle assembly factors (SAFs). SAFs have a NLS and are expected to be nuclear in interphase. How RanGTP activates MT nucleation is yet not fully understood. One of the main targets of RanGTP is TPX2 (targeting protein for Xklp2). TPX2 interacts with a specific MT nucleation complex formed by γ-TuRC, NEDD1 and RHAMM (hyaluronan-mediated motility receptor) to trigger nucleation[44]. This interaction is regulated by the kinase Aurora A, also activated by TPX2 (Figure 6 A). The phosphorylation of a specific serine residue on the substrate NEDD1 by Aurora A is essential for this pathway. This mechanism does not suggest a pre-defined site for the nucleation to happen. Other RanGTP dependent SAFs (CDK11, CHD4, ISWI, HURP, MCRS1, Mel28) have been described to play a role in MT nucleation, stabilization and organization[45,46]. By promoting MT nucleation and stabilization close to chromosomes, the RanGTP pathway cooperates with the “search and capture” mechanism increasing the MT capture in the kinetochores and favours via “chromatin stabilization” the MT capture, k-fiber formation and spindle assembly.

Kinetochores are the “hot spot” of nucleation around chromatin if compared to the chromosome arms[47]. Different observations lead to the idea that kinetochores could directly nucleate MTs. Indeed, experiments in *Xenopus laevis* egg extract showed that spindles could assemble in the absence of a RanGTP gradient[48]. MTs would nucleate in response to the activation of the CPC complex. The CPC complex is a four-protein complex consisting of the chromatin targeting subunits Survivin and Borealin, the scaffold protein inner centromere protein (INCENP) and the kinase Aurora B. It localizes mainly to the innter centromere region[49]. However, how the MTs could nucleate through this pathyway and assemble a spindle is not clear (Figure 6 B). The γ-TuRC has not been reported to be involved in the “kinetochore nucleation”. Besides, nucleation from the kinetochore would oppose the regular orientation of MTs in the spindle by locating, at least transiently, minus-ends in the kinetochore instead of plus-ends. Hence, it is more likely that the CPC complex is involved in MT stabilization around the kinetochore. It could do so by the negative regulation that Aurora B imposes in some factors promoting MT catastrophes (MCAK or stathmin1)[33,45]. The RanGTP pathway and the CPC pathway could cooperate to first nucleate and then stabilize MTs. Additionally, the CPC complex is involved in kinetochore-MT attachment error correction[49].

MT amplification

MTs are not only generated at centrosomes and chromosomes but also along the spindle body[35]. This is possible thanks to the recruitment of γ-TuRC to pre-existing MTs to amplify the MT mass. The recruitment is mediated by the augmin complex (also named HAUS complex in human cells). The complex consists of eight proteins. One of them, FAM29A (family with sequence similarity 20, member A/HAUS6) binds to γ-TuRC through NEDD1[50] while another, HICE1 (Hec1-interacting and centrosome-associated 1/HAUS8) targets the lattice of a pre-existing MT(Figure 6 C)[45]. The branch angle between the new MT and the template MT is shallow and MTs tend to grow parallel along the template. This is very convenient as new MTs preserve the polarity of the pre-existing MT[35]. Newly grow MTs can be then sorted towards the spindle poles[41].

Recent studies have related the MT amplification pathway to the RanGTP dependent pathway. They propose TPX2 as necessary for branching MTs from pre-existing MTs[51]. As shown in egg extract and *in vitro* experiments, TPX2 would have the capacity to directly recruit both γ-TuRC and augmin to the MT lattice[52,53]. According to this model TPX2 would be activated by RanGTP and participate in the chromatin-dependent nucleation and also transported to the spindle body for its role in MT amplification. Nevertheless, there is a lack of agreement in the field about the role of TPX2 in branching MTs. Other studies in *Drosophila* cells and *in vitro* suggest that TPX2 is dispensable for the MT amplification[54,55].

MT amplification is important to proper spindle assembly. Depletion of components of the augmin pathway reduces the MT density within the spindle and cells display chromosome segregation deffects[35,56,57].

c) Spindle MT dynamics

MTs in the cell cannot be permitted to grow and shrink in a stochastic manner. MT dynamics are controlled by numerous proteins, which can be grouped into microtubule-associated proteins (MAPs) in the cells[58].

MAPs regulate MT growth and disassembly. MT polymerases promote MT growth or rescue depolymerizing MTs by favoring the straight tubulin dimer conformation (i.e: XMAP215) whereas MT depolymerases induce catastrophe by promoting the intrinsic curvature of the tubulin dimer (i.e: kinesin-13, kinesin-8 and kinesin-14 families). MT dynamics are also regulated by MT plus-end tracking proteins (+TIPs), which recruit other MAPs. The main family of +TIPs are the end-binding proteins (EBs). Other MAPs can suppress catastrophe and promote rescue, it is the case of the cytoplasmic linker protein (CLIP)-associated proteins (CLASPs)[14,35]. To date, most of the described MAPs are regulators of the plus-ends dynamics. Some recently characterize minus-end binding proteins (-TIPs) will be described in section 1.4.

MT dynamics are also the target of many agents such as taxanes and vinca alkaloids that are employed in cancer chemotherapeutics to inhibit cell proliferation. One of the most common used drugs is Taxol (Tx). The Tx molecule binds to the luminal face of β-tubulin and impedes the “MT curling” preventing depolymerization[12].

1.3. Kinetochore fibers

Kinetochore fibers (K-fibers) are parallel bundles of MTs that connect the kinetochores to the spindle poles. K-fibers are formed by kinetochore MTs (KMTs) and have their minus-ends embedded at the centrosomes and their plus-ends at the kinetochores.

a) Functions

The K-fibers are the main generators of forces in the spindle. In the initial stages of mitosis, the nascent k-fibers exert pushing forces that drive centrosome separation[39]. During prometaphase, the KMTs extending from one centrosome “search and capture” the kinetochore of one of the chromatids. When the sister kinetochore attaches to the KMTs growing from the other centrosome, the chromosome bi-orients and congress in the center of the MT array. The sister chromatid pair “oscillates” as one k-fiber grows and the other shrinks until the chromosomes are aligned. Then, the cell is in metaphase. It is important to mention that the cells can also cope with the KMT attachment errors and replace them while forming the metaphase plate. In anaphase, the k-fibers shorten by depolymerization at both ends thereby segregating the chromosomes to the opposite poles.

b) Structure

Their specific structure and dynamics allow the k-fibers to satisfy all the functions mentioned above. The majority of the structural information about the k-fibers has been obtained by electron microscopy and more recently, electron tomography. The number of MTs that form the fiber depends on the cellular type and increases while mitosis progresses. In microscopy studies, bundles of MTs have been described to have in between 20-30 MTs in Ptk1 cells in metaphase. In HeLa cells, k-fibers have 17 MTs in average. Nonetheless, the number of MTs does not depend only on the cellular type and the mitotic phase but also on the definition of k-fiber *per se*. If strictly considering the MTs in contact with the kinetochore as KMTs, HeLa-Kyoto cells have been recently shown to have 9.5 MTs in average (*Kiewisz R. and Müller-Reichert T. personal communication*). The k-fiber would get enriched in this model by neighboring MTs that do not directly reach the kinetochore. Not all MTs in the fiber necessarily extend between the kinetochore and the spindle pole (*Kiewisz R. and Müller-Reichert T. personal communication*).

The k-fibers are the most robust population of MTs in the spindle. In fact, k-fibers are the last MT subclass to depolymerize in response to cold-treatment or MT depolymerizing drugs. The bundling of the MTs in the k-fiber increases their stability. In a metaphase cell, the KMTs are held together through a network of MT connectors. The network of MT connectors is termed "the mesh"[59]. Each connector has up to four nodes so it can link up to four MTs. "The mesh" is composed of protein complexes containing TACC3/ch-TOG (transforming acidic coiled-coil-containing protein 3 / CKAP-5 Cytoskeleton-associated protein 5) and clathrin[60] and it is key to maintain the integrity and stability of the k-fiber (Figure 7). K-fiber stabilization is also achieved through the microtubule-bundling activity of hepatoma up-regulated protein (HURP; also known as DLGAP5)[61] (Figure 7). The functional effect of k-fiber MT stability could be to generate a rigid connection to chromosomes so that forces are transmitted efficiently and not lost by bending or splaying of individual MTs[62].

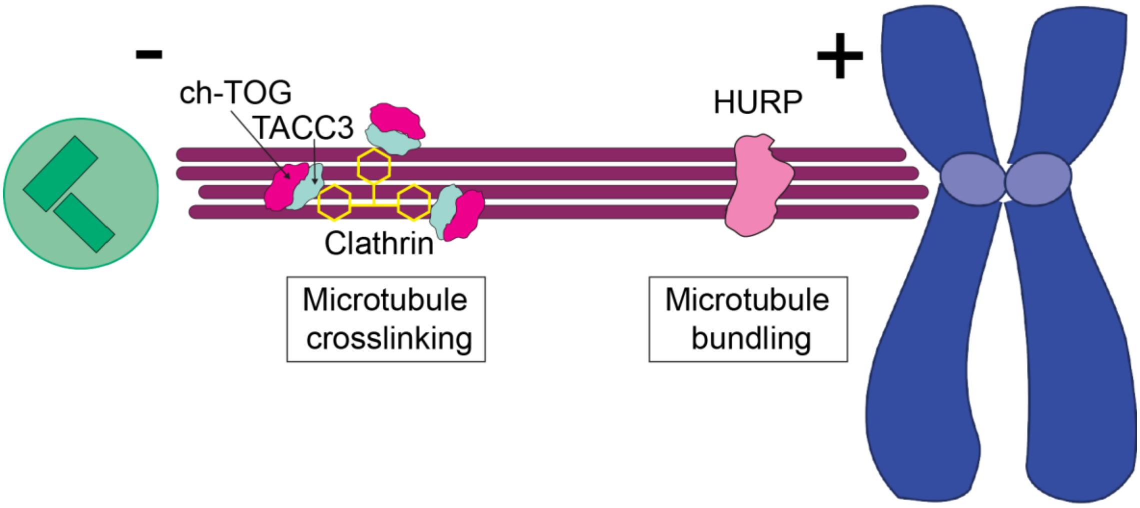

Figure 7. K-fiber structure. K-fibers are bundles of MTs that connect the kinetochore of the chromosomes (blue) to the spindle poles (represented by the centrosome in green). The structure is stable thanks to the bundling and crosslinking of MTs mediated by proteins such as HURP and the complex formed by clathrin, ch-TOG and TACC3.

How the k-fibers form is not yet fully understood. The process can be divided in two steps: formation and maturation of the k-fiber. After NEBD, dynamic MTs emanating from the centrosomes grow and shrink in all directions, having the chance to reach the kinetochore. If a MT eventually gets captured and stabilized at the kinetochore by the Ndc80 and Ska complexes it can set the basis of a k-fiber. Likewise, the first MT of a nascent fiber can form at the kinetochore and get captured by the spindle pole *via* dynein/NuMA[63]. K-fibers mature by stepwise addition of new MTs. The new MTs may grow from the spindle pole region along the existing fiber. Kinesin-14 motors bind the plus-end of a MT and guide its growth along another MT. Equally, MTs can grow and swivel around the spindle pole and the chromosomes exploring the space. When getting close to another MT, they could bind each other via crosslinkers such as Ase1/PRC1, favouring the bundling. Finally, MTs in the k-fiber could also get “amplified”. MTs nucleated from pre-existing MTs grow at shallow angles and preserving the polarity of the mother MT, which is very convenient for the formation of a parallel bundle. Most likely, formation and maturation of the k-fibers occur simultaneously but how the whole process is orchestrated remains to be investigated. Indeed, after NEBD the cell only needs 15-20 minutes to establish the metaphase plate. This could only be explained as a result of the simultaneous work of both routes in mammalian cells.

Although kinetochores can bind up to 20 MTs in HeLa cells, low occupancy at kinetochores permits bipolar spindle formation and satisfaction of the spindle assembly checkpoint (SAC). However, partial occupancy increases the number of lagging chromosomes. Therefore, high occupancy would be important to provide robust merotelic attachments[64].

c) Dynamics

During metaphase, k-fibers show a remarkable dynamic behavior. K-fibers in metaphase undergo poleward flux. Tubulin heterodimers added at the kinetochore move constantly poleward as tubulin disassembles at the minus-ends (Figure 8 A). As a result of the poleward flux, even when the length of the fiber remains constant the subunits “flux” poleward through the k-fiber[65], which implies that both plus-end and minus-end dynamics are tightly coordinated. Flux is driven mainly by two activities: polymerization and depolymerization. At the plus-ends, CLASP proteins promote incorporation of tubulin dimers into the k-fibers. CLASP recruitment to the k-fiber plus-ends is also supported by EB1[66]. At the minus-ends, members of the kinesin-13 family of depolymerases, namely kif2a and MCAK promote the disassembly of tubulin subunits[66,67] (Figure 8 B). Additionally, MTs must translocate towards the spindle poles. Motor proteins such as Eg5 are known to transport MTs poleward[68]. The functionality of poleward tubulin flux has always been under debate. What is clear is that both MT polymerization and depolymerization generate forces[69]. Thus, flux provides the force to align and move chromosomes in the metaphase plate and is also fundamental to make the metaphase spindle mechanically stable. In anaphase, both plus and minus-end depoymerize to promote chromosome segregation.

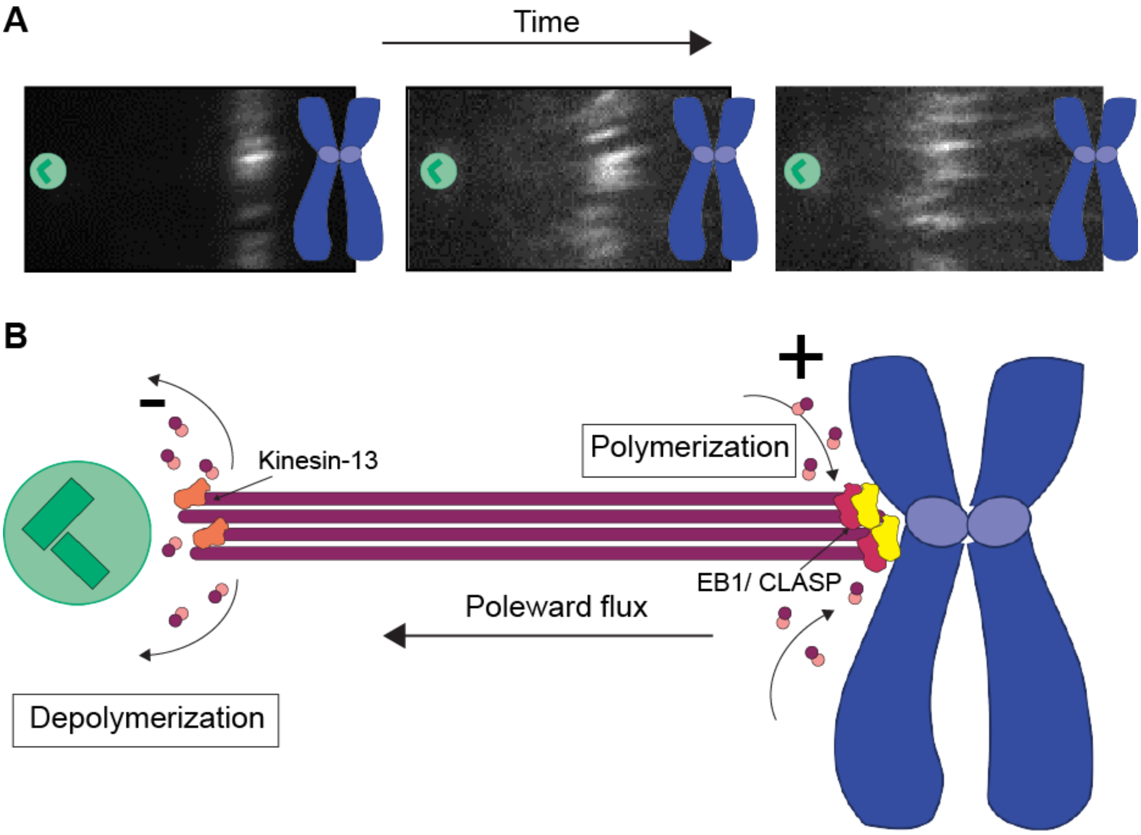

Figure 8. K-fibers undergo poleward flux in metaphase. A) Tubulin is transported poleward in the mitotic spindle. Snapshots at different time-points of a photoactivated tubulin in a metaphase spindle. Over time, the patch of activated tubulin moves from the spindle midzone to towards the spindle poles (adapted from[70]). B) The poleward flux is driven by two activities: net polymerization at the plus-ends and depolymerization at the minus-ends. EB1 and CLASP promote microtubule polymerization at the plus-ends while members of the kinesin-13 family disassemble tubulin subunits at the k-fiber minus-ends (adapted from[32]).

Interestingly, even if overall k-fiber plus-ends exhibit net tubulin incorporation in metaphase, when taking a snapshot of the plus-ends of an individual k-fiber, a mixture of polymerizing and depolymerizing MTs co-exist[24]. Indeed the individual MTs can alternate between phases of growth and shrinkage in order to satisfy the functions they perform. Initially, these dynamics allow for the “search and capture” in which kinetochores bind MTs thanks to the action of the motor proteins dynein and CENP-E. Once attached, the kinetochore-KMT interface remains highly dynamic in order to correct erroneous connections. KMTs can form monotelic, syntelic and merotelic attachments that have to be corrected for proper bi-orientation and chromosome segregation prior to entry in anaphase. For the error correction, the spindle relies on the kinase Aurora B. When interkinetochore distances are low, Aurora B phosphorylates the Ndc80-complex, one of the big protein assemblies involved in chromosome attachment. This phosphorylation promotes KT-MT detachment for error. In this context, depolymerization by kinesin-13 helps to dettach the wrong connections and polymerization favoured by CLASP/EB1 proteins promotes the binding to a new kinetochore. Additionally, chromosomes undergo oscilliations during metaphase, in which one sister chromatid associates with depolymerizing MTs while the other attaches elongating MTs. These oscillations facilitate chromosome alignment and congression. Finally, chromosome segregation is driven in anaphase by plus-end (and minus-end) depolymerization ("Pac-Man")[71]. While undergoing such complicated cycles of depolymerization and polymerization, KMTs have to remain properly connected to the kinetochores. For this purpose, kinetochores are formed by big protein assemblies (> 100 proteins) such as the Constitutive Centromere-Associated Network (CCAN) and the Knl1-Mis12 complex-Ndc80 complex (KMN) network[72]. The Ncd80 complex recruits Ska1 to the kinetochore. Interestingly, Ska1 tracks both polymerizing and depolymerizing KMTs and therefore, allows the kinetochore to associate with dynamic MTs[73]. Additionally, CENP-E remains stably attached to the kinetochores and is flexible to move bi-directionally to track dynamic MTs tips[74] In turn, these associations permit the transduction of the energy from tubulin dynamics into power to move chromosomes[75]. All these mechanisms to promote end-on MT attachments and correct them are crucial for mitotic progression. When the kinetochores are not properly connected to the KMTs, they activate the SAC that prevents cell cycle progression[76]. The KMT plus-end dynamics are subjected to regulation by many protein factors locating in the proximity of the kinetochores that have been thoroughly characterized (reviewed in [71,75]). Additionally, plus-end dynamics are controlled remotely from the spindle poles. For example, HURP, a RanGTP regulated protein, accumulates on k-fibers depending on their length and stabilized their plus-ends. At the same time, centrosomes set the k-fiber length thereby controlling plus-end dynamics[77]. Therefore, it is clear that plus and minus-end dynamics cannot be uncoupled.

While MT plus-end dynamics have been extensively characterized, much less is known about the dynamic nature of the k-fiber minus-ends and their regulation. This is manly due to the lack of structural information. The minus-ends of the fibers are supposed to be mostly focused and anchored at the spindle poles, embedded in the PCM. The spindle pole area is a very dense region and lacks contrast. This complicates the visualization of the ultrastructure of the minus-ends. To date, there is no information on the k-fiber minus-end structure in the mammalian mitotic spindle. Because k-fibers undergo poleward fux, their MT minus-ends are believed to constantly depolymerize in metaphase. Members of the kinesin-13 family drive minus-end depolymerization. The contribution of the minus-end disassembly to the flux is important for spindle stability, and chromosome alignment in metaphase. Indeed, minus-end depolymerization solely generates forces that put the spindle under tension. Upon blocking of the MT plus-end dynamics specifically, the disassembly at the minus-ends alone leads to centromere hyperstretching, k-fiber shortening and an increased number of attachment errors followed by chromosome mis-segregation[78]. In anaphase, minus-end depolymerization helps to segregate chromosomes. Depolymerizing minus-ends are conveniently anchored at the spindle poles. Applying an external force directly on the k-fibers of the spindle can break them in the middle but not detach them from the kinetochores[79]. However, it is not known how the spindle poles can have such persistent connection with MT tips that are depolymerizing. Additionally, spindle poles are robust while suffering a continuous remodeling. Spindle poles can incorporate newly nucleated KMTs thanks to the concerted action of the dynein and NuMA. They also sustain opposite forces coming from the kinetochores[63,80]. Despite being fundamental for proper mitosis, k-fiber minus-end structure and dynamics are poorly understood. There are not many factors described to target specifically the k-fiber minus-ends and modulate their dynamics. To date, the MCRS1-KANSL-complex is the only factor that directly targets k-fiber minus-ends and fine-tunes their dynamics[81,82].

1.4. Microtubule minus-end targeting proteins in mitosis

The majority of MT minus-ends in the spindle are located at the poles. The spindle poles are the sites where spindle MTs are focused and bundled and where the proteins controlling MT minus-end nucleation, dynamics and interactions with other partners such as MT severing enzymes and MT depolymerases are concentrated. In fact, these minus-end targeting proteins (-TIPs) together with minus-end-directed motors mediate the formation of the spindle poles.

The –TIPs must recognize specific structural features at the minus-ends that depend on the dynamic *momentum* of the MT[83]. Here, it is important to remark that currently the minus-ends in the spindle are thought to be either stable or depolymerizing. Hence, -TIPs must bind to stable minus-ends or most likely, track depolymerizing ends in the spindle. How this specific interaction takes place is yet to be described for most of the –TIPs.

The main –TIP is the γ-TuRC ring complex, the major MT nucleator in the cell. It “caps” minus-ends and blocks the exchange of tubulin dimers. Minus-ends capped by γ-TuRC are therefore, stable (depicted in Figure 9 as a triangle). Nonetheless, its structure and activity were already discussed before (1.1 C).

To date, only three additional proteins or protein complexes have been shown to have specific autonomous minus-end binding activity. These are CAMSAP/Patronin, ASPM/Asp and the KANSL complex[84]. Other factors are candidates such as NuMA are potential candidates still to be investigated (Figure 9).

The Drosophila protein Patronin was the first protein shown to cap and stabilize minus-ends *in vivo*. Patronin localizes to MT minus-ends in interphase and in mitosis. In mitosis, in the absence of Patronin, minus-ends lose subunits through the action of the kinesin-13 MT depolymerase (Klp10A in Drosophila), leading to short and disorganized mitotic spindles. The same activity has been confirmed *in vitro.* Patronin binds autonomously to MT minus-ends and protects them from the depolymerization activity of kinesin-13[85] (Figure 9). However, so far, the effect of Patronin on dynamic MTs has not been investigated. Further studies, showed that the CC+CKK domain of Patronin is responsible for binding MT minus-ends and stabilizing them[86]. Nonetheless, to which specific population of the spindle MTs Patronin binds is not known. Recent studies show that Patronin dynamically binds MTs bundles within the spindle. The authors propose that Patronin can target free minus-ends of MTs generated from the non-centrosomal pathways and helps bundling and stabilizing them. This hypothesis remains to be validated with future experiments[87].

The members of the calmodulin-regulated spectrin-associated protein (CAMSAP) family are the homologues of Patronin in mammals. The family is composed of three members: CAMSAP1, CAMSAP2 and CAMSAP3 which have the ability to recognize the minus-ends of non-centrosomal MTs[84]. Most of the CAMSAP proteins play a role in interphase. In fact, CAMSAP2 and CAMSAP3 are removed from MT in mitosis by phosphorylation[88]. CAMSAP1 dynamically tracks MT minus-ends in mitosis but its depletion only causes a mild reduction of spindle length[80]. *In vitro* CAMSAP1 CKK globular domain binds in a unique site between two tubulin dimers at the inter-protofilament interface. The site coincides with the lattice transition from regular to curved[83]. CAMSAP1 autonomously tracks only growing MT minus-ends but it does not affect their growth rate[89]. In fact, the binding of the CKK domain to the lattice hinders the interaction of kinesin-13 which could provide mechanistic hints of the effect in spindle length as in the case of Patronin[83]. The functions of CAMSAP1 in mitosis remain to be further explored.

Another protein that can autonomously recognize dynamic MT ends and inhibit their growth is abnormal spindle-like microcephaly-associated protein (ASPM in; Asp in Drosophila). ASPM localizes to the spindle poles in mitosis where it participates in spindle organization, spindle positioning and cytokinesis[90]. It has not been described whether ASPM shows preferential binding to any MT population in the spindle. In drosophila, Asp localizes to the minus-ends of MT bundles and amplified MTs. It is fundamental for spindle pole focusing, likely due to its MT minus-end binding and crosslinking activities[91]. *In vitro* ASPM accumulates at growing minus-ends and inhibits their growth. The first three CH domains (CH1-CH3) are sufficient to target ASPM to the minus-ends[92]. Additional investigations have shown that ASPM forms a complex with the severing enzyme katanin, both *in vivo* and *in vitro*. ASPM and katanin localize to spindle poles in a mutually dependent manner and control MT disassembly (Figure 9). The mis-regulation of this process can lead to microcephaly[92]. Indeed, mutations in ASPM gene are the most common cause of autosomal recessive primary microcephaly (MCPH), a disorder characterized by a small brain and associated mental retardation[90].

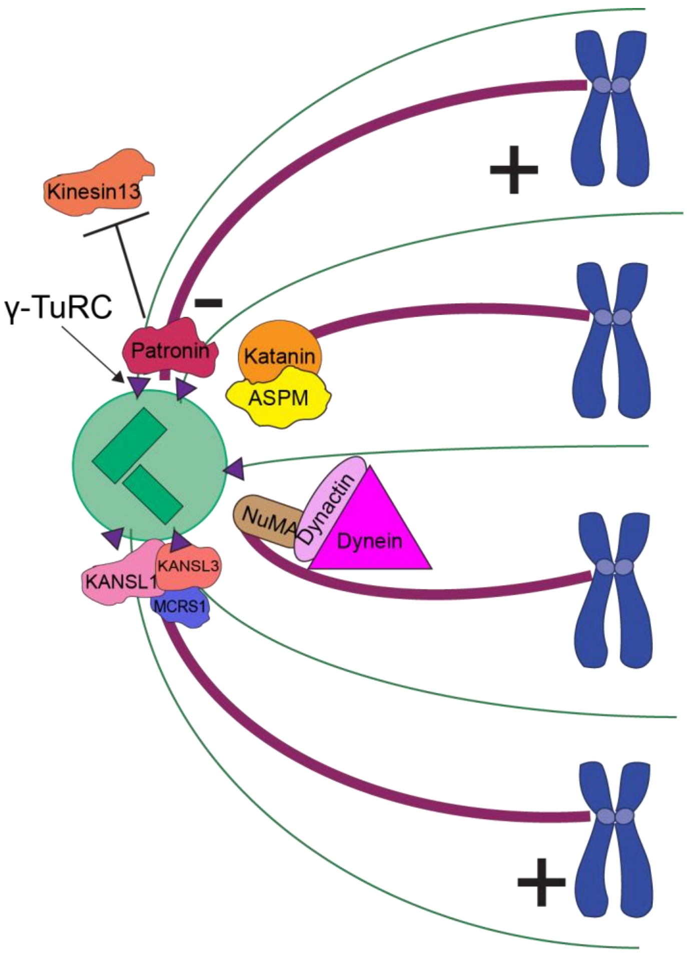

Figure 9. Microtubule minus-end targeting proteins in mitosis. The main minus-end binding protein is the γ-TuRC ring complex. Some MTs at the spindles poles are capped by this complex (represented as a purple triangle). The Drosophila protein Patronin binds MT minus-end in the spindle and stabilizes them against the action of the depolymerase kinesin-13. ASPM binds minus-end in the spindle in complex with katanin and regulate their dynamics. The motor complex dynein is targeted to the minus-ends through binding to NuMA. Whether NuMA directly targets minus-ends remains to be investigated. The MCRS1-KANSL-complex specifically binds k-fiber minus-ends in the spindle and regulate their dynamics.

At this point, it is interesting to mention that although minus-ends are supposed to be stable or mostly depolymerizing in metaphase, neither CAMSAP1 nor ASPM have been shown to track depolymerizing minus-ends *in vitro*. They rather target polymerizing ends. Indeed, the severing enzyme spastin is the only protein that has been demonstrated to track a depolymerizing end, the plus-end, *in vitro*[93]. The dynamics of the minus-ends *in vitro* are “slow” and the polymerization is followed by a rapid catastrophe. These technical issues could hinder the visualization of the tracking of a minus-end depolymerizing.

Nuclear mitotic apparatus protein (NuMA; Mud in Drosophila) is another protein associated to minus-ends. NuMA is nuclear in interphase and relocates to the spindle in mitosis in a RanGTP dependent manner[94]. In mitosis NuMA is important for spindle orientation, spindle bipolarity and pole focusing[95]. It is rapidly recruited to freshly generated minus-ends upon laser ablation of k-fibers in the spindle. The recruitment is independent of other known autonomous minus-end binding MAPs. In this way NuMA targets dynactin to minus-ends and localizes dynein activity serving as a cargo adaptor. Recent studies showed that the intrafragellar transport protein (IFT88) accumulates at k-fiber minus-ends and controls the binding of NuMA, thereby facilitating the incorporation of the k-fibers in the spindle[96]. All together they promote pole focusing[80]. Nevertheless, the origin of NuMA preference for minus-ends is currently not clear since it has not been shown to have direct affinity for minus-ends *in vitro*[96].

The members of the KANSL-complex, a chromatin modifier in interphase, have also been shown to preferentially bind MT minus-ends. In mitotic cells, MCRS1, KANSL1 and KANSL3 localize specifically to the minus-ends of k-fibers. Its depletion increases the depolymerization rate at minus-ends and compromises spindble stability and chromosome segregation. *In vitro*, KANSL3 and possibly KANSL1 target specifically minus-ends but their activity on dynamic minus-ends has not yet been described. Understanding how the KANSL-complex targets minus-ends and regulates k-fiber dynamics is the objective of this thesis and therefore, the KANSL-complex will be described in more detail in the chapter 1.5.

1.5. The KANSL complex

The KANSL-complex is an epigenetic regulator that controls the expression of many genes in interphase by regulating the compaction level of the chromatin. In mitosis, some of the members of the KANSL-complex relocate to the spindle where they fine-tune the dynamics at the k-fiber minus-ends. By having a dual-role the KANSL-complex coordinates both faithful expression and inheritance of the genome during cell cycle.

a) The KANSL-complex in interphase

The human KANSL-complex is composed of nine subunits. From these nine subunits, KANSL1, KANSL2, KANSL3 and PHF20 have only been identified as part of the KANSL-complex to date[97]. KAT8 (MOF), MCRS1, WDR5, OGT and HCF1 are part of the complex but also constituents of other complexes in interphase (Figure 10 B). The KANSL-complex is highly conserved and orthologues of the complex have been identified in many organisms: *D. melanogaster* (NSL-complex)*, C. elegans, M. musculus, D. rerio, A. Thaliana.*

From the nine members of the complex only KAT8 and OGT do have a catalytic function. KAT8 is a lysine acetyl transferase that marks histone 4 lysine 16 in the chromatin (H4K16ac). OGT (UDP-N-acetylglucosamine-peptide N-acetylglucosaminyltransferase) catalyzes the transfer of a single N-acetylglucosamine to a serine or threonine residue (Figure 10 C). Other members, mainly KANSL1, KANSL2 and KANSL3, are thought to act as scaffolds to stabilize the complex. PHF20 acts as the recruitment factor to bring the KANSL-complex to active promoters.

The structure of the KANSL-complex in interphase has been studied through structural and biochemical methods. KANSL1 is unstructured and believed to act as the major scaffolding protein within the NSL complex. KANSL1 binds KAT8 through its PEHE domain. It also interacts with PHF20 and MCRS1 via its N-terminal domain. At the same time, KANSL1 interacts with WDR5 and WDR5 binds KANSL2. However, it remains unknown how KANSL3, OGT and HCF1 are connected to the core complex. OGT has been proposed to O-GlcNAcylate KANSL3 and HCF1 and to be required for the stability of KANSL3[98] (Interactions are depicted in Figure 10 A for the human KANSL-complex).

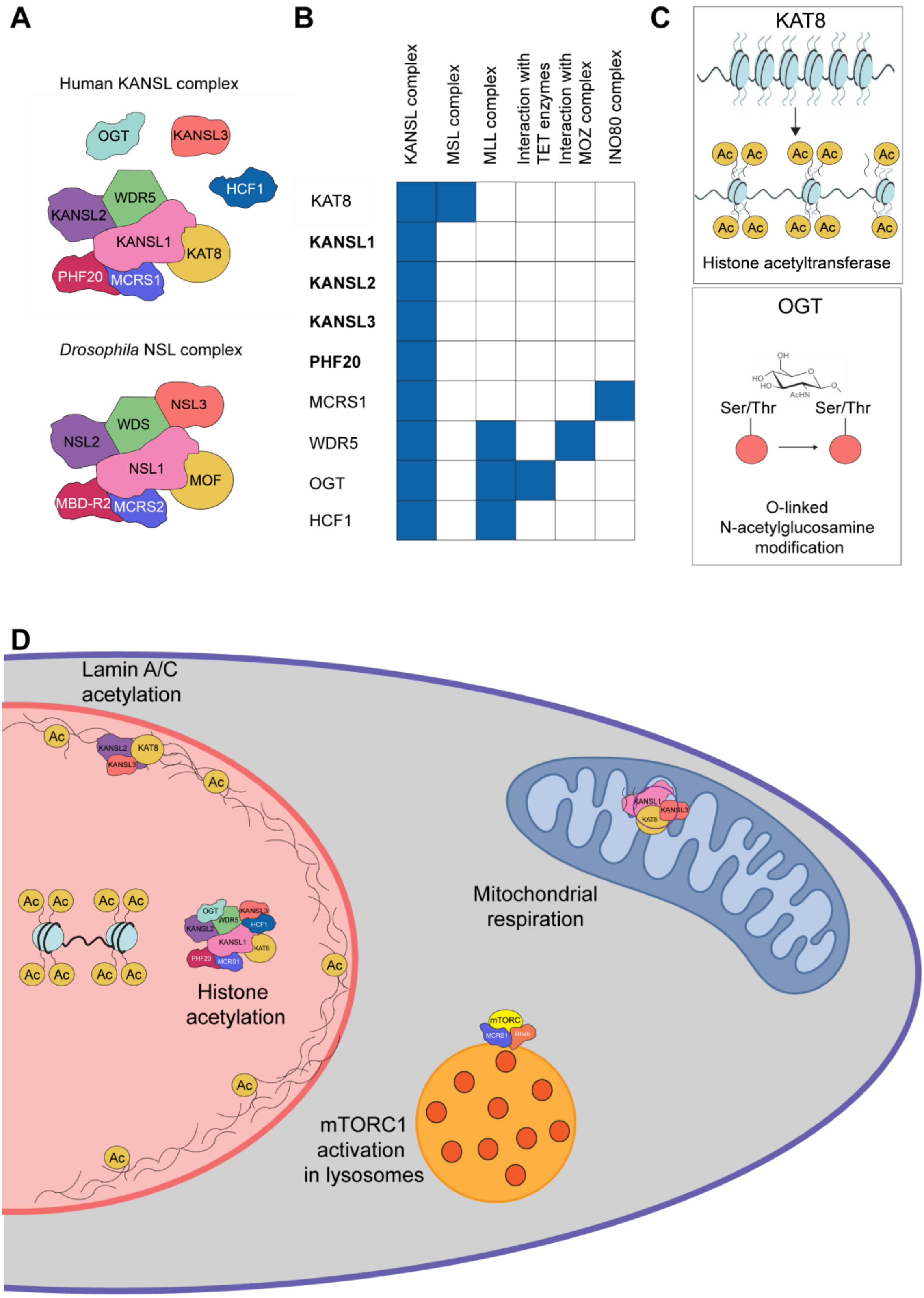
A
Human KANSL complex
OGT
KANSL3
HCF1
WDR5
KANSL2
KANSL1
KAT8
PHF20
MCRS1
Drosophila NSL complex
NSL3
WDS
NSL2
NSL1
MOF
MBD-R2
MCRS2
B
C
KAT8
Ac
Histone acetyltransferase
OGT
OH
HO
HO
O
AcHN
Ser/Thr
Ser/Thr
O-linked
N-acetylglucosamine
modification
D
Lamin A/C
acetylation
KANSL2
KAT8
KANSL3
Ac
OGT
WDR5
HCF1
KANSL1
PHF20
MCRS1
Histone
acetylation
Mitochondrial
respiration
KANSL1
KANSL3
KAT8
mTORC
MCRS1
Rheb
mTORC1
activation
in lysosomes

	KANSL complex	MSL complex	MLL complex	Interaction with TET enzymes	Interaction with MOZ complex	INO80 complex
KAT8	■	■				
KANSL1	■					
KANSL2	■					
KANSL3	■					
PHF20	■					
MCRS1	■					■
WDR5	■		■		■	
OGT	■		■	■		
HCF1	■		■			

Figure 10. The KANSL-complex in interphase. A) Components of the KANSL-complex. Top: members of the human KANSL-complex. Proteins are depicted taking into account the described interactions. It is not known how KANSL3, OGT and HCF1 connect to the other members of the complex. B) Bottom: ortologues of the KANSL-complex in *Drosophila.* The representation does

not take into account the interactions within the complex. B) Core versus shared components of the KANSL-complex. Core components are depicted in bold characters. KANSL1, KANSL2, KANSL3 and PHF20 are unique members of the KANSL-complex. Blue squares mark the complexes with whom other components are shared. C) Components of the KANSL-complex with enzymatic activity. KAT8 is a histone acetyltransferase. OGT catalyzes the transfer of a single N-acetylglucosamine to a serine or threonine residue. D) Components of the KANSL-complex play a role in a variety of functions in interphase Sme of the functions are depicted in the drawing (adapted from[99]).

Interestingly, it seems that the KANSL-complex is recruited to the chromatin in a specific order and that this order is fundamental for the stability of the complex. In *Drosophila* depletion of MCRS2 (MCRS1 in humans), NSL1 (KANSL1 in humans) or NSL3 (KANSL3 in humans) leads to reduced levels of the other complex members whereas depletion of MOF (KAT8 in humans) does not affect the stability of the other members. Besides, MCRS2 RNAi leads to lower levels of MOF, NSL1 and MBD-R2 at the chromatin. The hierarchy of recruitment suggests that the complex could assemble on the chromatin and then recruit the activity of the histone acetyltransferase MOF to a specific location. Experimental details providing insights on the recruitment of other members of the complex is yet not available.

The majority of roles of the KANSL-complex in interphase are chromatin-dependent. The binding and function of the complex have been investigated by chromatin immunoprecipitation (ChIP) followed by next-generation sequencing (NGS) and silencing experiments in *Drosophila* and mammalian cells. In *Drosophila* the NSL members mostly bind active promoters of housekeeping genes[99]. However, it is not clear if by targeting those promoters, the NSL-complex regulates the target genes. Some studies propose that depletion of the members of the NSL-complex affects the expression levels of most of its target genes by impaired transcription initiation, since it correlates with reduced levels of RNA polymerase II at gene promoters[100]. Whereas others find that in fact, only a defined subset of bound genes have their expression regulated by the complex[101]. Which role does the acetylation activity of MOF play in the regulation is also not clearly defined. Depletion of NSL-complex members does not lead to a bulk reduction in H4K16ac levels, so it is hypothesized that MOF acetylation could be more important in the context of the other complex it belongs to (Figure 10 B)[102]. Alternatively, it is speculated that MOF acetylation activity in the context of the NSL-complex could be addressed to chromatin regulators or the transcriptional machinery, which remains to be determined in the future.

In mammalian cells the members of the complex tend to localize to promoters of transcriptionally active genes as well. Some of these genes are housekeeping but the complex also targets developmental genes and enhancers in mouse embryonic stem cells (ESCs). Indeed, the binding of KAT8 and KANSL3 to the second group is lost in most differentiated cells. This binding appears to be important for proliferation [103].

Nonetheless, KANSL-complex functions are not limited to its binding to chromatin in interphase. For instance, KAT8, KANSL1 and KANSL3 have been reported in the mitochondria of HeLa cells. There, KAT8 localizes to the D-loop of mitochondrial DNA depending on KANSL3 to control the expression of respiratory genes (Figure 10 D). Downregulation of either KAT8 or KANSL1 in these cells leads to impaired mitochondrial respiration[104].

Recently, the KANSL-complex has been shown to help maintaining the nuclear architecture stability. Loss of KAT8, KANSL2 or KANSL3 leads to a stochastic accumulation of nuclear abnormalities, including blebbing and micronuclei, associated with genomic instability patterns. In this context, lamin A/C was identified as a substrate of KAT8 lysine acetyltransferase activity beyond chromatin (Figure 10 D). Mechanistically, loss of lamin A/C acetylation results in its increased solubility, defective phosphorylation dynamics and impaired nuclear mechanostability. Therefore, the nuclear lamina loses integrity and eventually the nucleus can break. Interestingly, the loss of lamin A/C acetylation also affects the epigenetic landscape within the nuclear abnormalities, leading to an enrichment of heterochromatin associated modifications[105].

Besides, some of the subunits have additional roles *a priori* independent of the complex. For instance, MCRS1 has been shown to be the essential link between the protein Rheb (Ras homolog enriched in brain) and mTORC1 activation. MCRS1 seems to maintain Rheb at the lysosome surface[106] (Figure 10 D). The same protein also engages in PCM transport through interactions with the motor protein dynein. The interaction between MCRS1 and the motor is critical for centriollar satellite formation and ciliogenesis in interphase[107].

Given the plethora of functions in which they are involved, KANSL proteins are essential in all species. Indeed, disruption of the respective genes in *Drosophila* is lethal for both, male and female flies at early larval stages, which led to name the complex as non-specific lethal (NSL)[100]. In humans, heterozygous mutations in KANSL1 underpin the Koolen-de Vries (KdV) syndrome, a severe developmental disorder which manifests with developmental delay, intellectual disability, facial dysmorphisms, low birthweight and a range of comorbidities. Furthermore, mosaic point mutations in KANSL2 locus which are predicted to induce splicing defects in transcripts have been related to severe intellectual disability. Additionally, deregulation of the KANSL-complex members KAT8, MCRS1 and KANSL2 as well as reduced levels of H4K16ac are reported in different cancer diseases[99].

Interestingly, the functions of the KANSL-complex are not restricted to interphase but some members of the KANSL-complex have been shown to be fundamental during mitosis.

b) The KANSL-complex in mitosis

After NEBD, nuclear proteins diffuse and are free to relocate to the mitotic spindle. This is the case of some of the members of the KANSL-complex. To date, MCRS1, KANSL1, KANSL3 and WDR5 have been shown to bind MTs in the spindle and control the proper segregation of the genetic material in mammals and or/in *Drosophila*[82,107–109].

MCRS1 contribution to spindle assembly was first identified in a genome-wide RNA interference screen of *Drosophila* S2 cells[110]. Initially under the gene name CG1135, MCRS1 was of particular interest due to its reported nuclear localization in interphase and its localization to the centrosome in mitosis[110], making of it a putative RanGTP-regulated SAF. Indeed, further experiments in mammalian cells showed that MCRS1 is nuclear in interphase and accumulates to the spindle poles from early mitosis, in a RanGTP-dependent manner as demonstrated in the *Xenopus laevis* egg extract system. Strikingly, MCRS1 localization is restricted to the minus-ends of k-fibers, which to date is a unique property[107] (Figure 11 A).

To investigate the function of MCRS1 in mitosis cells were silenced by RNAi. Interestingly, MCRS1-depleted cells undergo a significant delay in mitosis while maintaining the SAC activated, spending up to 8 hours while trying to assemble the bipolar spindle. Further experiments to gain insights into the role of MCRS1 in spindle assembly showed a marked defect in MT assembly around chromatin, similar to the loss of function phenotype of TPX2. Consistent with this phenotype, MCRS1 only localizes to the chromosomal MTs both in cells and in *Xenopus laevis* egg extracts, another unique feature that suggests that MCRS1 is involved in chromosomal MT assembly. MCRS1 depletion led to shorter and less stable k-fibers. In these cells, poleward flux is more rapid, which connects to a faster removal of tubulin subunits at the minus-ends. Taken together, all these characteristics indicate that MCRS1 targets k-fiber minus-ends to protect them against MT depolymerization[107,111] (Figure 11 C).

In this context, the depolymerase MCAK (KIF2C, kinesin-13) emerged as a possible counter partner of MCRS1. Indeed, MCAK silencing could rescue chromosomal MT assembly in MCRS1-depleted cells. Accordingly, experiments in *Xenopus laevis* in egg extract and *in vitro* showed that MCRS1 can counteract the activity of MCAK, most likely by competing with its binding at MTs. Therefore, MCRS1 could protect k-fiber minus-ends against MTdepolymerization[81] (Figure 11 E).

Recently published studies have related MCRS1 to other depolymerase of the kinesin-13 family, KIF2A. They find that MCRS1 interacts with KIF2A and promotes its recruitment to the spindle poles. Consistingly, depletion of MCRS1 leads to reduced levels of KIF2A in the poles, longer spindles and problems in chromosome alignment[112] (Figure 11 E).

The activity of MCRS1 in mitosis has been proposed to be regulated by phosphorylation through two different kinases: Aurora-A and Mps1. Aurora-A kinase phosphorylates MCRS1 in mitosis on the residues Ser35/Ser36. This phosphorylation does not affect MCRS1 localization but it is important for k-fiber formation and dynamics. Based on different experiments, it is proposed that at the onset of mitosis MCRS1 would be released by RanGTP to cap the nascent k-fibers that emanate from the chromosomes and protect them from depolymerization. In a second step, once k-fibers are fully formed, Aurora-A would phosphorylate MCRS1 and switch its activity towards the control of k-fiber minus-end dynamics[113,114]. Likewise, Mps1 phosphorylates MCRS1 on the Ser64/Ser65 sites. This phosphorylation is also not responsible for the specific localization of MCRS1 but it enhances the recruitment of KIF2A to the spindle poles and facilitates precise chromosome segregation[112] (Figure 11 G).

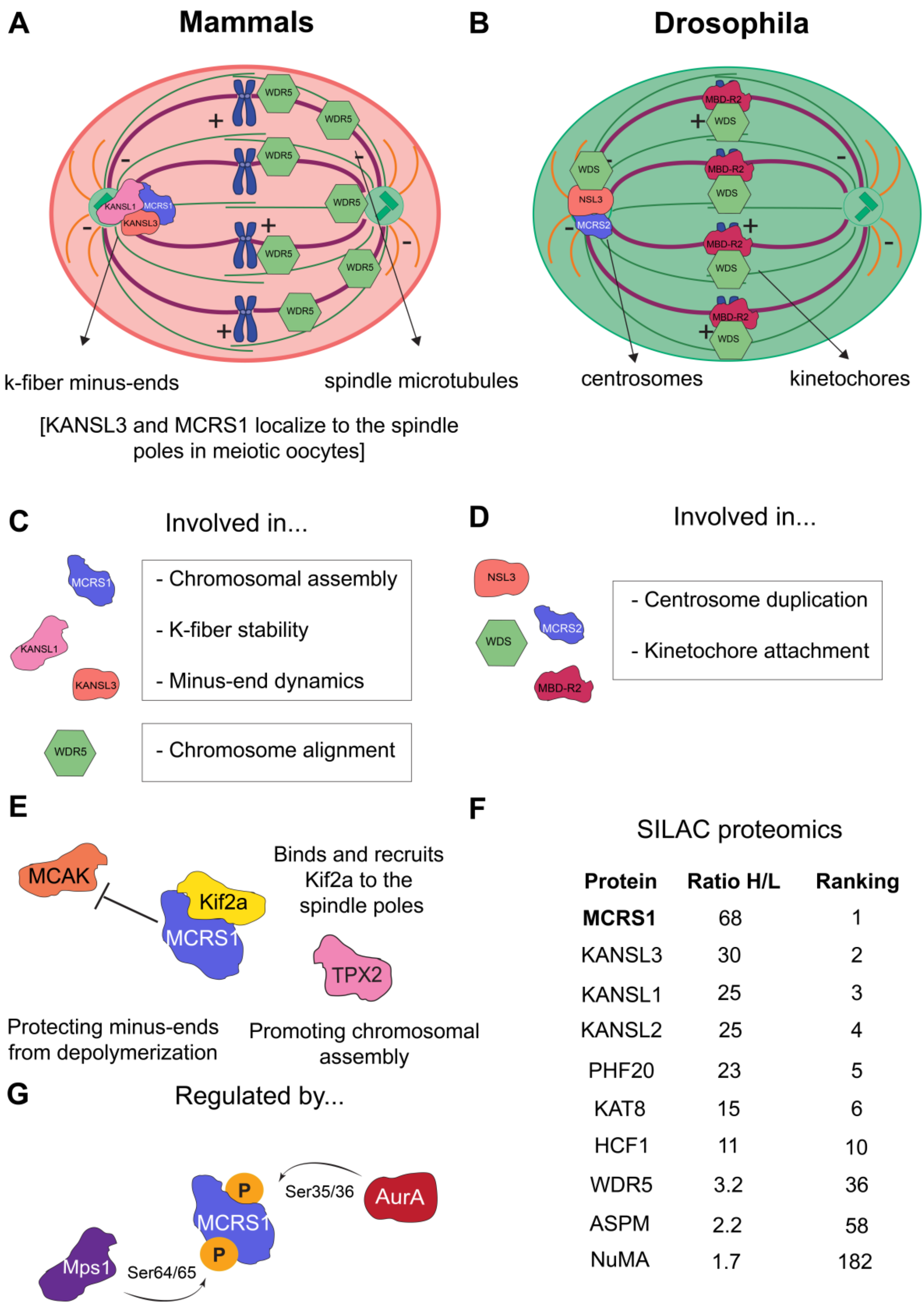
A
Mammals
WDR5
KANSL1
MCRS1
KANSL3
+
-
k-fiber minus-ends
spindle microtubules
[KANSL3 and MCRS1 localize to the spindle poles in meiotic oocytes]
B
Drosophila
MBD-R2
WDS
NSL3
MCRS2
centrosomes
kinetochores
C
Involved in...
MCRS1
KANSL1
KANSL3
WDR5
- Chromosomal assembly
- K-fiber stability
- Minus-end dynamics
- Chromosome alignment
D
Involved in...
NSL3
WDS
MCRS2
MBD-R2
- Centrosome duplication
- Kinetochore attachment
E
MCAK
Kif2a
MCRS1
Binds and recruits Kif2a to the spindle poles
TPX2
Protecting minus-ends from depolymerization
Promoting chromosomal assembly
F
SILAC proteomics
G
Regulated by...
P
MCRS1
Ser35/36
AurA
Mps1
Ser64/65

Protein	**Ratio H/L**	**Ranking**
MCRS1	68	1
KANSL3	30	2
KANSL1	25	3
KANSL2	25	4
PHF20	23	5
KAT8	15	6
HCF1	11	10
WDR5	3.2	36
ASPM	2.2	58
NuMA	1.7	182

Figure 11. The KANSL-complex in mitosis: mammalian cells and Drosophila. A) Localization of the members of the KANSL-complex in the mitotic spindle of mammalian cells. MCRS1, KANSL3 and KANSL1 localize specifically to the k-fiber minus-ends whereas WDR 5 localize all along the spindle MTs. B) Localization of different members of the NSL-complex in the mitotic spindle of *Drosophila* cells. NSL3 and MCRS2 localize to the centrosomes. MBD-R2 binds DNA and WDS localizes to centrosomes and kinetochores C) Functions in which the KANSL-complex is involved in the mammalian mitosis. D) Functions in which the NSL-complex participates in *Drosophila* mitosis. E) Mitotic partners of the KANSL-complex. MCRS1 counteracts MCAK in

mitosis. It also recruits Kif2a to the spindle poles. MCRS1 seems to interact with TPX2 to promote chromosomal assembly. F) SILAC proteomics. Mitotic partners of MCRS1 as revealed by SILAC-quantitative proteomics (adapted from[82]). G) The function of MCRS1 in mitosis is regulated by phosphorilation. Aurora A and Mps1 phosphorilate MCRS1 in different residues.

In vitro MCRS1 seems to bind along the length of MTs which raised the question as how it concentrates towards the poleward ends of k-fibers[111]. A SILAC-based quantitative proteomic approach revealed that MCRS1 in mitosis interacts with other members of the KANSL-complex[82,115] (Figure 11 F). At least two other subunits of the complex, KANSL3 and KANSL1, localize to the spindle poles in a RanGTP-dependent way. KANSL3 and KANSL1 are important for the chromosomal MT assembly and k-fiber stability. Both proteins regulate k-fiber minus-end dynamics. As a consequence, they are essential for spindle assembly and chromosome segregation. All these phenotypic features remind of those of MCRS1 described before. Moreover, KANSL3 was shown to be required for MCRS1 localization to the spindle poles. These data suggest the existence of a functional MT-binding subcomplex formed at least by MCRS1, KANSL3 and KANSL1 in mitotic cells. *In vitro* KANSL3 autonomously binds MT minus-ends of stabilized MTs. Therefore, KANSL3 may bind MCRS1 and recruit it to the spindle poles[82]. However, how this interaction takes place and the activity of the KANSL proteins on dynamic minus-ends *in vitro* have not yet been described[84].

Interestingly, MCRS1 and KANSL3 have been reported to localize to the spindle poles of meiotic spindle in mouse oocytes, cells lacking centrosomes. Although their specific role in meiosis has not yet been studied, this localization suggests that the part of the KANSL-complex may play a role in acentrosomal assembly and dynamics both in mitosis and meiosis[116].

In *Drosophila* the orthologues of MCRS1, Rcd5, and KANSL3, Rcd1, localize to the centrosomes in metaphase. On the contrary, the orthologue of PHF20, MBD-R2, binds DNA in metaphase whereas WDR5, Wds, is located both at the centrosomes and at the kinetochore (Figure 11 B). Despite the different localizations in mitosis, depletion of any of these four members of the complex leads to problems in centrosome duplication and chromosome alignment and segregation (Figure 11 D). The authors propose that these is primarily due to a reduced transcription of genes encoding centromere and kinetochore components. However, the fact that each protein binds a specific region of the spindle also implies some direct functions that remain to be further characterized[109].

In mitotic mammalian cells WDR5 localizes all over spindle MTs (Figure 11 A). Cells depleted of WDR5 display a clear delay in mitotic progression as a result of the problems to align the condensed chromosomes in the metaphase plate (Figure 11 C). In the same study, WDR5 has been shown to directly interact with and recruit the depolymerase KIF2A to the spindle poles, thereby controlling the chromosome alignment. It does so in the context of the MLL-complex, as it requires its interaction with MLL[108].

Objectives

Objectives

2. Objectives

1) To obtain structural insights on the k-fiber microtubule minus-ends by electron tomography.

2) To determine the impact of the MCRS1-KANSL complex on k-fiber assembly and MT minus-ends dynamics.

3) To unravel how the MCRS1-KANSL complex recognizes and binds specifically to the MT minus-ends and the consequences on their dynamics.

Results

3. Results

3.1. Structure of the k-fiber minus-ends in metaphase

The understanding of the structure and dynamics of the MT minus-ends is limited. In the mitotic spindle minus-ends are located at the spindle pole. The area is very dense and therefore, difficult to investigate. To our knowledge, there is no structural (and dynamic) information on the minus-ends of the mammalian spindle. Therefore, we set out to gain insights into the MT minus-end structure in the spindle, specifically that of the k-fibers To date, the best approach to reveal ultrastructural details on MT ends is electron tomography (ET). ET ensures good preservation of the structure when rapid freezing is applied and provides 3D information of the ends[117]. In collaboration with Robert Kiewisz from the group of Thomas Müller-Reichert (TU Dresden) we investigated the structure of k-fiber minus-ends of metaphase HeLa-Kyoto cells.

a) Tomographic reconstruction of k-fibers

We first checked that ¼ of the spindle that the tomograms of a ¼ of spindle could be representative enough to obtain solid data on the k-fibers based on full spindle tomograms obtained by our collaborator.

To reconstruct the k-fibers of metaphase spindles from HeLa-Kyoto cells the protocol was the following[118]. First, the mitotic fraction of the cells was selected by “shake-off” and cryo-immobilized by high-pressure freezing. The samples were processed for ET and screened by electron microscopy in the search for cells with chromosomes aligned in metaphase. Series of tilted views of the selected cells were recorded in an electron microscope (ET). Mitotic spindles were then 3D reconstructed (12 A).The full HeLa-Kyoto spindle shown in Figure 12 B consists of 4884 MTs.

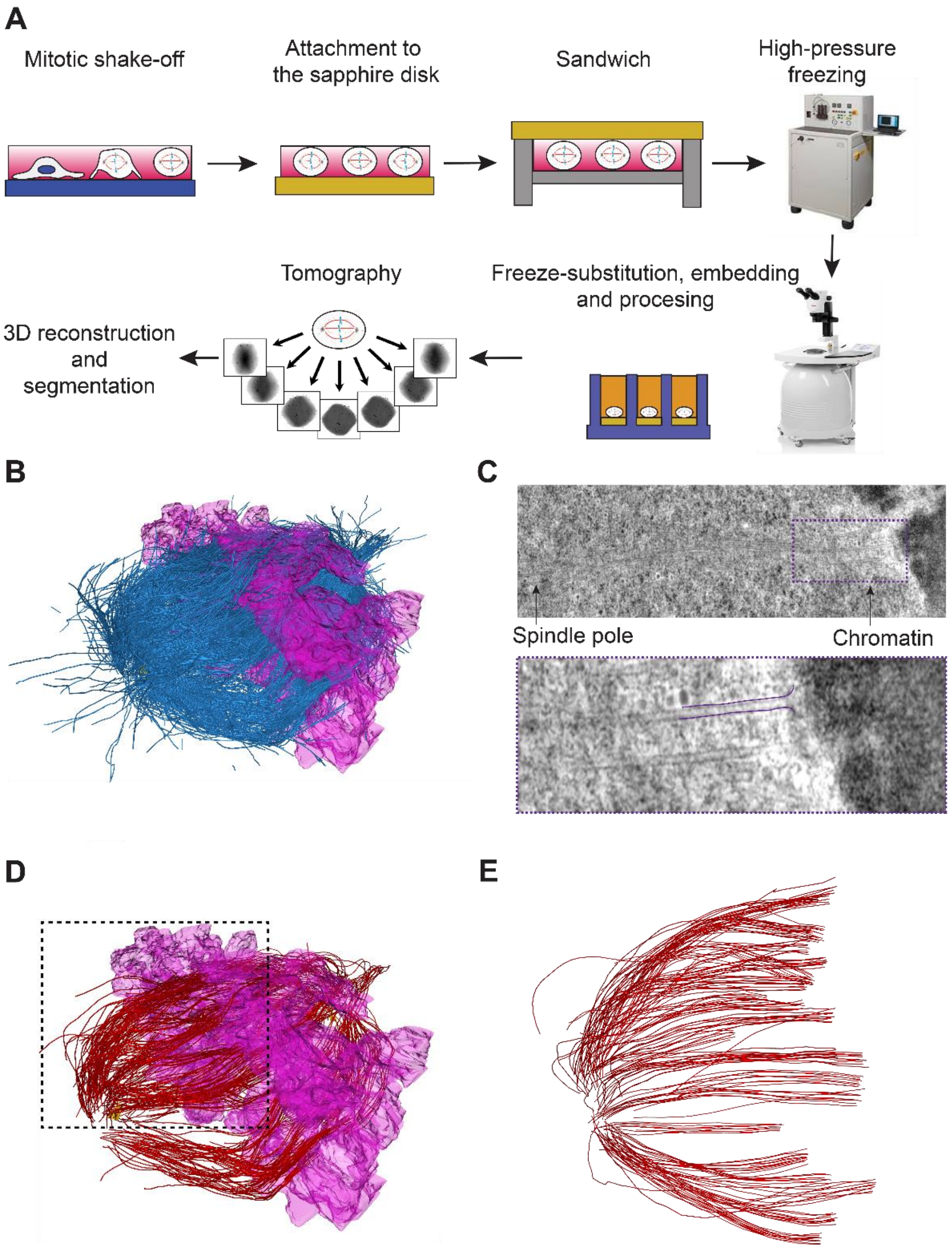
A
Mitotic shake-off
Attachment to the sapphire disk
Sandwich
High-pressure freezing
Freeze-substitution, embedding and procesing
Tomography
3D reconstruction and segmentation
B
C
Spindle pole
Chromatin
D
E

Figure 12. Tomographic reconstruction of the k-fibers. A) Representation of the process of ET of mitotic cells. B) Model of a full HeLa-Kyoto metaphase spindle after tomographic reconstruction. MTs are depicted in blue (N= 4884), chromosomes are in purple and one of the centriole pairs in yellow. C) Criteria to select the kinetochore MTs (KMTs). Electron microscopy image of part of a k-fiber. A MT in direct contact with the kinetochore is highlighted in purple. The electron dense dark grey region is the chromatin. D) Model of the k-fibers of a full metaphase spindle after tomographic reconstruction. MTs are depicted in red (N= 792), chromosomes are in purple and one of the centriole pairs in yellow. The dashed square represents the region selected for reconstruction in the actual experiments. In the pole-to-pole axis, the region spans from one of the spindle poles to the beginning of the KMTs of the other spindle pole. In the vertical axis, from below the centriole up to the top end of the spindle. E) Top view of the tomographic reconstruction of the ¼ of k-fibers reconstructed for our project. Having a full spindle from another cell as a reference, the model represents the region selected in D (The beginning of the second set of k-fibers is not shown in the model). The volume includes 205 KMTs organized in 22 k-fibers. The full reconstructions shown in B and D as an example belong to our collaborator Robert Kiewisz. The reconstruction shown in figure E is our data and the starting point of our analysis.

From the whole MT population, the subset of MTs belonging to the k-fiber was defined as those MTs in direct contact with the kinetochore of the chromosomes (from now on kinetochore MTs (KMTs)) (12 C). A full spindle, like the one in 12 B, has 792 KMTs, which represent ~14% of all MT population (Figure 12 D). To confirm that a ¼ of the spindle displays the same features as a full spindle, we divided the spindle in Figure 12 D in four quarters. Each quarter region corresponded to the volume contained in the dashed-line rectangle depicted in Figure 12 D. In the pole-to-pole axis, the region spans from one of the spindle poles to the beginning of the KMTs of the opposite spindle pole. Perpendicular to this axis, it extends from below the centriole pair to the top part of the spindle. In this region, we measured the interkinetochore distance and number of KMTs per k-fiber of each ¼ and compared it to that of the full spindle (Data shown in the annex, Figure A A and A B). We did not find significant differences among the quarters and the full spindle.

Thus, we went on to reconstruct a ¼ of volume of a HeLa-Kyoto cell following the same protocol for our characterization of the k-fiber MT minus-end morphology. As our interest was on the k-fibers, we only reconstructed the k-fibers for this new cell (Figure 12 E, the beginning of the second pair of kinetochores is not shown in the model). The reconstructed volume contains 22 k-fibers made out of 205 KMTs (Figure 12 E). The k-fibers were only considered if all the KMTs were fully inside of the volume.

To ensure that the reconstructed cell was in a metaphase stage, we used the interkinetochore distance as a stage marker. As the interkinetochore distance is an estimate of the stretch and the strech varies in the different mitotic stages, it serves as a readout of the mitotic state of the cell[119]. For a metaphase HeLa cell, we took as a reference an interkinetochore distance of 1.19±0.03 µm, measured after immunofluorescence of fixed HeLa cells[120]. For the measurement, we manually selected sister kinetochores by looking for the closest neighboring kinetochore. The center of each sister kinetochore was determined to be the median position of all the KMTs plus-ends associated with that kinetochore. The distance between the two sister kinetochores (interkinetochore distance) was calculated as the 3D Euclidean distance between the two paired centers[118]. The mean interkinetochore distance for the HeLa-Kyoto spindle is 1.158 ± 004761 µm, which is in agreement with the value measured in fixed cells. The pole-to-pole distance for this cell was 13.31 µm (measured from centriole to centriole). Having reconstructuted part of the k-fibers of a metaphase cell, we continued by investigating their minus-end morphology.

b) K-fiber minus-ends in metaphase are both, open and closed

To learn details about the k-fiber MT end morphology, we looked at the end structure obtained after 3D reconstruction. Previous studies *in vitro* and in cells have correlated MT end morphology with the dynamic state of MTs. Growing or shriking MTs appear to have flared ends whereas stable MTs usually have a "cap-like" structure at their tips. Thus, as contradictory as it sounds, we can infer the dynamic nature of the MTs from a static picture. In other words, MT end morphology serves as a readout of dynamics.

In our case, after reconstructing the KMTs of a metaphase cell, MT tips were selected out of the MT length by segmenting automatically the filaments 2 µm away from their ends. A first qualitative classification revealed the existence of three different categories of MT morphologies: closed, open or undefined. Closed ends had a higher electron density at their tips as shown in 13 A. MTs classified as open had a flared structure at the ends as depicted in 13 B. Finally, undefined ends were those either not appearing complete in the tomogram or indistinguishable due to the lack of contrast in the specific region 13 C.

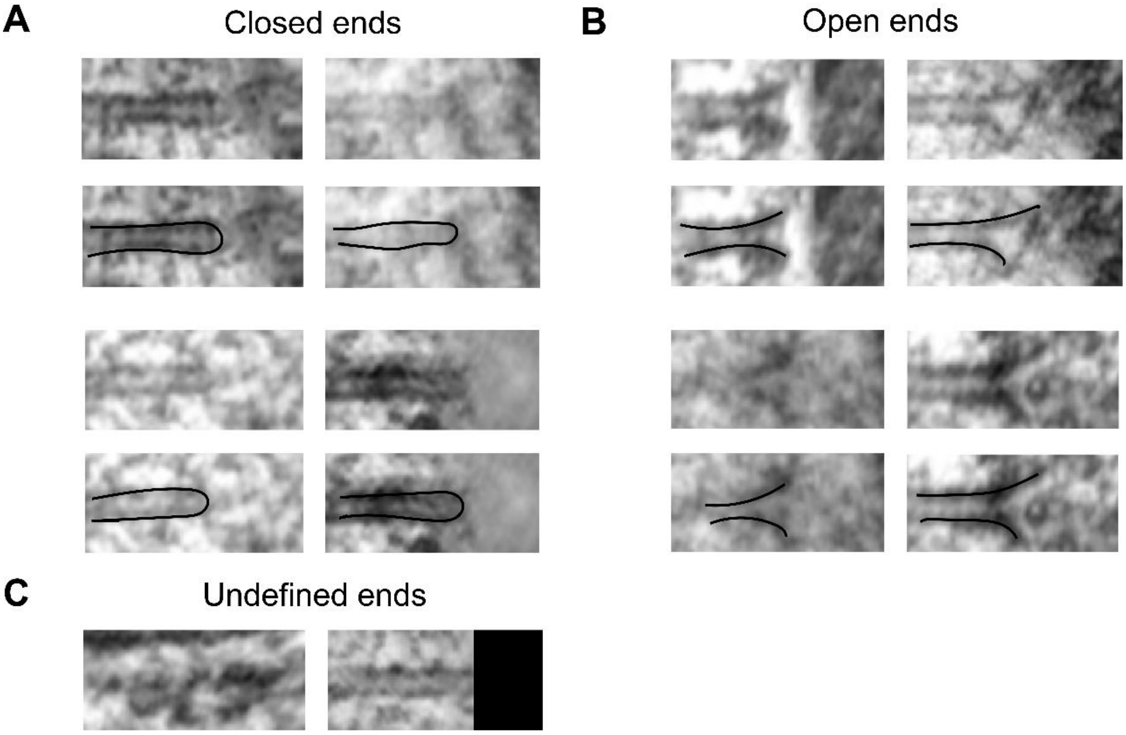

Figure 13. Microtubule end morphology as a readout of dynamics. A) Open end morphology. Representative examples of sheet-like (left), curved (middle) and blunt (right) ends, classified as opened. Open ends are assumed to be dynamic. B) Closed end morphology. Representative examples of "capped" ends, defined as closed and stable. C) Undefined ends. Ends indistinguishable (left image) or incomplete in the tomogram (right image) were classified as undefined.

It is important to mention that MT end classification is very complicated and time consuming. ET images have usually a low signal-to-noise ratio, specially at the area of the spindle poles, and MTs are very abundant in this area. Classifications are currently done manually although different machine learning approaches were applied to improve the process. The accuracy of the algorithms when compared to the manual classification of three agreeing experts was at maximum 82%, which is not more optimal than manual counting[121]. Taking this into account, we went on to quantify the proportion of the different subclasses of ends in the reconstructed quarter of the WT spindle. We performed a manual classification of the ends in duplicate. We reasoned that two independent "classifiers" would lead to more confident determinations. Additionally, the end annotation was blind. We only got to correlate the location of the MT end in the spindle and its morphology after having done the classification. Next, we determined MT polarity to identify plus and minus-ends. In a single KMT, the plus-end was assumed to be the one in direct contact to the kinetochore (Figure 12 C) and the other MT end was defined as the minus-end. A splines mathematical model with random effects was used to combine the measurements of the two observers and to estimate the proportion of open ends at a certain position depending on the distance to the spindle pole (relative distance). The unclassified ends were discarded from this analysis and therefore, the proportion of open ends was calculated only taking into account the total population of open and closed MT ends.

For the WT quarter cell we manually assigned 410 MT ends, 205 of which correspond to the minus-ends. We discarded 41 ends classified as undefined (20%). The models shown in Figure 14 A and B highlight the morphology of the minus-ends as assigned by one of the two "classifiers". Green circles correspond to open ends whereas pink circles show closed ends. Interestingly, from a first look it can already be observed that both types of ends coexist at the spindle pole, where the majority of the minus-ends are located. At position 0.0 which coincides with the position of the centrioles, 70% of the minus-ends are estimated to have an open morphology (credible interval (CI) between 37.35% and 91.44%). The percentage of open ends drops ~18% (CI= -25% to -8%) while moving away from the centrosome area (> 0.2) (so does the absolute number of minus-ends (the centrosome area was estimated as the region with a high concentration of MT minus-ends and set a relative distance of 0.2).

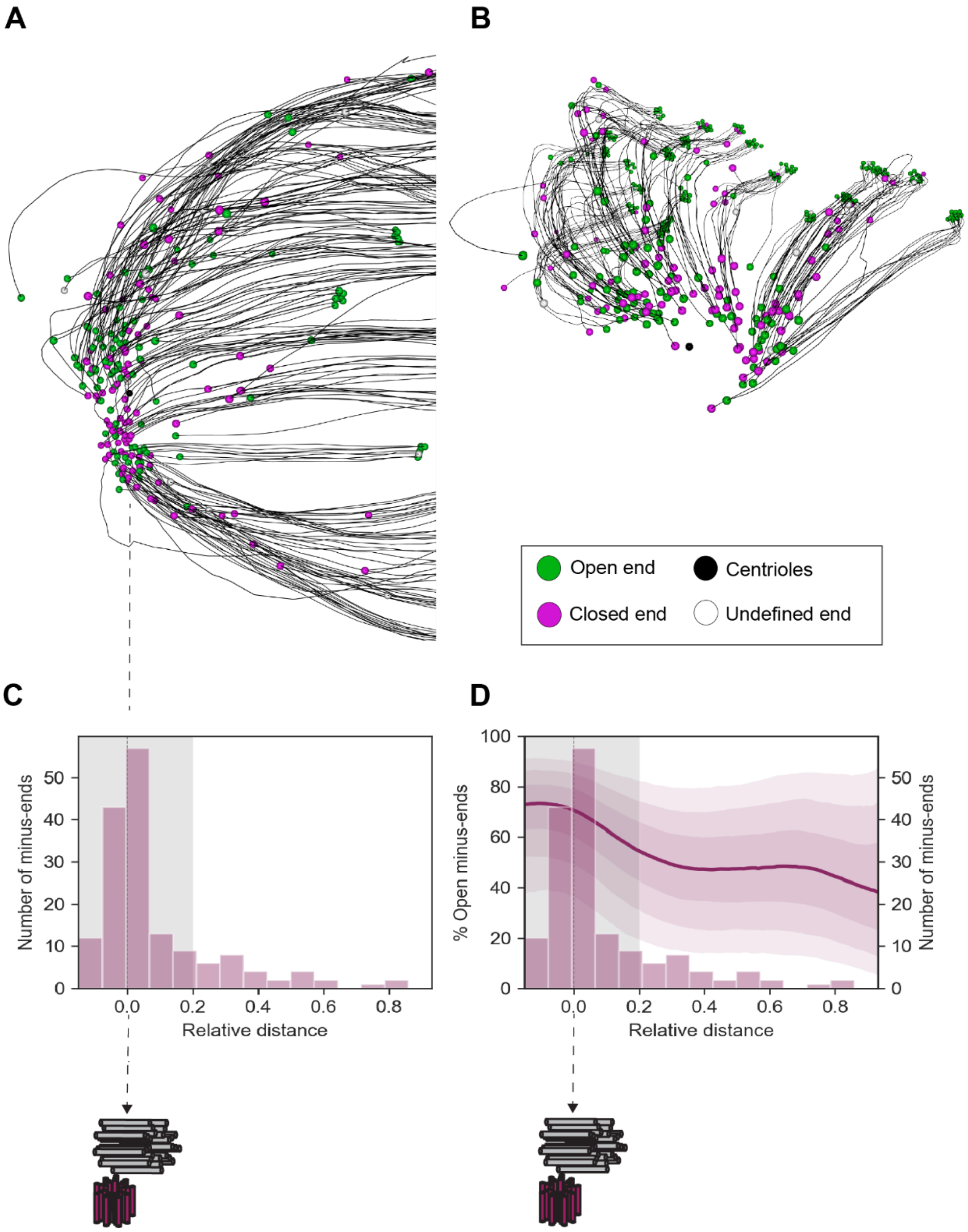

Figure 14. Characterization of the K-fiber minus-end distribution and morphology. A) Top view model of a tomographic reconstruction of the k-fibers in a WT cell (1/4 volume). MTs are depicted in black and MT ends, with a focus on the spindle pole, are represented by circles with different colors. Green circles represent open ends, pink closed ends and white circles undefined ends. The localization of the centriole-pair is shown as a black circle. The model shows the classification done by one of the two classifiers. B) Same as in A) but viewed from the spindle pole towards the midzone. C) Histogram representing the absolute number of minus-ends quantified at different relative distances. Undefined ends are not considered. The centrioles are located at position 0.0 and the kinetochores at position 1.0 relative to the centrioles. A) and C) are aligned along the relative distance (from 0.0 to 1.0). The shadow represents the limits of the centrosome area of influence. Total number of minus-ends = 164. D) Graphical representation combining the minus-end distribution histogram with the splines model estimating the percentage of open ends at different spindle positions. Around 70% of minus-ends are open in the spindle pole area (CI = 37.35% to 91.44%) versus ~47% in the region in between the spindle pole and the kinetochore (CI = 13.13% to 80.80%). The shadow represents the credible interval (CI) (there is 95% probability to find the true value within the interval). Total number of minus-ends = 164.

Consistently, the proportion of open minus-ends remains similar when only taking into account the ends in which both classifiers agree (Annex, Figure B). 77 MT minus-ends were labelled as open by both classifiers and 34 as closed. Specifically, at position 0.0, 75% of minus-ends were classified as open and 25 % as closed (Annex, Figure B). The last result give us confidence on the fact that we clearly detect both, open and closed MTends at the spindle pole.

Thus, having assessed that at the spindle poles there are both open and closed minus-ends, we wondered whether individual k-fibers would all had the same conformation (open or closed) or it would be more hetereogeneous. We performed a likelihood ratio test between models that included or ignored the k-fiber as a random effect. The model taking into account the k-fiber showed no significant increase in the explained variance compared to the model without k-fiber effects (p-value = 1). This suggests that the minus-end morphology of a KMT within the k-fibers is independent from the morphology of the minus-ends of the MTs in the same k-fiber. Therefore, both type of minus-ends co-exist also within the same k-fiber.

After characterizing the k-fiber minus-ends in the spindle, we conclude that they are not homogeneous and closed and open ends coexist, although there is a majority of open ends. Since MT structure serves as a readout of dynamics, we can also infer that there are both stable and dynamic MT minus-ends at the spindle pole. In addition, this is true in the context of an individual k-fiber. Interestingly, two distinct morphologies, open and closed, were described in the mitotic centrosome of *C.elegans*[20]. Here, we characterize for the first time the morphology of the k-fiber MT minus-ends in mammalian cells. Our data suggest that in each Kfiber, some MTs are dynamic whereas others may be more stable. This is unexpected since the tubulin flux occurring from the spindle midzone towards the spindle poles in metaphase involves the net incorporation of tubulin at the midzone and the net MT depolymerization and loss of tubulin at the spindle poles.

3.2. K-fibers and their minus-ends are altered in MCRS1-silenced cells

MCRS1, together with other members of the KANSL-complex, has been described to have unique properties. In mitosis, it localizes specifically to the k-fiber MT minus-ends and fine-tune their dynamics. Spindles assembled without MCRS1 undergo higher poleward flux. Besides, MCRS1 is essential for non-centrosomal MT assembly and k-fiber stability[81]. Having obtained structural insights on the morphology of the k-fiber MT minus-ends in a metaphase spindle, we decided to explore whether and how MCRS1 silencing could change the morphology and dynamics of the k-fiber MT minus-ends. Additionally, MCRS1 could serve as a “molecular tool” to deepen our understanding on k-fibers structure and dynamic regulation.

a) Spindle morphology is altered in MCRS1-silenced cells

As ET is a very time consuming technique, we were aware that we would not be able to reconstruct many MCRS1-silenced cells to average their phenotype as in regular immunofluorescence experiments. Therefore, we first looked at the spindles of silenced cells in the search for specific features that , in combination with high levels of silencing, could allow us to select downregulated cells before undergoing the reconstruction procedure.

To study the specific features of the mitotic spindles assembled in the absence of MCRS1, we transfected HeLa-Kyoto cells with specific siRNAs as previously described [81]. Next, we analyzed the efficiency of MCRS1-silencing after 72h by WB. MCRS1 levels were reduced to 46% in silenced cells (Annex, Figure CA). We also fixed the cells, performed immunostaining and observed them under a fluorescence microscope (Figure 15 A). Mitotic spindles could assemble in absence of MCRS1 but they had an altered morphology. The half spindle angle (Figure 15 B, top image) was visibly narrower in MCRS1-silenced cells compared to cells treated with scramble siRNA. In addition, the outer MTs in the spindle appeared to be more splayed out in the silenced cells (Figure 15 B, bottom image). We went on to quantify manually quantified both features, as indicated in Figure 15 B. The mean half spindle angle in siScramble cells was 86,34 ± 1,168, significantly higher than 73,09 ± 0,8201 in MCRS1-silenced cells (p-value < 0.0001 at 5% CI) (Figure 15 C Left graph). In the case of the MT angle, the mean was

151,4 ± 0,6822 in siScramble cells and 167,8 ± 0,8478 in silenced cells, significantly lower (p-value < 0.0001 at 5% CI) (15 C Right graph).

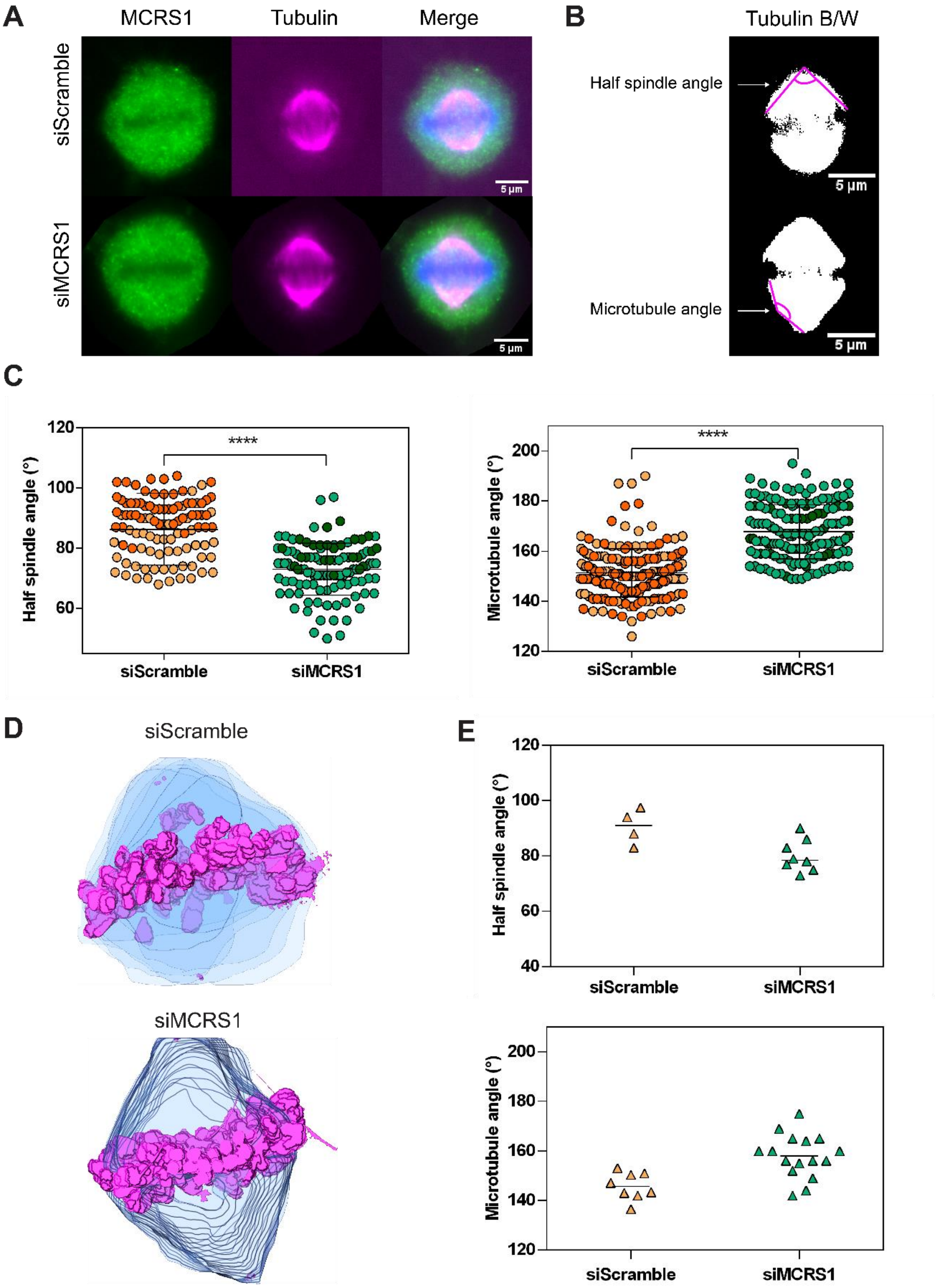
A
MCRS1
Tubulin
Merge
siScramble
siMCRS1
5 µm
5 µm
B
Tubulin B/W
Half spindle angle
Microtubule angle
5 µm
5 µm
C
Half spindle angle (°)
120
100
80
60
****
siScramble
siMCRS1
Microtubule angle (°)
200
180
160
140
120
****
siScramble
siMCRS1
D
siScramble
siMCRS1
E
Half spindle angle (°)
120
100
80
60
40
siScramble
siMCRS1
Microtubule angle (°)
200
180
160
140
120
siScramble
siMCRS1

Figure 15. Characterization of spindle morphology in MCRS1-silenced cells (legend next page).

A) Immunofluorescence staining of control and MCRS1-silenced cells. DNA is shown in blue, MTs in magenta and MCRS1 in green. MCRS1 staining can be observed as tiny spots at spindle poles in the control cell. Upon silencing, MCRS1 cannot be detected anymore. B) Black and White images of the control and silenced spindles from A). The magenta lines show the angles that were measured for the half spindle (top) and for the MTs in the outward position of the spindle (bottom). C) Spindles assembled in MCRS1-silenced cells have narrower half spindle angles and straight outer MTs compared to siScramble spindles. Left: scatter plot representing the quantification of the half spindle angle from immunofluorescence images. Measurements from two biological replicates are depicted by dots in different colors. N= 2 siControl n= 105; siMCRS1 n= 110. Bars, mean±SD; p-value < 0.0001 according to unpaired two-tailed t-test. Right: scatter plot representing the quantification of the MT angle from immunofluorescence images. Measurements from two biological replicates are depicted by dots in different colors. N=2 siControl n= 201; siMCRS1 n=161. Bars, mean±SD; p-value < 0.0001 according to unpaired two-tailed t-test D) Models of the mitotic spindle shape after EM screening. Chromosomes are shown in pink and MTs are in blue. F) Altered morphology in MCRS1-silenced spindles can be observed after EM acquisition. Top: scatter plot of the quantification of the half spindle angle after EM. Bottom: scatter plot of the quantification of the MT angle after EM.

After having characterized the specific features of MCRS1-silenced mitotic spindles by immunofluorescence, we validated if the same characteristics were recognisable in EM after screening of the spindles assembled in silenced cells. Since for this experiment we seeded a bigger volume of cells, after 48h they had reached confluency. Thus, we splitted and reseeded them. At 60h, we treated the cells again with the specific siRNAs. After 72h, we high-pressure froze the cells and processed them as previously described for EM (and ET) microscopy. We analyzed MCRS1 protein levels by WB. With the “double transfection” we reached 88% reduction in MCRS1 protein levels (Annex, Figure CB). Then, we acquired electron microscopy stacks of the different cells assembled in the scramble control and MCRS1 and estimated the volume occupied by the spindle (Figure 15 E). In this way, we could determine the half spindle and MT angles for the different candidates, as previously done in the immunofluorescence experiments (Figure 15 C). After quantifying several mitotic spindles for both conditions (Figure 15 F), we could see that the morphological pattern observed in immunofluorescence studies was also recognisable by EM. (Figure 15 E and F).

We chose for ET acquisition a cell transfected with a scramble siRNA, to discard an effect of the treatment, and a MCRS1-silenced cell.

b) The MT of K-fibers assembled in MCRS1-silenced cells have their minus-ends further away from the spindle pole

After ET, we reconstructed a quarter of volume of the k-fibers for the scramble and MCRS1-silenced cells as previously described. The resulting model is shown in Figure 16 A. We measured the distance between the sister kinetochore pairs. The mean of the interkinetochore distance for the control spindle was 1.023± 0.04965 µm for the cell treated with the siScrambled and 1.024±0.03432 µm for the MCRS1-silenced cell. These values are in the range of expected values for a metaphase cell. Besides, we did not find significant differences between to two of them (p-value > 0.05 at 95% CI). To discard the possible effect of the transfection reagent we also compared statistically the mean interkinetochore distance previously calculated for the HeLa-Kyoto spindle to that of the siScramble spindle. We again did not find significant differences (p-value > 0.05 at 95% CI) (Annex, Figure D). These results suggest two things. On one hand, we are confident that the spindles we reconstructed were all in metaphase. On the other hand, the transfection of the cells had no consequences on spindle morphology. The scramble cell had a pole-to-pole distance of 13.41 µm and the MCRS1-silenced cell of 15.41 µm.

We could clearly recognize similar morphological features in the reconstructed spindles to those observed by immunofluorescence. The k-fibers in the MCRS1-silenced spindle appeared more stretched compared to those in the scramble (and control) spindles (Figure 12 F and Figure 16). While the k-fibers in the siScramble cell are more rounded at the spindle pole, the k-fibers assembled without MCRS1 appear to be under a higher tension. A higher tension in the k-fibers could indicate higher pulling forces on the k-fibers, in agreement with previously published data[81]. However, for this specific cell, it did not translate into a “stretching” of the sister kinetochores.

A new characteristic feature we could only observe after tomographic reconstruction is the minus-end displacement from the spindle pole in the spindles assembled without MCRS1. When looking at Figure 16 A, in the control cell (left), the centriole pair is embedded within the mass of MT minus-ends. In the MCRS1-silenced cell (right), there is a gap between the centrioles and the end of the MTs. To quantify this observation, we made “bins” at different relative minus-end distances and counted the number of minus-ends in each bin for each condition, siScramble and siMCRS1. We also included the control spindle previously characterized. It is important to mention that the relative position on the pole-to-pole axis (centriole localization 0.0) to the kinetochore (1.0) was normalized to be able to compare the distribution of the minus-end positions in the three different conditions.

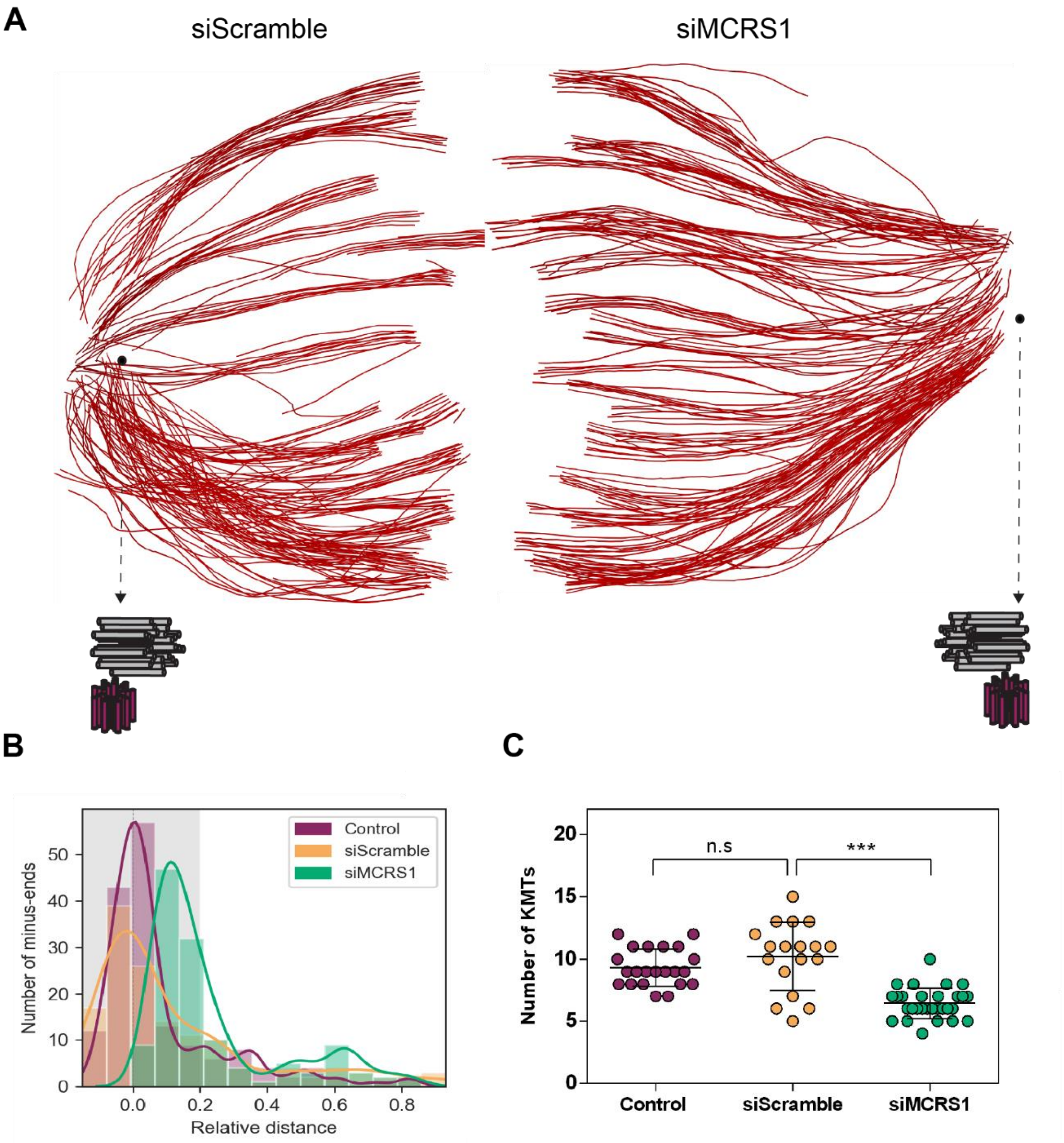

Figure 16. Tomographic reconstruction of k-fibers assembled in the absence of MCRS1. A) Top view model representing the tomographic reconstruction of the k-fibers of a siControl (left) and a siMCRS1 spindle (right). The k-fibers in the silenced cell appear to be more stretched than those in the control cell. B) Histogram representing the absolute number of minus-ends at different relative distances from the centrioles (0.0). The line represents the gaussian kernel density distribution. The majority of minus-ends in the control and siScramble spindles are in the close proximity of the centriole-pair. In the MCRS1-silenced cell, the minus-ends are displaced from the centrioles. The shadow represents the limits of the centrosome area. Number of minus-ends: WT = 205; siControl = 184; siMCRS1= 187. C) K-fibers assembled without MCRS1 have less KMTs. Scatter plots showing the number of KMTs per k-fiber in the three different conditions. Measurements correspond to ¼ of spindle cell per condition. Control n= 22; siScramble n= 18; siMCRS1 n= 29. Differences in the number of KMTs per k-fiber were analysed using a Generalized Linear Model (GLM) with Poisson likelihood and log link function, using siMCRS1 and siScramble as covariates. The estimated average for the control = 9.32, for the siScramble= 10.22 and for the siMCRS1= 6.45. p-value < 0.001 (***). n.s = non-significant (p-value = 0.362).

In the Control and siScramble spindles (Figure 12 E, 16 B), the majority of minus-ends are located at position 0.0, which coincides with the centriole location. However, most of the k-fiber MT minus-ends in the MCRS1-silenced cell do not reach the centrioles but are away from them at a relative distance of 0.1. This area still belongs to the centrosome area region. In all three cases the number of k-fiber MT minus-end drops to values below 10 further away from the spindle pole (>0.2 – 1.0). Thus, the main difference in the position of the k-fiber MT minus-ends at the spindle poles is within the centrosome area.

c) K-fibers in MCRS1-silenced spindles have less kinetochore MTs

We also counted the number of k-fibers and KMTs in the reconstructed volumes of the control and MCRS1-silenced cells. Strikingly, the siScramble spindle contains 20 k-fibers that altogether have 205 KMTs whereas the MCRS1-silenced spindle has 29 k-fiber with altogether 187 KMTs. The reconstructed spindle from the HeLa-Kyoto cell (control) had 22 k-fibers and 205 KMTs. The MCRS1-silenced spindle has overall less KMTs organized in a higher number of k-fibers, which could only happen with a lower number of KMTs per k-fiber, or at least in some of them.

Thus, we automatically quantified the number of KMTs per k-fiber. The control spindle has a mean of 9.32 KMTs per k-fiber, the siScramble has 10.22 KMTs and the MCRS1-silenced spindle has 6.45 KMTs (Figure 16 C). We analyzed the differences in the number of KMTs per k-fiber using Poisson likelihood with siScramble and siMCRS1 as covariates. We could see that indeed, the MCRS1-silenced cell has significantly less KMTs per k-fiber (p-value < 0.001) whereas we could not detect differences in the number of MTs between the control and siScramble spindles.

A lower number of KMTs could originate from a defect in MT nucleation or assembly or it could result from disassembly of some KMTs. In any case, the lower number of KMTs is in full agreement with previous reports showing that k-fibers in MCRS1-silenced spindles are less resistant to cold-treatment compared to control cells[81]. Besides, a reduced number of KMTs could potentially explain the higher “pulling forces” or stretch observed in the k-fibers assembled without MCRS1. At equal pulling forces from the spindle pole, holding a “lighter structure”, the k-fiber with less KMTs, would could generate more stretching.

After characterizing the k-fiber ultrastructure, we went on to investigate the morphology of the MT minus-end morphology in the MCRS1-silenced spindle.

d) K-fiber MT minus-ends in MCRS1-silenced spindles seem to have a higher proportion of open ends at the spindle poles

To learn details on the k-fiber minus-end morphology in MCRS1-silenced cells, we looked at the 3D reconstruction. As for the ¼ control HeLa-Kyoto cell, we classified the ends into three different categories: open, closed and undefined (Figure 13). Two “classifiers” did a manual annotation of the end morphology without previous information on the location of the specific MT end within the spindle. The polarity of the MT was determined as before, the plus-end of the KMT reaching directly the kinetochore was labeled as the plus-end and the other end was defined as the minus-end. A splines mathematical model with random effects was used to combine the measurements of the two observers and to estimate the percentage of open-ends at each position (relative position). We also added to the analysis the HeLa-Kyoto control cell characterized in the first chapter. The unclassified ends were discarded from this analysis and therefore, the proportion of open-ends was calculated from the total population of open and closed MT ends.

For the siScramble quarter cell we manually assigned 368 MT ends, 184 of which corresponding to the minus-ends. We discarded 42 ends classified as undefined (23%). In the siMCRS1 we classified 374 MT ends, 187 of which are minus-ends. 60 ends marked as undefined were not taken into account for the analysis (32 %). The models in Figure 12 A are a representation of the MT minus-end classification for the siScramble (left) and siMCRS1 (right) cells as done by one of the two “classifiers”. The mathematic analysis for the three cells is depicted in

Figure 17 B. In the region surrounding the centrioles, where the majority of the minus-ends are located in all three cells (Figure 17 B), the inferred percentage of open minus-ends for the siMCRS1 cell is 77.71% (CI = 44.50% to 95.30%) whereas the estimate for the siControl is 69.62% (CI = 37.92% to 90.34%). The control spindle is estimated to have a 66.58% of open ends (CI = 36.05% to 88.35%) These results suggest that the k-fibers in the MCRS1-silenced cells have a slightly higher proportion of open minus-ends at the spindle pole. Further away from the centrosome (relative distance > 0.2) less MTs are found and the proportion of open ends seems to drop to a mean of 47.16% in the control spindle (CI = 14.72% to 79.70%) and a mean of 50.35% in the siScramble (CI = 16.85% to 83.12). The percentage of open ends is even lower for MCRS1-silenced k-fibers at that interval, 36.38% (CI = 8.31% to 79.76%).

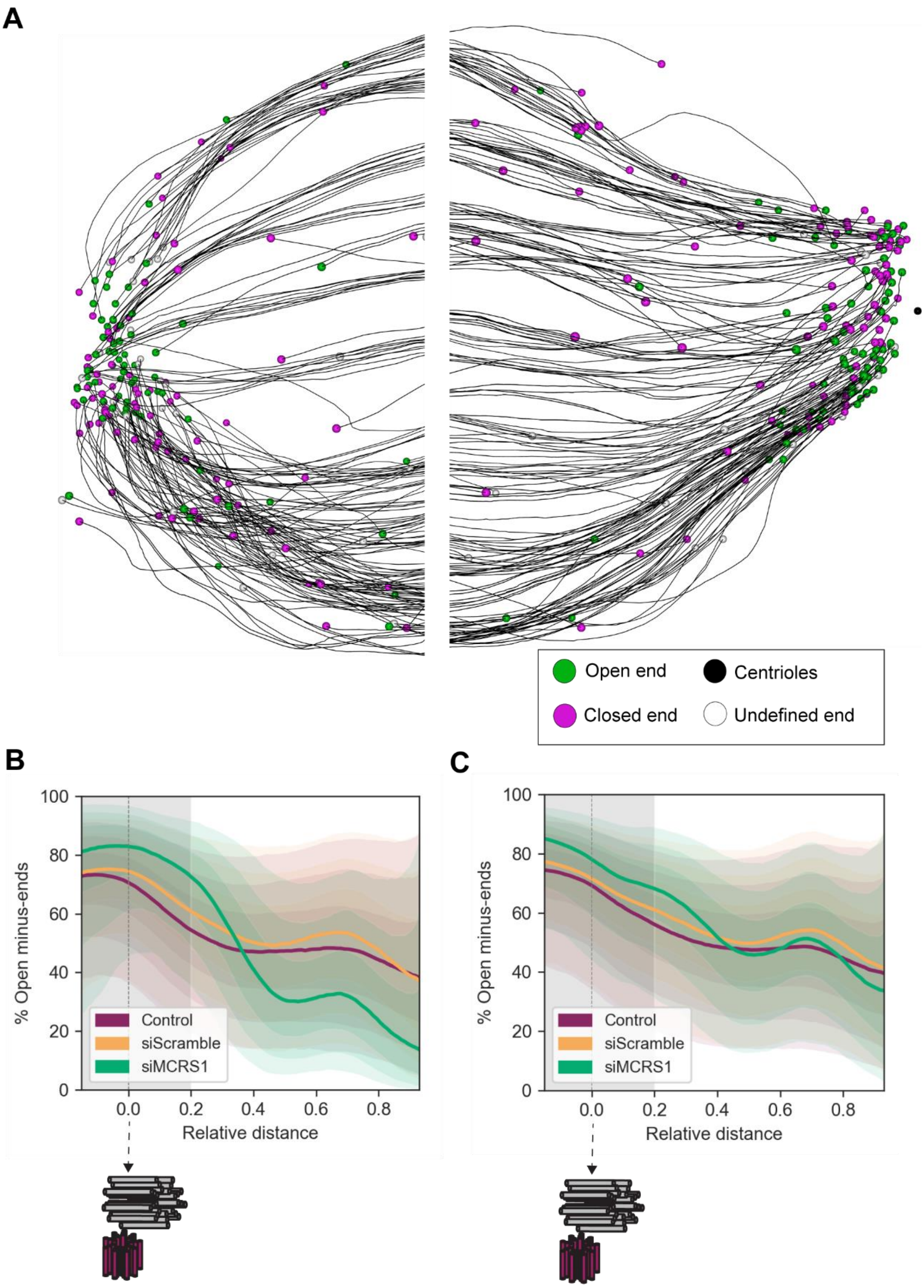

Figure 17. Characterization of the k-fiber minus-end morphology in MCRS1-silenced cells (legend next page).

A) Top view model representing the tomographic reconstruction of the k-fibers in a siScramble (left) and a siMCRS1 spindle (right). MTs are depicted in black and the morphology of their ends is represented by circles: green represents open ends, pink closed ends and white undefined ends. The localization of the centriole-pair is shown as a black ball. The models show the classification done by one of the two classifiers B) Graphical representation of the splines model estimating the percentage of open ends at different spindle positions (relative distances). Around 77.71% of minus-ends are open in the MCRS1-silenced k-fibers (credible interval 44.50% to 95.30%). The estimate for the siScramble is 69.62% (credible interval 37.92% to 90.34%) and for the control 66.58% (credible interval 36.05% to 88.35%) at the spindle pole region (< 0.2). These values drop to 47.16% in the WT (CI 14.72% to 79.70%), 50.53% in the control (CI 16.85% to 83.12%) and 36.38% in the siMCRS1 (CI 8.31% to 79.76%). The shadow around the line represents the credible interval (CI) (there is 95% probability to find the true value within the interval). Total number of minus-ends: Control= 164; siScramble= 142; siMCRS1= 127. C) Graphical representation of the splines model estimating the percentage of open ends at different spindle positions (relative distances) including three additional MCRS1-silenced spindles. The estimated percentage of open-ends in the siMCRS1 is 77.94% (CI = 49.95% to 93.30%) in the spindle pole region (< 0.2). The mean proportion of open ends drops to 49.44% (CI = 17.42% to 78.54%) at a relative distance >0.2. Total number of minus-ends: siMCRS1= 342.

Being aware of the limitations imposed by extracting data from only one cell per condition for such delicated classifications, we decided to reconstruct three additional MCRS1-silenced spindles. We verified that phenotypic features such as spindle altered morphology, number of KMTs per k-fiber or distance from the spindle pole were similar to those characterized before and proceeded to classify the end morphology as previously explained. We added the new data to the splines mathematical model (Figure 17 C).

The number of analyzed minus-ends in the MCRS1 silenced spindles was increased to 454, from which 112 were discarded as undefined (24.67%). The estimated percentage of open-ends was 77.94% (CI = 49.95% to 93.30%) in the spindle pole region (< 0.2). The mean proportion of open ends dropped to 49.44% (CI = 17.42% to 78.54%) at a relative distance >0.2, more in the line with the distribution observed in control and siScramble spindles.

The percentage of open ends at the spindle poles in the MCRS1-silenced cells is also slightly higher as compared to the two other conditions (control and siScramble). Additionally, it can be seen that the expected proportion of open ends decreases further away from the centrosomes, and the few MTs ends detected are more likely to be closed in all three conditions (it can be observed as a majority of pink circles in Figure 17 A). These data are interesting as it could indicate that those MTs may nucleate around the chromatin. Nonetheless, as the classifications are very complicated, the variability between “classifiers” generates wide credible intervals. In the future, it could be useful to include additional independent “classifiers” to obtain more certainty in the measurements and to increase the number of cells characterized.

Overall, these results indicate that the absence of MCRS1 from the spindle poles could affect directly the minus-end morphology at the poles and thus, their dynamics. This new phenotypic feature would fit with the idea of an in increase in the depolymerization rates and as MT depolymerization generates forces, could help explaining the higher tension in the spindle. As k-fiber minus-end dynamics cannot be uncoupled from plus-end dynamics, we decided to take a look at the plus-end morphology at the kinetochores.

e) K-fiber MT plus-ends have an open morphology at the kinetochore

K-fiber MT plus-end dynamics have been widely studied. KMTs plus-ends are directly engaged in the mechanism for correction of errors in MT-kinetochore attachment for the proper segregation of chromosomes. This is possible thanks to highly regulated dynamics. KMTs can switch between polymerization and depolymerization and to our knowledge MT plus end morphology has always been determined to be open (Figure 3, Introduction). We went on to classify plus-end morphology in the three conditions.

We annotated the same number of MT plus-ends as for the minus-ends. From the control, we classified 205 ends from which we discarded 14 as undefined (~7%). In the siScramble cell, 184 ends, 24 discarded (13%) and for the MCRS1-silenced spindle we classified 187 ends and removed from our analysis 26 (14%). Compared to the spindle pole region, where the majority of the minus-ends lie, the kinetochore area has a better signal-to-noise ratio and therefore, the percentage of ends classified as undefined is slightly lower.

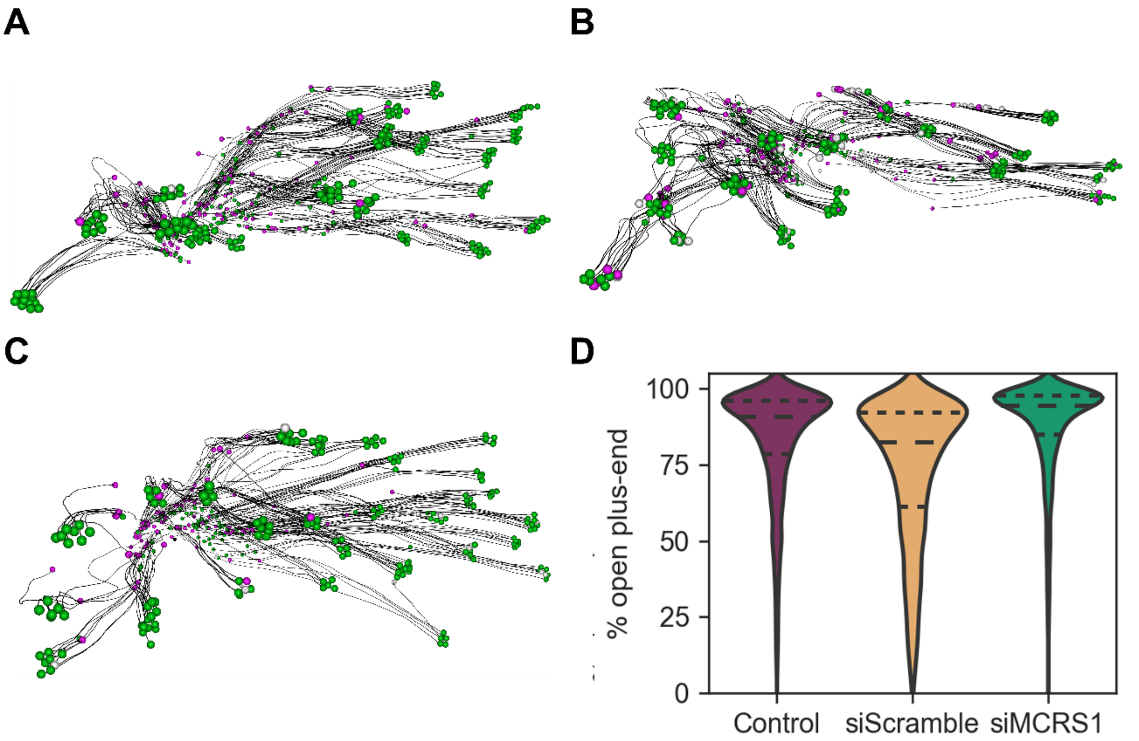

Figure 18. Characterization of the k-fiber plus-end morphology. At the kinetochore the majority of the KMTs have their plus-ends open. A) Front view of the control model with the end classification done by one of the two “classifiers”. B) Front view of the siScramble model with the end classification done by one of the two “classifiers”. C) Front view of the siMCRS1 model with the end classification done by one of the two “classifiers”. D) Graphical representation of the expected proportion of open plus-ends at the kinetochore. The majority of MT ends are expected to be open. For the WT the mean is 83.87% (CI = 33.47% to 98.84%), for the siControl = 74.04% (CI = 16.39% to 97.71%) and for the siMCRS1 = 88.16% (CI = 40.77% to 99.45%).

As it can be easily observed, in the models of the kinetochore region, the vast majority of k-fiber plus-ends are labelled as green, meaning open (Figure 18 A, B, C). Indeed the mathematical model predicts high proportions of open ends in all three conditions (Figure 18 D). We can therefore, conclude that open ends are basically open in the three conditions.

3.3. *In vitro* reconstitution assays to investigate the targeting of the MCRS1-KANSL-complex to the k-fibers MT minus-end

The previous results suggest that the lack of MCRS1 impairs k-fiber structure and alters the proportion of open minus-ends at the spindle poles. Previous data also indicate that MCRS1 does so by localizing specifically to the k-fiber minus-ends in cells, probably together with other proteins from the KANSL-complex[82]. Additionally, now we know from our data that within the k-fiber, there are KMTs with open minus-ends, probably dynamic, and closed ones, probably less dynamics or stable. Therefore, considering this information, we wondered how the MCRS1-KANSL-complex could associate such complex structure, either by binding dynamic, stable ends or both types of ends.

In vitro MCRS1 was shown to decorate taxol-stabilized MTs whereas KANSL3, and possibly KANSL1, had some preferential binding towards the MT minus-end. Besides, the localization of MCRS1 at the spindle poles was lost upon KANSL3 silencing, which suggested that KANSL3 could target MCRS1 to the k-fiber minus-ends in mitosis. To investigate further how the MCRS1-KANSL-complex could localize to the MT ends and how it could affect their dynamics, we performed *in vitro* reconstitution assays.

a) MCRS1, KANSL3 and KANSL1 expression and purification for *in vitro* TIRF experiments

As individually MCRS1, KANSL3 and KANSL1 were shown to directly interact with Taxol-stabilized MTs in spin-down experiments, we decided to work with these proteins tagged with a fluorescent label for TIRF microscopy. In this way, we aimed at understanding better their binding to MTs and their effect on MT dynamics.

KANSL1 and KANSL3 are big proteins, 121 kDa and 96 kDa respectively. The structure of a short fragment of KANSL1 (585–589) has been solved by chrystallography in complex with other proteins. However, more than half of its secondary structure is predicted to be a random coil (66.61%). In the case of KANSL3, the percentage of predicted random coil is 55%. MCRS1 is a 58 (or 52?) kDa protein and it is predicted to have a 62% of alpha helixes in its secondary structure. None, of the three proteins contains a canonical MT binding site in its structure. However, interestingly, KANSL3, contains 5 SxIP motifs, 4 of them at its C-terminus. KANSL1 has one of these motifs. These short consensus motifs of serine any- amino acid- isoleucine mediate the binding to +TIPs proteins such as EB1(Figure 19 A).

Previous experiments revealed that KANSL1 and KANSL3 were not soluble after bacterial expression, fitting the predicted disordered secondary structure. MCRS1 can be purified soluble from bacteria but for our purposes, we used insect cells as the expression system of choice for the three proteins. MCRS1 was tagged with a mCherry at its C-terminus for TIRF imaging and KANSL1 and KANSL3 with a mGFP: In all three cases, the proteins were also tagged with a purification tag containing 10 histidine residues, a zz-tag and a TEV-cleavage site at their N-terminus (Figure 19 A).

All three protein were expressed in insect cells. Next, we purified them using zz-tag affinity, TEV cleavage and size exclusion chromatography in a one-day protocol (Figure 19 B).

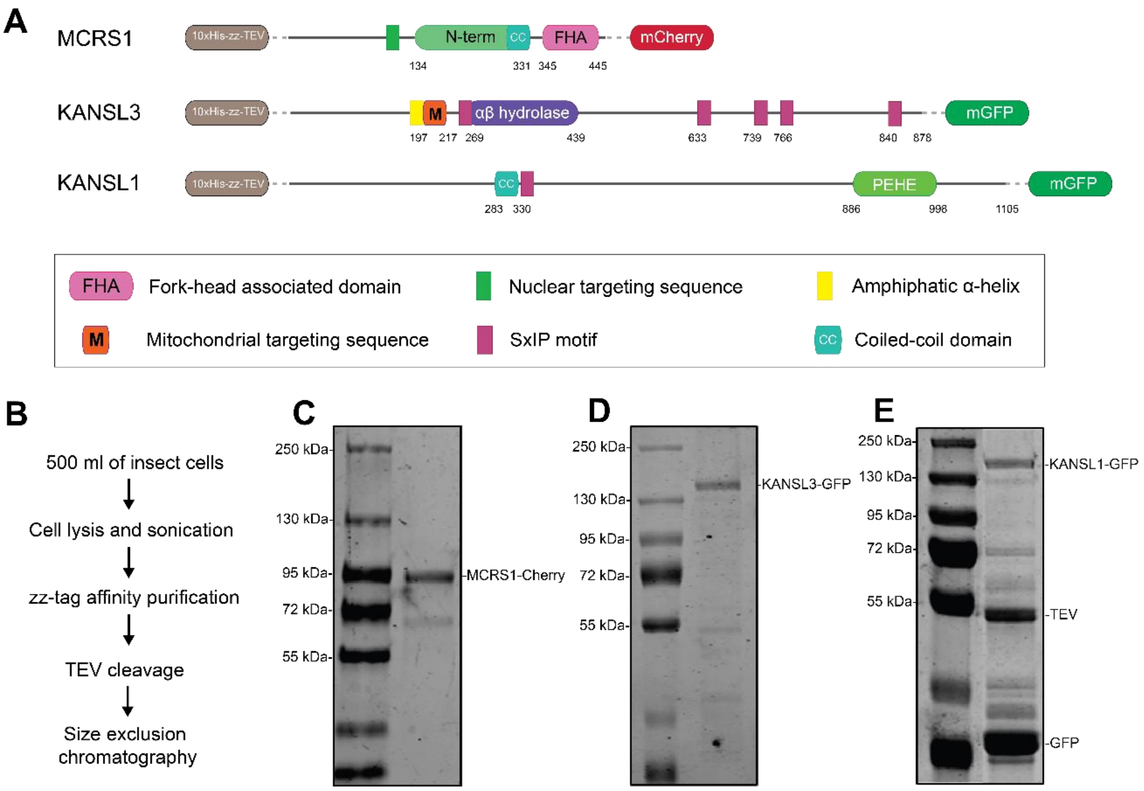
A
MCRS1
10xHis-zz-TEV
N-term
CC
FHA
mCherry
134
331
345
445
KANSL3
10xHis-zz-TEV
M
αβ hydrolase
mGFP
197
217
269
439
633
739
766
840
878
KANSL1
10xHis-zz-TEV
CC
PEHE
mGFP
283
330
886
998
1105
FHA Fork-head associated domain
Nuclear targeting sequence
Amphiphatic α-helix
M Mitochondrial targeting sequence
SxIP motif
CC Coiled-coil domain
B
500 ml of insect cells
Cell lysis and sonication
zz-tag affinity purification
TEV cleavage
Size exclusion chromatography
C
250 kDa
130 kDa
95 kDa
72 kDa
55 kDa
MCRS1-Cherry
D
250 kDa
130 kDa
95 kDa
72 kDa
55 kDa
KANSL3-GFP
E
250 kDa
130 kDa
95 kDa
72 kDa
55 kDa
KANSL1-GFP
TEV
GFP

Figure 19. MCRS1-Cherry, KANSL3-GFP and KANSL1-GFP structure and purification from insect cells. A) Sketch of the domains and motifs in MCRS1, KANSL3 and KANSL3 structure as well as the fluorescent tags added for TIRF imaging at their C-terminus and the purification tag at their N-terminus. The purification tag contains 10 histidine repeats, a zz-tag and a TEV cleavage site. B) Overview of the protein purification steps. C) InstantBlue stain of the SDS-PAGE of MCRS1-Cherry after size exclusion chromatography. D) InstantBlue stain of the SDS-PAGE of KANSL3-GFP after size exclusion chromatography. E) InstantBlue stain of the SDS-PAGE of KANSL1-GFP after TEV cleavage. KANSL1-GFP was not soluble after size exclusion chromatography.

The MCRS1-Cherry protein was purified soluble at an estimated concentration of 4 µM (Figure 19 C). KANSL3-GFP was also soluble (Figure 19 D) but more diluted (~ 0.78 µM) and most probably formed oligomers as detected by its FPLC elution profile. The peak had an estimated molecular 800 kDa. Different lysis buffers were used to try to increase the protein concentration without success. Besides, the protein always eluted as an oligomer independently on the buffer after FPLC. KANSL1-GFP was not soluble after size exclusion chromatography (Figure 19 E). It was initially difficult to get it soluble from insect cells and precipitated mostly to the cell pellet. Then, it degraded over the purification steps and was not detectable by InstantBlue SDS-PAGE after FPLC. Therefore, we could only work with KANSL3-GFP and MCRS1-Cherry TIRF experiments with MTs. As KANSL3 had shown preferential binding towards the MT minus-end in spin-down experiments, we started by studying if this property was maintained upon the addition of the GFP-tag.

b) KANSL3-GFP seems to preferentially bind one of the MT ends *in vitro*

To study the localization of KANSL3-GFP to the MTs, we performed localization assays on Tx-stabilized MTs by TIRF imaging. We carried out these assays in 2 mm-wide flowcells in which we could introduce step-wise different solutions and then, imaged the bottom of the glass surface thanks to a customized metal holder adaptor on the TIRF microscope. Within the flowcell, we immobilized rhodamine-labelled-Tx-MTs to a cover glass covered with anti- β-tubulin antibodies and added different concentrations of KANSL3-GFP together with an oxygen scavenger system to avoid photobleaching. Next, we imaged the glass surface by TIRF imaging which allows optical sectioning to reduce fluorescence background (Figure 20).

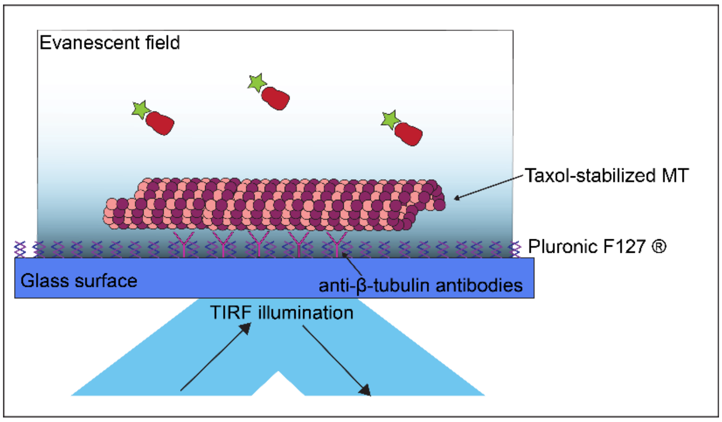

Figure 20. Schematic of TIRF setup for the localization assays on Taxol-stabilized MTs. Tx-MTs were immobilized on a sylanized glass surface blocked with Pluronic F127 ® via. anti-β-tubulin antibodies. Different concentrations of KANSL3-GFP were added to the channel together with an oxygen scavenger system. After incubation, the glass surface was imaged using a TIRF microscope[122].

After incubating KANSL3-GFP with Tx-MTs, we acquired images to study the localization of the protein on the MT lattice (Figure 21 A). We observed that at low protein concentrations (~39.2 nM) (Figure 21 A, first row), the protein rarely binds the MT lattice. Upon increasing slightly the protein concentration (~78 nM), some extra protein dots colocalize with MTs (Figure 21 A, middle row). However, when adding double protein concentration (156 nM) (Figure 21 B, last row), we observed more binding events along the MT lattice. At that higher concentration, we also observed some MTs having KANSL3-GFP associated with an extremity as indicated by the white arrows (Figure 21 B, last row). In order to analyze if this localization was preferential, we measured the KANSL3-GFP fluorescence intensity over the MT lattice and normalized it to the tubulin intensity for the three different concentrations. At each concentration, we averaged the KANSL3-GFP/ tubulin ratio at different positions by aligning the MTs at their ends and plot the intensity using a logarithmic scale. This analysis is depicted in the plot in Figure 21 B with a sketch of a MT below as a representation of the different positions. At the two lower concentration (39.2 nM and 78 nM), the MT ends cannot be distinguished as a drop in the fluorescence ratio, which indicates that KANSL3-GFP is almost not binding to the MT lattice. Besides, there are no evident differences in intensity at different positions along the lines, which suggest that the protein does not have a higher affinity for any of the positions. Interestingly, at the highest concentration, the protein distribution changes dramatically. The ends of the MT can be perfectly inferred from the plot and additionally, there is a peak at both ends compared to the middle, which indicates a higher affinity of the protein for the ends compared to the middle of the MT lattice (Figure 21 B, 156 nM).

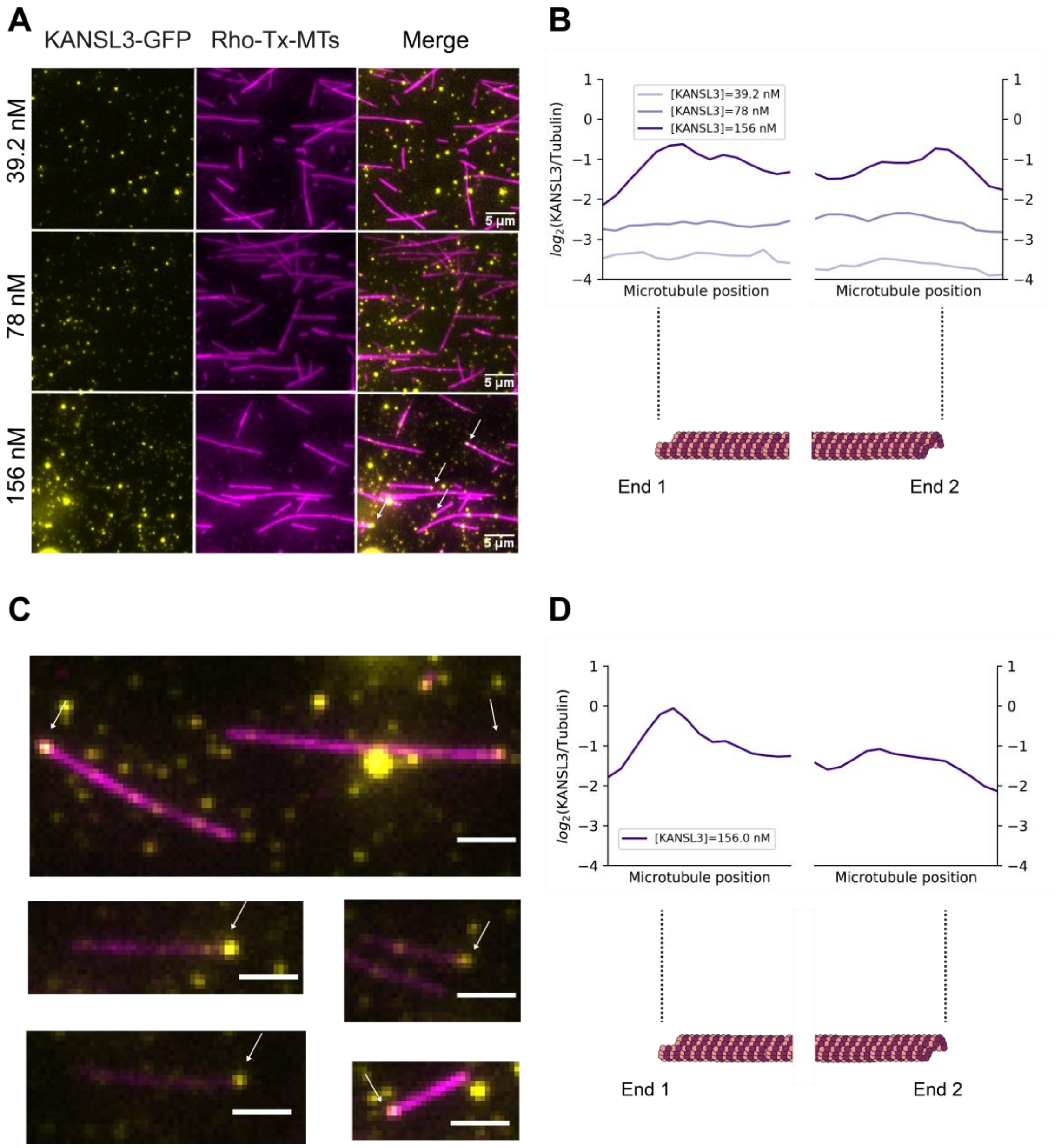

Figure 21. KANSL3-GFP preferentially binds one of the MT ends of Taxol-stabilized MTs. A) Representative TIRF images of KANSL3-GFP on Tx-MTs at three different concentrations. The 488 nm channel depicting KANSL3-GFP is shown in yellow and the 532 nm channel depicting the Tx-MTs labelled with rhodamine in magenta. A merge of both channels is shown in the last column. B) Line plot representing the average of KANSL3-GFP/ tubulin at different MT positions. MTs are aligned at their ends for the averaging. [39.2 nM] = 10 MTs; [78 nM] = 20 MTs; [156 nM] = 19 MTs. C) Representative TIRF images of KANSL3-GFP decorating one of the two MT ends only (merge) (from the third experiment in A). The white scale bar corresponds to 2 µm. D) Line plot representing the average of KANSL3-GFP/tubulin at different positions (third experiment in A). MTs are aligned by the end with higher intensity (End 1) [156 nM] = 19 MTs.

By looking in detail at the protein localization at the highest concentration (Figure 21 A, last row), we observed that the majority of MTs had a brighter spot decorating only one of the two ends (Figure 21 C). Thus, we decided to repeat the intensity analysis for this specific concentration by aligning the MT ends from their end with a highest intensity. In this way, we clearly observed that the intensity peak appears only at one of the ends

(Figure 21 D). These data suggest that binding is preferential towards one of the MT ends. Unfortunately, we have not been able to determine yet if the end to which the protein binds is the minus-end, which remains to be investigated in the future.

Besides, these results suggest that the preferential binding previously reported on MT spin-down experiments, happens also when the protein is tagged with GFP. However, could not compare both binding efficiencies. Additionally, under the microscope, we could observe protein oligomers of different sizes. The size of these oligomers of KANSL3-GFP increased at higher protein concentrations and over time, which indicates that KANSL3-GFP may have a tendency to aggregate (some of these big oligomers can be seen in Figure 21).

Overall, it seems that KANSL3-GFP has some preferential binding towards one of the MT ends in vitro. Nonetheless, we went on to determine how many MTs had their end decorated by KANSL3-GFP. At the highest concentration, only 30% of MTs are decorated by KANSL3-GFP, which seems not to suffice for proper targeting of the KANSL-complex. Therefore, we can especulate that KANSL3-GFP may need of other binding partners to recognize the minus-ends more efficiently in cells.

c) MCRS1-cherry seems to preferentially bind one of the MT ends *in vitro*

MCRS1 was described to decorate the MT lattice in spin-down experiments *in vitro* [82]. We tested whether tagging with a Cherry-tag at its C-terminus interfere with its binding properties by TIRF imaging.

The protein was purified in a high concentration after size exclusion chromatography (4 µM) and therefore, we could investigate the binding of the protein to Tx-MTs at high concentrations (~400 nM). Indeed, in those conditions, MCRS1-Cherry completely associated with the MT lattice, as previously described (Figure 22 A, third row). However, at a slightly lower concentration (~320 nM) (Figure 22 A, second row), we observed that although most MTs are fully covered with MCRS1-Cherry, there seems to be an enrichment of protein at some MT ends (Figure 22, white arrows in the second row).

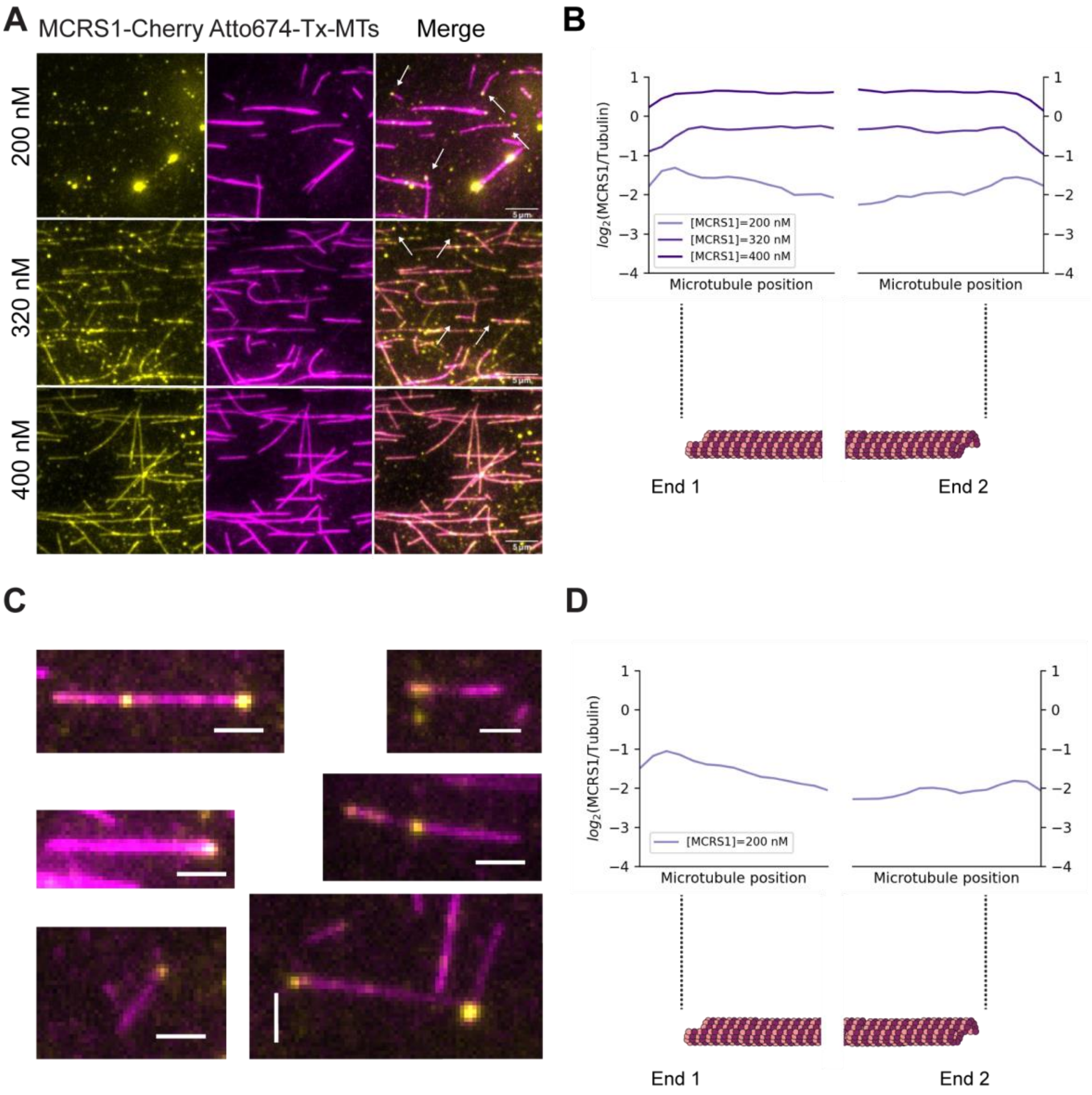
A
MCRS1-Cherry
Atto674-Tx-MTs
Merge
200 nM
320 nM
400 nM
5 µm
B
log₂(MCRS1/Tubulin)
1
0
−1
−2
−3
−4
[MCRS1]=200 nM
[MCRS1]=320 nM
[MCRS1]=400 nM
Microtubule position
Microtubule position
End 1
End 2
C
D
[MCRS1]=200 nM

Figure 22. MCRS1-Cherry preferentially binds one of the MT ends of Taxol-stabilized MTs. A) Representative TIRF images of MCRS1-Cherry on Tx-MTs at three different concentrations. The 532 nm channel depicting MCRS1-Cherry is shown in yellow and the 647 nm channel depicting the Tx-MTs labelled with Atto647 in magenta. A merge of both channels is shown in the last column. B) Line plot representing the average of MCRS1-Cherry/ tubulin at different MT positions. MTs are aligned at their ends for the averaging. [200 nM] = 19 MTs; [320 nM] = 28 MTs; [400 nM] = 10 MTs. C) Representative TIRF images of MCRS1-Cherry decorating one of the two MT ends only (merge) (from the first experiment in A). The white scale bar corresponds to 2 µm. D) Line plot representing the average of MCRS1-Cherry/tubulin at different positions (first experiment in A). MTs are aligned by the end with higher intensity (End 1) [200 nM] = 19 MTs.

We decreased further the protein concentration to 200 nM (Figure 22 A, first row). Strikingly, we could see that although MCRS1 associated with the MT lattice, some MTs had a brighter spot of protein at their tips (white arrows). As we did for KANSL3-GFP, we quantified the intensity profile of MCRS1-Cherry over the MT lattice and normalized it to the tubulin for the three different concentrations (Figure 22 B). At the highest concentration, the line is perfectly flat, meaning the protein is bound with equal affinity all along the MT. At the intermediate concentration, the situation is almost the same.

However, two tiny peaks start to emerge at the MT ends. At the low concentration, we observe that the peak becomes more prominent, which means that although the protein readily binds the MT lattice, it accumulates at the ends in this range of concentration. Following the same reasoning as before, we observed that most of the MTs had only one of the two ends occupied with a brighter spot (Figure 22 C). When aligning all analyzed MTs by their end with higher intensity, a peak appears only at one of the MT ends (Figure 22 C). These data suggest that the binding may be preferential towards one of the MT ends. Analysis of the MT polarity are still required to determine to which end is MCRS1-Cherry binding.

MCRS1-Cherry compared to KANSL3-GFP tends to aggregate less at the working conditions and has a higher affinity for the MT lattice. Thus, it prefers to bind the MT lattice rather than the glass surface. If MCRS1-Cherry is an end binding protein, we would expect that at lower concentration, it will rather bind only the end and not the lattice. It is worthy to mention that we did try to image MCRS1-Cherry at lower concentrations but due to technical limitations specific for the 532 nm laser beam, it is difficult for us to carry out consistent single-molecule experiments that would allow us to discriminate between the protein and the background. Something that should be investigated in the future.

Overall, these results suggest that MCRS1-Cherry could be a new end-binding protein, which needs to be further confirmed in the near future. Interestingly, analyzing the binding efficiency of MCRS1-Cherry, we found that 68 % of MTs have their end decorated with the protein spot at 200 nM concentration. This opens up two interesting questions. On one hand, if both proteins, KANSL3-GFP and MCRS1-Cherry have some preferential binding to the MT end, one possibility is that together they may have a higher affinity for the MT ends. This question will be targeted in the last chapter of the results. On the other hand, we could investigate if these two proteins can target the dynamic MT ends and influence their dynamics. We started by studying the effect of MCRS1-Cherry on MT dynamics, as it was the protein with a higher affinity.

d) MCRS1-cherry has no obvious MT end tracking *in vitro*

To investigate a potential MT end tracking ability of MCRS1-Cherry, we moved to dynamic assays with MT seeds under the TIRF microscope. We used GMPCPP seeds for these assays as having taxol in the flowcell would have impaired MT dynamics. The MT seeds contained biotinylated-tubulin and were tethered to the biotinylated glass surface via neutravidin.

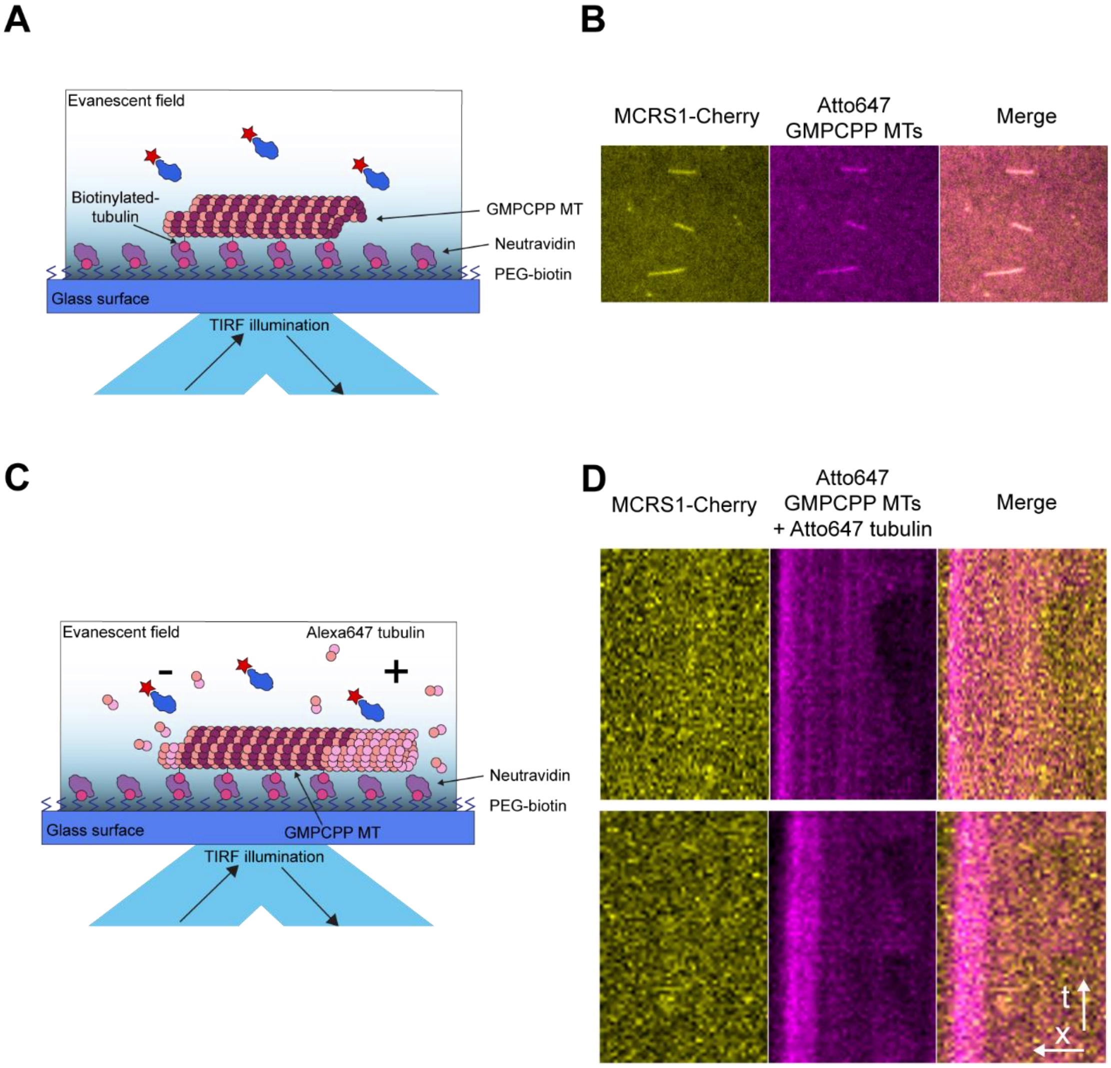
A
Evanescent field
Biotinylated-tubulin
GMPCPP MT
Neutravidin
PEG-biotin
Glass surface
TIRF illumination
B
MCRS1-Cherry
Atto647 GMPCPP MTs
Merge
C
Evanescent field
Alexa647 tubulin
-
+
Neutravidin
PEG-biotin
Glass surface
GMPCPP MT
TIRF illumination
D
MCRS1-Cherry
Atto647 GMPCPP MTs + Atto647 tubulin
Merge
t
x

Figure 23. MCRS1-Cherry binds to GMPCPP-seeds and soluble tubulin. A) Schematic of the MT seeds setup. GMPCPP-MT seeds were immobilized on a biotynilated glass surface via neutravidin. MCRS1-Cherry was added to the channel together with an oxygen scavenger system. The channel was imaged by using TIRF[123]. B) Representative images of the GMPCPP-MT seeds covered with MCRS1-Cherry. The channel 532 nm depicting MCRS1-Cherry is shown in yellow. The GMPCPP-MT seeds in the 647 nm channel are in magenta. A merge of both channels is also shown. C) Schematic of the dynamic MT seeds assays. Free tubulin and GTP were added together with MCRS1-Cherry and an oxygen scavenger system to promote MT growth. D) Representative kymographs (representation of the spatial position over time) of dynamic MTs. MCRS1-Cherry in the 532 nm channel is shown in yellow. In the 647 nm channel, GMPCPP-MT seeds are shown as a brigher región and the dynamic plus-end is visible as a prolongation of the MT seeds. The minus-end starts to grow from the other side of the MT seed

and is more difficult to visualize. We did not find any localization of MCRS1-Cherry on the dynamic ends.

First, we studied if the protein binding observed in the localization assays with Tx-MTs was also present in the same setup by incubating GMPCPP-MT seeds with MCRS1-Cherry alone (Figure 23 A). Representative images of MCRS1-Cherry bound to the MT-seeds can be seen in Figure 23 A. MCRS1-Cherry decorates the MT-lattice consistent with our previous results with Tx-MTs. Next, we continued by adding free labelled-tubulin and GTP to the setup, together with the protein, to promote MT dynamics (Figure 23 C). MT ends started to grow from the seeds. Plus-ends showed phases of growth and catastrophes (Figure 23 D). Minus-ends grew slower and also had some catastrophes but less frequently, as expected (not seen in the Figure). Surprisingly, upon addition of free tubulin and GTP to the setup, MCRS1-Cherry did not localizing anymore to the MT seeds nor to the dynamic ends. These results were reproducible in several independent experiments, in which we also tried to vary the protein / free tubulin ratio. The data indicate that MCRS1-Cherry binds to free tubulin with higher affinity than to polymerized tubulin, which precludes any study of its end “tracking activity”. However, MCRS1-Cherry could affect MT dynamics without directly binding MT ends. This possibilty remains to be investigated as well as the tracking activity of KANSL3-GFP that will be studied in the near future.

3.4. *In vitro* reconstitution assays to investigate the architecture of the MCRS1-KANSL-complex

At least three members of the KANSL-complex localize to the k-fiber minus-ends in the mitotic spindle. *In vitro* KANSL3 and possibly KANSL1 localize specifically to the MT minus-end. Additionally, here, we have described MCRS1 as a candidate end targeting protein. Understanding the binary interactions of the three candidates may help us to reconstitute a minimal complex that may target the MT minus-ends to investigate its effect on MT dynamics by TIRF imaging.

SILAC quantitative proteomics in cells synchronized in mitosis using MCRS1 as a bait, retrieved KANSL3 and KANSL1 as the most prominent preys (Meunier 2015). Besides, pulling from KANSL3 after co-expression of all the members of the KANSL-complex allows the retrieval of the full complex, including MCRS1 and KANSL1. However, the only described direct interaction between NSL1 (KANSL1) and MCRS2 (MCRS1) in *Drosophila* (Figure 24 A is a summary of all these interactions). To our knowledge, the binding hierarchy among MCRS1, KANSL1 and KANSL3 in humans is not known. To try to map the potenital interactions, we obtained data from a yeast two-hybrid screening and performed different *in vitro* pull-downs with the members of the complex.

a) KANSL1 and MCRS1 directly interact *in vitro*

To gain more information on the binary interactions, Mireia Garriga (Maurer lab, CRG), did a yeast two-hybrid screening which included all the seven proteins of the KANSL-complex (at that moment HCF1 and OGT were not assigned to the complex). The only interactions retrieved from this screening are depicted in Figure 24 B. Human MCRS1 interacts with itself and also with KANSL1. In order to validate this interaction, we performed *in vitro* pull-downs. We purified GST-MCRS1 from bacteria and incubated it with an insect cell lysate containing recombinant GFP-KANSL1. GFP pull-down from KANSL1 retrieves GST-MCRS1 as shown in the Western Blot in Figure 24 C.

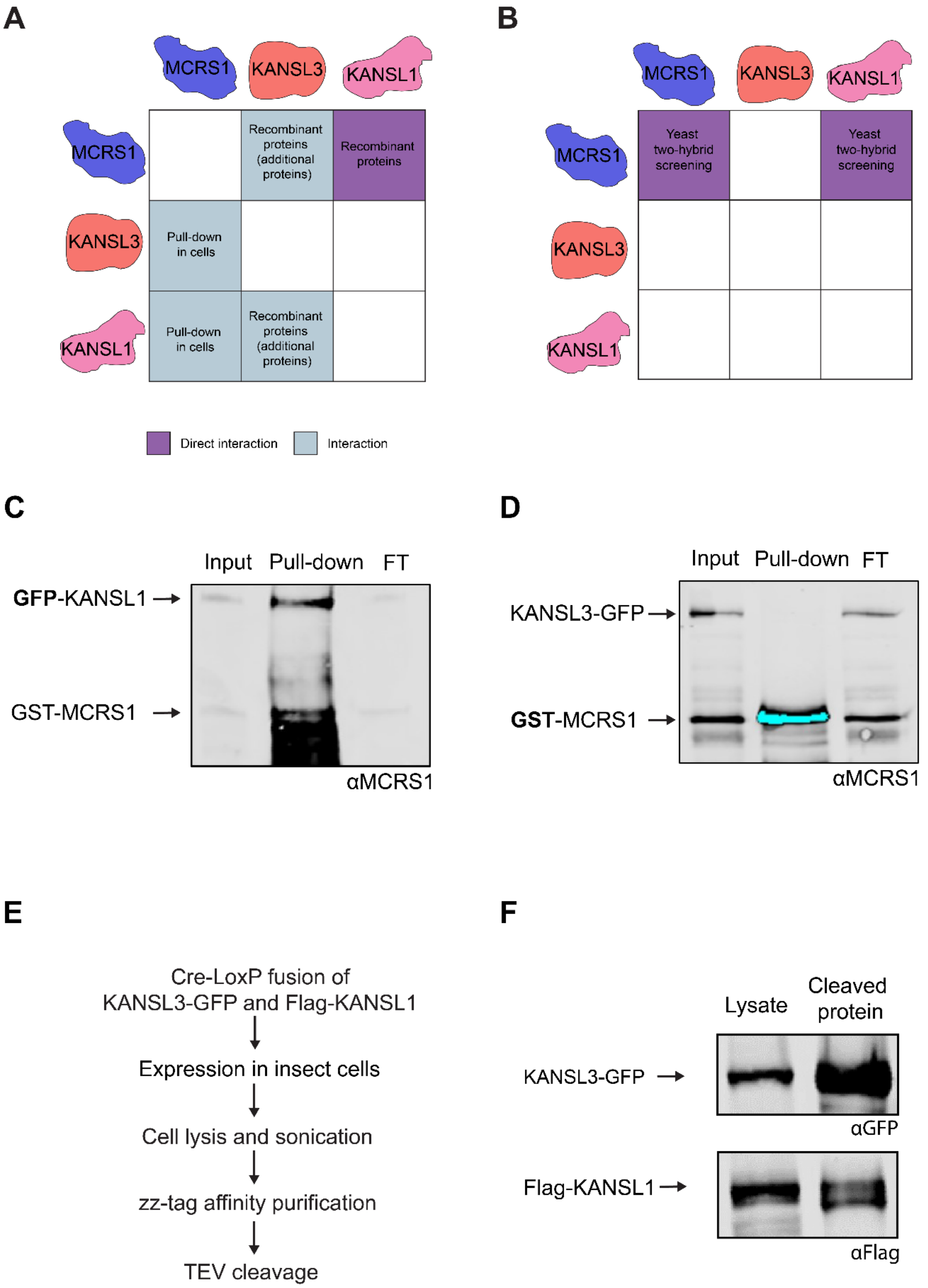
A
B
C
D
E
F

A

	MCRS1	KANSL3	KANSL1
MCRS1		🟦 Recombinant proteins (additional proteins)	🟪 Recombinant proteins
KANSL3	🟦 Pull-down in cells		
KANSL1	🟦 Pull-down in cells	🟦 Recombinant proteins (additional proteins)	

B

	MCRS1	KANSL3	KANSL1
MCRS1	🟪 Yeast two-hybrid screening		🟪 Yeast two-hybrid screening
KANSL3			
KANSL1			

🟪 Direct interaction 🟦 Interaction

Input
Pull-down
FT
GFP-KANSL1
GST-MCRS1
αMCRS1
Input
Pull-down
FT
KANSL3-GFP
GST-MCRS1
αMCRS1
Cre-LoxP fusion of KANSL3-GFP and Flag-KANSL1
Expression in insect cells
Cell lysis and sonication
zz-tag affinity purification
TEV cleavage
Lysate
Cleaved protein
KANSL3-GFP
αGFP
Flag-KANSL1
αFlag

Figure 24. MCRS1, KANSL1 and KANSL3 interactions(legend next page).

A) Schematic summary of the previously described interactions. B) Schematic summary of the new interactions shown by the yeast two-hybrid screening. C) GST-MCRS1 interacts with GFP-KANSL1 in *in vitro* pull-downs. WesternBlot showing the GFP-pull-down from KANSL1. As GFP-KANSL1 is cloned with a zz-tag (a region of protein G), it can be detected indirectly by the antiMCRS1 antibody. The black band below the protein band shows the degradation of the protein during the incubation time. D) KANSL3-GFP does not interact with GST-MCRS1 in *in vitro* pull-downs. WesternBlot showing the GST-pull-down from MCRS1. KANSL3 does not appear in the pull-down line. As for GFP-KANSL1, KANSL3-GFP is detected indirectly. E) Scheme of the co-expression and co-purification procedure for KANSL3-GFP and Flag-KANSL1. A recombinant construct was generated by Cre-LoxP fusion for co-expression of both proteins in insect cells. KANSL3-GFP has an affinity purification tag containing 10 histidine residues-zz-tag-TEV cleavage site. F) KANSL3-GFP and Flag-KANSL1 interact *in vitro.* Western Blots showing the co-purification of KANSL3-GFP and Flag-KANSL1. After affinity purification and TEV cleavage, both proteins are together. The detection is done in different membranes as both proteins have a similar molecular weight (121 kDa and 122 kDa respectively).

b) KANSL3 and MCRS1 do not interact *in vitro*

KANSL3 was shown to be required for MCRS1 to localize to the spindle poles in cells. Besides, both proteins (tagged with fluorophores) seem to have a preferential binding towards one of the MT ends. Together with the previously described interaction data, this suggests that KANSL3 and MCRS1 may directly interact. Although the interaction did not appear in the yeast-two hybrid screening, we decided to do an *in vitro* pull-down to investigate it.

We mixed GST-MCRS1 purified from bacteria with insect cell lysates expressing KANSL3-GFP. GST pull-down from MCRS1 does not retrieves KANSL3-GFP (Figure 24 D). Therefore, it seems that KANSL3 does not interact directly with MCRS1.

c) KANSL1 and KANSL3 interact *in vitro*

The last possible combination of proteins to connect the three members was KANSL1 and KANSL3. As KANSL1 alone was not purifiable (Figure 19 E) and had a tendency to degrade in insect cell lysates (Figure 24 F), we thought that co-expression in insect cells together with KANSL3-GFP could aid in its stability. Therefore, using the MultiBac technology for protein complexes, we co-expressed and co-purified KANSL3-GFP and Flag-KANSL1 following the procedure shown in Figure 24 E. For the purification we pulled of the zz-affinity tag contained in KANSL3-GFP and then, did a TEV cleavage to detach the protein (and its potential binding partners) from the affinity beads. After TEV cleavage, we analyzed the protein contents by Western Blot. Both proteins are present in the lysate after TEV-cleavage, which is only possible if Flag-KANSL1 is binding KANSL3-GFP (Figure 24 F).

All these three results together indicate that KANSL3 may bind to KANSL1 that in turn may bind MCRS1. To date, there was no information on how KANSL3 connects to the other members of the KANSL-complex (Introduction, Figure 10). We propose that it is through a direct interaction with KANSL1.

Being aware of the influence that big protein tags can have on protein structure and protein-protein interactions, the next step would be to the three proteins without any tag or only very small ones ligther tags and try to copurify them to confirm their interaction. Next, it would then be interesting to study in our TIRF setup how this subcomplex, containing possibly proteins that recognize the MT ends, interacts with MTs.

Discussion

4. Discussion

Life relies on cell division, the process by which a parental cell divides to produce two daughter cells with the same genetic material. The mitotic spindle is the molecular machine that segregates the duplicated chromosomes. The spindle is formed by two arrays of antiparallel MTs with their plus-ends contacting the chromosomes or establishing antiparallel connections in the spindle midzone and their minus-ends focused forming the spindle poles. The kinetochore fibers (k-fibers) are bundles of MTs that attach the two sister kinetochores of each chromosome to the two spindle poles and drive their segregation. The K-fiber MT plus-end dynamics has been extensively characterized but to date, not much is known about their minus-end dynamics. K-fiber MT minus-ends are thought to depolymerize constantly thereby driving tubulin poleward flux, which is fundamental for spindle stability and chromosome alignment in metaphase and contributes to chromosome segregation in anaphase. Indeed, it has been shown that MT minus end depolymerization generates enough forces to pull on the kinetochores under conditions that selectively block K-fiber MT plus-end dynamics, generating kinetochore hyperstretching[78,124]. However, how the k-fiber MT minus-end dynamics are established and regulated is poorly understood. The main aim of this thesis was to obtain some insights into the K-fiber MT minus ends morphology/ies and on the mechanism that ensures a controlled depolymerization in the metaphase spindle.

4.1. Structure of the k-fiber minus-ends using electron tomography

The minus-ends of the k-fibers are mostly focused at the spindle pole. After nucleation from the chromosome region, KMTs grow back and are transported poleward. Then, their minus-ends enriched in NuMA are captured by cytoplasmic dynein that clusters them into the poles. Other motors such as HSET and Eg5 also participate in this organization[41]. The spindle poles are robust as they can sustain high forces and tension generated at the paired sister kinetochores but at the same time a rapid MT turnover that allows attachment errors corrections. K-fibers can be entirely re-built and they can also incorporate new MTs[80]. In principle, these newly nucleated MTs have their minus-ends “capped” by the γ-TuRC nucleation complex. Regarding dynamics, k-fiber minus-ends are believed to continuously depolymerize and contribute to MT poleward flux. These ideas originate from observations of cells in metaphase. A stripe of photo-activable tubulin stripe photoactivated by laser illumination in the proximity of the aligned chromosomes at the metaphase plate rapidly move towards the spindle poles where it vanishes[10,70]. This was interpreted as the result of the net incorporation of tubulin subunits at the plus ends of the MTs attached to (or in the proximity of) the kinetochores in combination with the removal of tubulin subunits at the MT minus-ends. These observations date back to 1986[70]. Since then, not much new information about the k-fiber minus-end dynamics has been gathered. Actually, MT minus-ends have not been the focus of attention as compared with the MT plus-ends. This may be because they are much more difficult to investigate because they are tighlty packed in the spindle pole area and therefore, difficult to image and until recently no specific binders had been identified. Thus, currently, there is a lack of structural information on the k-fiber minus-ends. In this work, we aimed at gaining novel insights on the k-fiber minus-end ultrastructure of the mammalian spindle.

To do so, we used ET as the technique of choice since it provides high-resolution structural data. Interestingly, previous studies mostly pefomed *in vitro* indicated a correlation between different types of MT end morphologies and their dynamic state (growth, shrinkage, pause) (Figure 3). We could therefore use the MT minus-end morphologies to infer their dynamic state at the time of fixation.

Strikingly, and unexpectedly, we observed that not all k-fiber MT minus-ends are open at the spindle pole in the mammalian metaphase spindle. Indeed, in the proximity of the centrioles at the spindle poles, we estimate that ~37.31% of the k-fiber MT minus-ends are capped or closed. Despite the inherent variability of the measurements, 25% of the MT minus ends were assigned as closed by two independent classifiers, providing confidence in the classification (Annex Figure B). This means that 2 out of 5 MT minus-ends at the spindle pole appear as closed while 3 of them are open. Inferring a dynamic state from the MT end morphology (Figure 3, introduction), these data suggest that 2 out of 5 MT minus-ends are stable and the other 3 are dynamic. Interestingly, we found no evidence of clustering of open ends at specific k-fibers. These data indicate that the MTs forming an individual K-fibers are not homogeneous in terms of their minus end dynamic state but are instead mixed showing open and close ends. The analysis of the K-fiber MTs minus-ends that do not reach the centrosome region suggest that more than half of them has a closed conformation (Figure 14). This result could be expected if MTs are newly nucleated in the chromatin region and have their minus-ends capped by the γ-TuRC nucleation complex.

However, the presence of K-fiber MT having closed minus-ends at the spindle poles was rather unexpected. As previously described, the MT poleward flux occurring in the spindle requires a constant removal of tubulin subunits from the minus-end. Thus, we expected that at the poles all the KMTs would have open minus-ends. This could be the result of an uncapping of the k-fiber MT minus-ends at the spindle poles in the proximity of the centrosome for instance by severing enzymes, and their depolymerization by the MT depolymerases, two clases of proteins enriched at the spindle poles. We expect the "uncapping" of the γ-TuRC to be irreversible in this context. However, this hypothesis does not fit well with our data. Some of the MT have closed ends and therefore may not depolymerize. Therefore based on the snapshot obtained by ET, our data suggest that not all the KMTs undergo depolymerization at the same time to drive the characteristic MT flux.

How do our results on KMT minus-end morphology change our understanding on what happens at the spindle pole region? Although more data are needed to get a clear picture, we can hypothesize that the "capped" MT ends serve as a stable anchor point of the k-fibers to the spindle pole in metaphase. They could permanently interact with other spindle MTs and provide mechanical stability to the mitotic spindle while other KMTs are permitted to flux and generate forces to "pull from" and align the chromosomes. When the cell enters into anaphase, an uncapping of all these KMTs could then contribute to increase the rate of MT flux and promote chromosome segregation. This is something to be investigated in the future.

It is currently not possible to define what component(s) may form the "cap" at the KMTs minus ends that we visualize as a higher electron density material closing the end of the MT. The γ-TuRC ring complex[41] has been visualized as a higher electron density shaped as a cone at the MT minus end (Figure 3, introduction). This MT nucleation complex is very large with an approximate molecular weight of 2353.97 kDa[28]. The electron dense material that we visualized could also correspond to other MT minus-end binding protein complex(es). Currently there are two possible candidates: ASPM-Katanin[92] and the MCRS1-KANSL complex. Interestingly the SILAC proteomic data from the lab suggest that MCRS1 and the KANSL complex may intereact with ASPM (Figure 11, introduction). We can speculate about the size of a MT minus-end binding complex. If considering only one copy for each of the KANSL subunits this would correspond to approximately 734 kDa. Now if we also take into account one copy each of ASPM and NuMA (that was also recovered in the SILAC proteomic experiments looking for MCRS1 interactors) (Figure 11, introduction), the resulting complex would be much larger at around 1382 kDa. This would be at least half the size of the γ-TuRC ring and therefore, we can speculate that it would produce an electron dense material visible in the tomograms. In agreement with this hypothesis we quantified a reduction of the proportion of closed K-fiber minus ends (therefore having a complex attached) in MCRS1 silenced cells.

In this case, we could imagine that within an individual k-fiber, the binding-unbiding, stochastic or regulated, of a specific protein complex at the MT minus-ends could provide a mechanism to control their dynamic state. Ideally, getting snapshots of the k-fiber minus-ends at different time-points could provide further support to this idea, but to date this is not technically possible.

The MT plus and minus-ends dynamics of the k-fibers must be coordinated and equilibrated to account for a stable spindle size and to mediate chromosome attachment and movements as well as error correction in the KMTs attachment. Recent studies showed that centrosomes (at the spindle poles) control k-fiber length via depolymerases and severing enzymes that shorten the MTs through their minus ends and generate MT poleward flux. Thus, depending on the K-fiber length, different plus-ends dynamics regulators such as HURP accumulation changes[77]. This sets the basis for the coordination between the plus and minus-end dynamics. Observations in yeast suggest that spindle pole bodies (SPB) remotely control cargo transport from the minus-ends to the plus-ends to regulate K-fiber dynamics[125]. The fact that we observed that some KMT minus ends are closed at the spindle poles while open at the plus-end suggests that there must also be a tight communication between the dynamics at each end. Indeed if the MTs plus-end would continuously incorporate tubulin subunits, and their minus end would maintain a cap, their overall length would increase affecting spindle stability and chromosome attachment. It would have been very interesting to test whether we can establish some kind of correlation between the minus-end dynamic state of a specific KMT and its plus-end dynamic state inferred from the ET snapshot. Previous investigations on the KMT plus-ends in Ptk1 cells tried to discriminate between depolymerizing and polymerizing MT plus-ends. They reported that 2 out 3 plus-ends are in a depolymerizing state even when the k-fiber exhibits net incorporation of tubulin at the plus-ends[24]. However, with the current resolution we achieved by ET, we could not distinguish if the ends classified as open correspond to growing or shriking states (plus or minus) (Figure 25). In our analysis, all of them showed a flared morphology, in agreement with recently published tomographic data[23].

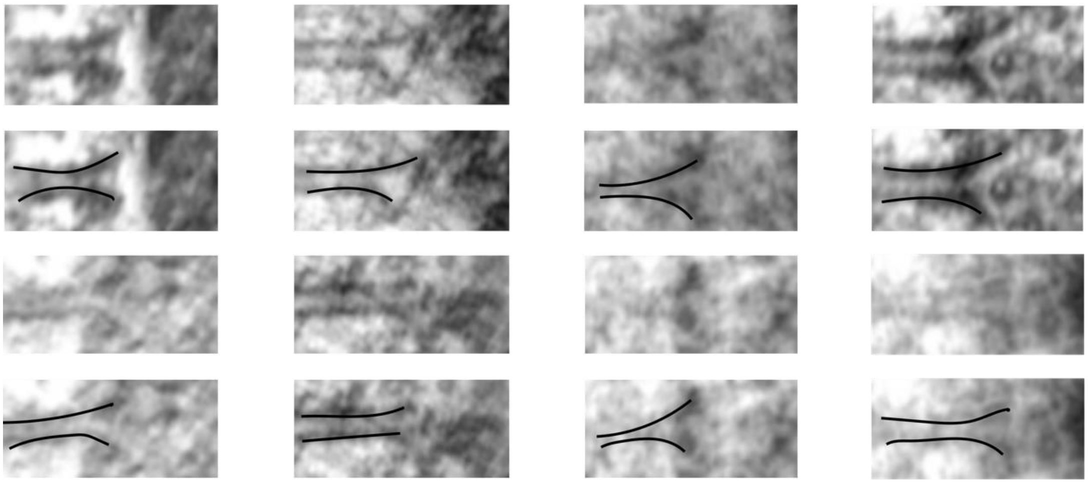

Figure 25. Open end morphology. Different types of MT open end conformations cannot be distinguished with the current resolution after ET reconstruction. Representative collection of open ends (without polarity assignement) showing a flared conformation.

Having described for the first time the morphology of the k-fiber minus-ends in a mammalian spindle as a combination of open and closed ends and having hypothesized about the implications of these finding, we went on to investigate how the minus-end dynamics may be regulated. The MCRS1-KANSL-complex has the unique feature to target specifically k-fiber minus-ends and fine-tune their dynamics. Therefore, it is the perfect “molecular tool” to characterize k-fiber MT minus-ends dynamics. But, since this complex has been characterized for its functions during interphase in the regulation of housekeeping genes expression, can we trust that the phenotypes observed in mitosis upon silencing of some of its components is completely specific?

4.2. The MCRS1-KANSL-complex has moonlighting activity

MCRS1 and the other members of the KANSL complex have been described as "moonlighting proteins". These proteins can perform a number of apparently unrelated functions that can even be exerted in different compartments[126,127]. The members of the KANSL-complex are transcription factors (TFs) bound to chromatin in interphase. However, some of them relocate to the mitotic spindle when the cell enters into mitosis. While being interesting from an evolutionary point of view, the fact that the members of the complex have a dual-role makes it much more complicated for disentangling their functions. In fact, recently published studies on the Drosophila NSL-complex showed that the orthologues of MCRS1, KANSL3, PHF20 and WDR5 localize to the spindle in mitosis and that their depletion leads to problems in centrosome duplication and chromosome alignment and segregation. However, the authors propose that the observed mitotic defects are originating from the function of the NSL-complex in gene expression regulation. They reported that a centromeric protein, Cid (CENP-A in humans), and a kinetochore protein, Ndc80, are downregulated after silencing the NSL-complex members suggestin that this could account for the defects they observed in mitosis. Therefore, if no direct function in mitosis can be demonstrated, these proteins would not fall into the category of "moonlighting proteins"[109].

In the case of the human KANSL-complex, the "moonlighting activity" is proven. In addition to the specific localization to the spindle in cells, the function of MCRS1, KANSL3 and KANSL1 was addressed through experiments performed in Xenopus egg extracts in which gene expression is inactive and purely *in vitro*. These experimetns revealed that these proteins bind to MTs and they promote MT growth in the presence of RanGTP [81,82]. In addition they seem to associate with different mitotic partners, f.i: TPX2, MCRS1, KANSL3 and KANSL1

Nonetheless, we cannot discard that the mitotic phenotypes observed upon silencing of KANSL proteins are due to an indirect effect on gene expression. To analyze a bit further this possibility, we looked onto the already available transcriptomics data in repositories. We found data obtained from mouse embryonic stem cells (MES), specifically, RNA-seq data comparing control and KANSL3-silenced cells and MCRS1 and KANSL3 ChIP-seq data (Annex Figure E A, E B). We crossed both types of data in order to look for promoters of genes bound by the KANSL-complex whose transcription was up or down regulated. We obtained a list of 1106 downregulated genes and 816 upregulated genes in silenced cells. We selected Nuf2, a component of the Ncd80-complex involved in kinetochore attachment, GTSE1, proposed to regulate k-fiber dynamics, Clasp2, a MT plus-end dynamics regulator and Katnal1, a variant of the katanin P60 subunit (Annex Figure E C) for further analysis by qPCR. We could not detect any significant difference in the expression levels of these genes in control and MCRS1-silenced cells, as expected from the transcriptomic analysis (Annex Figure E D). For example, we did not find a reduction in Nuf2 levels (Ncd80-complex) in MCRS1 silenced cells (Annex Figure E D) as previously reported in Drosophila[109]. It would be interesting to also assess protein levels by WB and immunofluorescence. Ideally, we could perform a transcriptomics analysis in the HeLa MCRS1-silenced cells that we used for ET. In any case our preliminary analysis suggests that defects in the expression of mitotic genes is not a concern when analyzing the phenotypes of silenced cells.

4.3. How does the MCRS1-KANSL-complex regulate k-fiber minus-end dynamics in mitosis?

In this thesis, we used ET to study the ultrastructure of the k-fibers assembled in MCRS1 silenced cells looking at their minus-end morphology to gain insights into the mechanism by which minus-end dynamics is regulated by the KANSL-complex. Regarding the ultrastructure of the k-fibers, we observed that the k-fibers in MCRS1-silenced cells are to be under more tension than in control cells (siScramble cells) since they appeared more "stretched". However, this does not translate into kinetochore hyperstretching as previously described[81]. We hypothesized that this may be due to the different protocols used for these different type of experiments. For immunofluorescence analysis, cells were fixed 72 h after transfection. Within this time, cells possibly struggled to form a stable mitotic spindle as previously described[81].Therefore, at the time of fixation, many of them were likely to have aberrant spindles due to a prolonged arrest. By contrast, the protocol for ET consisted of two successive mitotic shake-offs spaced by 2 h. Therefore the cells subjected to high-pressure freezing had spent at maximum 2 h trying to assemble a bipolar and go into anaphase. In this case the spindles may not be as aberrant.

ET allowed us to obtain single MT resolution and therefore, we could accurately count the number of KMTs attached to a particular kinetochore at the time of fixation. Strikingly, MCRS1-silencing resulted in k-fibers with less MTs than control cells (on average 3 KMTs less than control and siScramble cells). A similar phenotype was observed in the ET of 3 additional MCRS1-silenced spindles. We are therefore confident that the results are reproducible and the effect is significative. They are also in agreement with previous reports indicating that K-fibers assembled in MCRS1 silenced cells are less stable to cold induced depolymerization[107]. The reduction of KMTs could originate from defects at the level of chromosomal MT assembly or from problems in kinetochore attachment and stability.

One exciting result from our analysis is that the proportion of open KMT minus-ends appears to increase at the spindle pole in the MCRS1 silenced cells. Although the effect is not major, we could quantify a ~10% increase it is highly reproducible since we could observed it in 4 spindles. In principle, we can assume that open MT minus-ends do not grow but only depolymerize. Therefore, the higher proportion of open ends would fit well with the previous report showing that the poleward flux measured in MCRS1-silenced is higher than in control cells[81]. Interestingly, we also observed that the K-fiber minus-ends in the MCRS1 silenced cells were further away from the spindle pole not reaching the centriole areas nor spanning over them as in control (siScramble) cells. This topology is actually reminiscent of that of Drosophila mitotic spindles (Figure 26 A), in which the centrosome is visibly separated from the spindle MTs. It is tempting to speculate that MCRS1-silenced cells may also have problems in the assembly of MTs from the centrosomal pathway and therefore, there would be a lesser overlap between the KMTs and the MTs emating from the centrosome. In the last scenario, it would be interesting to exert forces on the MCRS1-silenced k-fibers to test if their anchoring to the spindle poles is preserved[128].

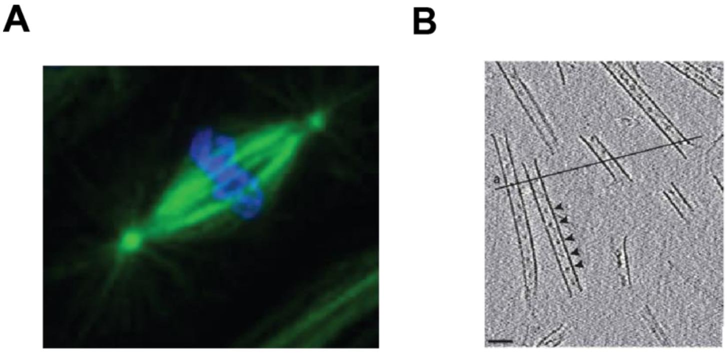

Figure 26. A) Drosophila S2 cell mitotic spindle (adapted from[129]). Centrosomes can be clearly distinguished from spindle MTs. B) Cryo-EM image of Taxol-stabilized-MTs. MT ends are blunt in this *in vitro* polymerized MTs (adapted from[130]).

Considering that MCRS1 indeed alters the minus-end structure of the k-fibers, we investigated how it could specifically target such structure, combining both, open and closed ends. *In vitro* reconstitution assays to study the localization of MCRS1 and KANSL3 on Tx-stabilized MTs revealed that both proteins have a preferential binding towards one of the MT ends. KANSL1 was also likely to have preferential binding towards one of the MT ends *in vitro*[82]. Here we also demonstrated that KANSL1 binds both MCRS1 and KANSL3 *in vitro*. Besides, KANSL1 silencing affects the level of expression of the other members of the complex[82], suggesting that it could be the core component of the subcomplex. Althogether, we could hypothesize that all three proteins in complex recognize one of the MT ends in Tx-stabilized MTs. These MTs have a blunt end morphology as seen in cryo-EM structures (Figure 26 B). Therefore, we could speculate that the complex binds such an end. The complex formed by MCRS1, KANSL3 and KANSL1 would have a size of 272 kDa if having a 1:1:1 stoichiometry, around ten times smaller than the γ-TuRC. Hypothetically, several subunits of this complex could "cap" the end of the MT.

Working with individual proteins that have a high molecular weight and a predicted highly disordered structure (namely KANSL1 and KANSL3) may not be optimal when they are part of a protein complex *in vivo*. For the future, it would be interesting to reconstitute such “minimal complex of proteins”, probably by co-expressing the three proteins.

Additionally, it would be interesting to test if the complex may track depolymerizing MTs. As we have shown in this thesis, k-fiber MT minus-ends are either closed or open in the metaphase spindle. The open ends at the spindle pole are assumed to be depolymerizing. Technically, it is challenging to mimic MT depolymerization *in vitro*. Often, the conditions in the *in vitro* MT dynamic assays only allow to observe plus and minus-ends either polymerizing or undergoing a catastrophe. Recent publications used a MT GMPCPP-seeds dynamic setup but without including free tubulin and with GTP to compete with the GMPCPP and promote controlled MT depolymerization[83]. This is probably a more suitable setup to study tracking of depolymerizing-ends in the future. Alternatively, other type of systems such as Xenopus egg extracts imaged under the TIRF microscope could provide more realistic depolymerization conditions (bearing in mind the presence of other components in the assay).

Finally, something else to be investigated is the interplay of the complex with other mitotic proteins, which can be important for its function and also for its minus-end targeting. The KANSL-complex was shown to interact with TPX2 and to counteract the activity of the depolymerase MCAK[82]. Here, we show that the KMT minus-ends in MCRS1-silenced cells have a higher proportion of open morphologies, which correlates with higher depolymerization rates. MCAK could have easier access to ends not decorated with the MCRS1-KANSL-complex. Other interesting mitotic members could be severing enzymes such as katanin or proteins localizing to the minus-end such as dynein, ASPM and NuMA (all included as mitotic partners in the SILAC proteomics). In addition, KANSL3 and KANSL1 contain several SxIP binding motifs (Figure 19A), characteristic of +TIP proteins and which mediate their binding to EB proteins[131]. Interestingly, MCRS1 associates with GST-EB1 in pull-downs in cell lysates[132]. These data indicate that the KANSL-complex might interact with EB1 in mitosis. This interaction could enhance the recognition of dynamic MT ends. To date, EB1 has only been observed to track polymerizing ends but we cannot discard that this is due to the technical limitations described before.

Taking everything together, we can propose a hypothetical model by which the MCRS1-KANSL-complex could fine-tune dynamics at the k-fiber minus-ends (Figure 22):

1) In a metaphase cell, the MCRS1-KANSL-complex would target uncapped-ends. Binding partners such as EB proteins could enhance the binding of the complex to the depolymerizing-ends. Upon binding of these protein complexes, the MT-ends would appear as "capped", constituting around 30% of the minus-ends of the KMTs at the spindle poles (as observed by ET). In this way, the complex could regulate the access of kinesin-13 (MCAK, kif2a) preventing active depolymerization of these MTs (Figure 27 A, left).

2) Since the k-fibers in metaphase continuously flux, MT minus-ends cannot be permanently "capped" by the MCRS1-KANSL-complex. Therefore, the MCRS1-KANSL-complex could bind on and off at the MT minus-ends. The binding could be regulated by phosphorylation. In this context, it is tempting to speculate that MCRS1 phosphorylation on Ser35/36 by the kinase Aurora A may play a role. Indeed, it was previously reported that this site phosphorylated by Aurora A is required for spindle and K-fiber assembly [113](Figure 27 A, right).

3) The k-fibers assembled in MCRS1-silenced cell have less KMTs than controls. This may be a consequence of the reduced efficiency of chromosome dependent MT assembly. These KMT have their minus-ends further away from the spindle pole and with a higher proportion of ends (~80%). These ends would be more accessible for depolymerization by kinesin-13, and could drive a higher poleward flux. The silenced cells do not manage to divide, confirming the importance of k-fiber MT minus-end dynamics regulation during mitosis (Figure 27 B).

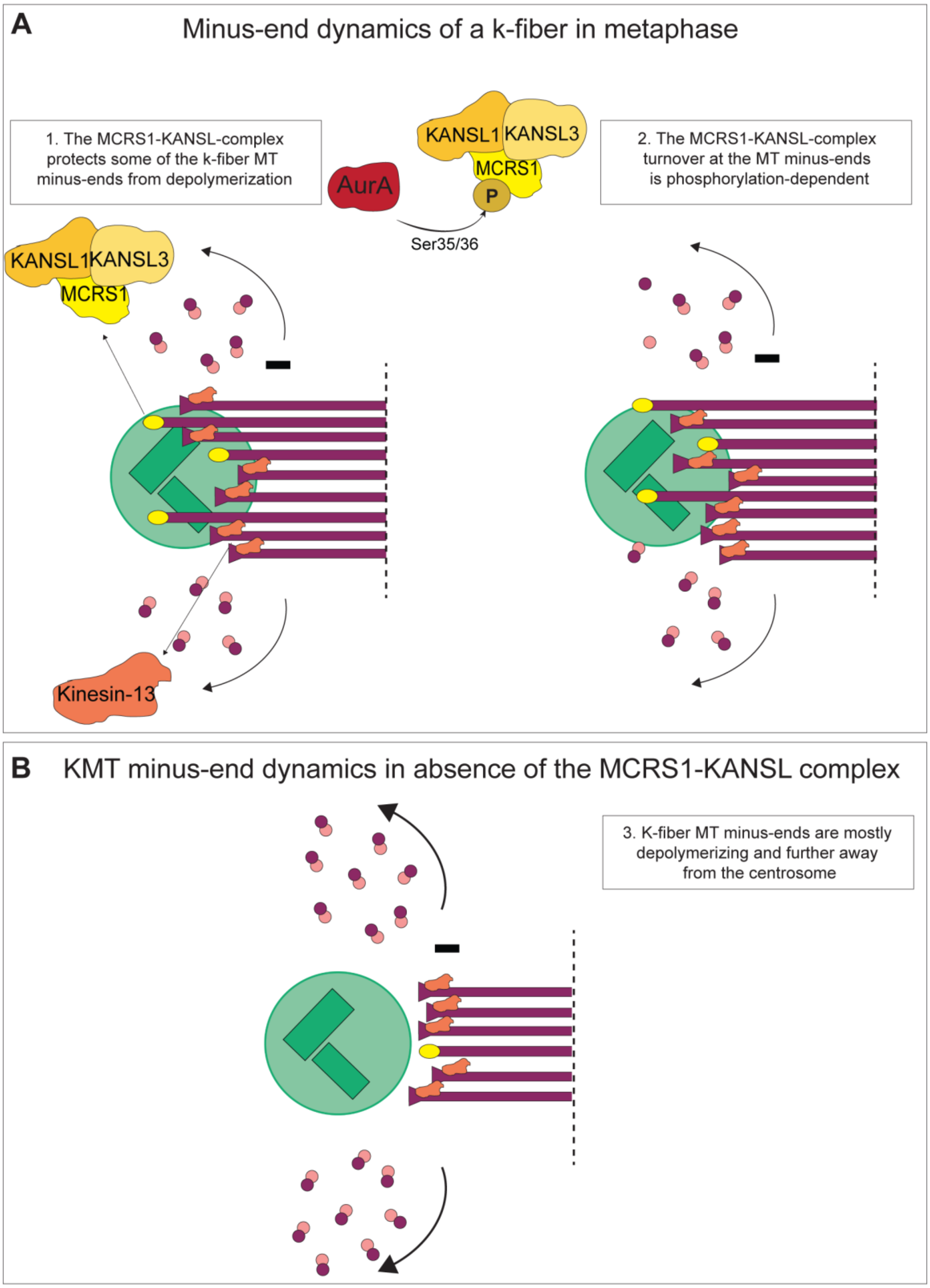
A
Minus-end dynamics of a k-fiber in metaphase
1. The MCRS1-KANSL-complex protects some of the k-fiber MT minus-ends from depolymerization
AurA
KANSL1
KANSL3
MCRS1
P
Ser35/36
2. The MCRS1-KANSL-complex turnover at the MT minus-ends is phosphorylation-dependent
KANSL1
KANSL3
MCRS1
Kinesin-13
B
KMT minus-end dynamics in absence of the MCRS1-KANSL complex
3. K-fiber MT minus-ends are mostly depolymerizing and further away from the centrosome

Figure 27. Possible model of KMT minus-end dynamics regulation by the KANSL-complex. A) KMT minus-end dynamics in metaphase. K-fibers have on average 9 KMTs (purple) directly contacting the kinetochore and spanning an area around the centrosome (green). Left: ~30% of their minus-ends are "capped" at the spindle poles (3 out of 9 in the model). The "cap" could be the MCRS1-KANSL-complex. The access of kinesin-13 to the "capped" minus-ends is restricted. Right: the MCRS1-KANSL-complex does not permanently bind the same KMT minus-ends. Its turnover on MT ends could be regulated by phosphorylation, for example by Aurora A on MCRS1. In this way, KMT minus-ends could switch between "capped", stable and "uncapped" states, thereby depolymerizing in a controlled manner to regulate minus-end dynamics. B) KMT minus-end dynamics in a MCRS1-silenced cell in metaphase. K-fibers have on average 6 KMTs directly

contacting the kinetochore. Their minus-ends are further away from the centrosome than in controls. MT minus-ends are mostly open (5 out of 6 in the model) since the MCRS1-KANSL-complex is absent or strongly reduced. This results in higher accessibility for depolymerization by kinesin-13.

The specific action of the MCRS1-KANSL-complex at the k-fiber MT minus-end would allow the regulation of dynamics at the minus-ends in metaphase. Hypotethically, the status of the KMT minus-end could be coordinated with the status of the KMT plus-ends. For instance, if a plus-end would be depolymerizing, the corresponding minus-end could be “capped” by the KANSL-complex to preserve the length of the k-fiber. In contrast, if a plus-end is growing, its partner minus-end could be at that moment depolymerizing. Overall, such mechanism could contribute to an equilibrium between the plus and minus-end dynamics in the k-fiber. This would be fundamental to permit chromosome alignment by oscillatory movements and error correction. A structure that is stable but at the same time dynamic.

4.4. Are the k-fiber MT minus-ends the new plus-ends?

Altogether, we could propose that the "k-fiber minus-ends are the new plus-ends". Until now, the MT plus-ends have received much more attention than the minus-ends. Here we hypothesize, based on our data, that plus and minus-ends share many features and that their regulation contribute to spindle fitness. In the next points, I develop why we think "the minus-ends could be the new plus-ends" and therefore, should be the object of more studies in the future.

- **Dynamics:** in principle when taking a snapshot of the plus and minus KMT ends of an individual k-fiber in a metaphase cell, a mixture of end morphologies co-exist. This was already known for the plus-ends, as polymerizing and depolymerizing ends co-exist. In this case, individual MT ends can, in principle, switch between growing and shrinking phases[24].
  Here, we describe a similar situation for the KMT minus-ends. Indeed, after having taken a snapshot on the minus-ends, we infer from their morphology that that dynamic depolymerizing and stable ends co-exist. We hypothesize that the individual MT ends can alternate between these two phases.

- **Structure:** both types of ends are dynamically but firmly attached to the structures that hold them. The plus-ends are attached to the kinetochore in a way that permits their dynamics while the minus-ends are properly anchored at the spindle poles, where they can sustain the addition of new MTs at the same time as tubulin dimers are released from some of the KMTs. The 'anchoring' of the k-fibers to the spindle poles was recently addressed. Biophysical studies applying forces on the k-fibers have shown that it is easier to break a k-fiber in its middle point than to detach it from its anchor points. K-fibers are indeed flexible to pivot around spindle poles[128]. The protein complexes holding the KMT plus-ends in the kinetochore have been extensively described[75]. KMT minus-ends are focused at the spindle poles by a NuMA-dynein dependent mechanism. How they are firmly anchored to the spindle poles while undergoing complex dynamics remains to be investigated.

- **Force generation:** both types of ends, by means of polymerization and depolymerization, can generate forces that are fundamental for the positioning of the chromosomes at the metaphase plate, the correction of attachment errors and finally, their segregation. These functions are carried out together with other associated MAPs.

- **Dynamics regulators:** to perform the fundamental functions they carry out, both are supported by a cohort of associated proteins. Many plus-ends binding proteins (+TIPs) have been described and their characterization has helped to understand k-fiber dynamic regulation: Ska1, CENP-A or CLASP proteins (Introduction 1.3)[75]. Most +TIPs associate with end binding (EB) proteins that can track the dynamic ends. In the case of the minus-ends, only recently specific –TIPs regulators are emerging (Introduction 1.4), which also complicated the study of their dynamics, as there were no “molecular tools” to interfere with them. It is interesting to speculate that the current EB proteins or a similar family of proteins might help also to recruit –TIPs to the depolymerizing k-fiber minus-ends, which to date is unknown. Among the –TIPs family, a prominent member which seems to regulate k-fiber minus-end dynamics is the MCRS1-KANSL-complex. As already explained, the MCRS1-KANSL-complex alters both k-fiber ultrastructure and minus-end morphology to regulate minus-end dynamics in metaphase.

- **Regulation by phosphorylation:** KMT plus-ends dynamics and error correction at the kinetochore rely on the kinase Aurora B. Aurora B acts as a tension sensor. Depending on the interkinetochore distance, Aurora B can/cannot phosphorylate its substrates (f.i: the Ndc80-complex). In this way, it can modulate KMT-attachments and plus-end dynamics. It is interesting to speculate that a similar regulatory mechanism could function at the spindle poles. Aurora A localizes to the centrosome where it phosphorylates multiple substrates. Aurora A is fundamental for centrosome maturation and separation, acentrosomal and centrosomal spindle assembly, kinetochore function and cytokinesis[133]. Additionally, Aurora A phosphorylates MCRS1 to regulate k-fiber minus-end dynamics[113].

Altogether, my results suggest that the dynamics of the k-fiber minus-ends are more complicated than previously anticipated. This opens up new interesting questions about their regulation to be investigated in the future. The MCRS1-KANSL-complex could play a fundamental role in their regulation by dynamically “capping” some K-fiber MT-minus-ends to regulate their depolymerization rates for proper cell division.

Conclusions

5. Conclusions

1) Electron tomography of metaphase spindles provides novel high-resolution structural data for k-fiber ultrastructure and MT end-morphologies in control and silenced cells.

2) In metaphase, KMT minus-ends can show an open and close conformation, although the majority are open.

3) In an individual k-fiber, open and closed KMT minus-ends co-exist.

4) MCRS1-silenced cells assemble mitotic spindles with an altered morphology: narrower half-spindle angles, outer MTs splayed out and KMTs appear straighter.

5) K-fibers in MCRS1-silenced cells have significantly less KMTs.

6) K-fiber MTs in MCRS1-silenced cells have their minus-ends further away from the spindle pole.

7) K-fiber MTs in MCRS1-silenced cells have a higher proportion of open minus-ends.

8) KANSL3-GFP shows preferential binding to one of the taxol-stabilized MTs in TIRF microscopy

9) MCRS1 may be a novel direct end-binding protein.

10) KANSL1 directly interacts with MCRS1 and KANSL3 *in vitro.*

11) The regulation of the dynamics of the k-fiber MT minus-ends may be more complex than previously anticipated and may show some parallels with the complex regulation occurring at their plus-ends.

Materials and methods

6. Materials and Methods

Standard techniques

Cell culture

HeLa cells (referencia) were grown at 37ºC in a 5% CO_2 atmosphere. The cells were cultured in Dulbecco's Modified Eagle Medium (DMEM) with 4.5 g/L glucose with L-glutamine with sodium pyruvate (Lonza, BE12-604F) supplemented with 10% fetal bovine serum (FBS) (Gibco^{TM}, A4766801) and an antibiotic cocktail containing 100 μg/ml streptomycin and 100 units/ml penicillin (Sigma-Aldrich, 15140122). HeLa cells were splitted when reaching around 80-90% confluency with 0.25% Trypsin (Sigma-Aldrich, T4049) and diluted 1:10 for regular maintenance.

Immunofluorescence

For immunofluorescence (IF) cells were typically grown on 18 mm round coverslip and fixed by immersion in cold methanol (-20ºC) during 10 minutes. Next, coverslips were blocked and permeabilized with immunofluorescence medium (IF medium) containing 0.5 % BSA (Panreac, A1391) and 0.1 % Triton X-100 (Sigma-Aldrich, T8787) in PBS 1x for at least 30 min. Next, a primary antibody solution (primary antibodies dissolved in IF medium) was added to the coverslips for 1 h at room temperature. The coverslips were washed thee times with IF medium. Then, a secondary antibody solution (secondary antibodies and Hoechst in IF medium) was added for 45 min at room temperature. Finally, the coverslips were washed twice with IF medium and twice with PBS 1x and mounted in 10 % Mowiol (home-made). The coverslips were protected from light and against drying during the whole process. The antibodies used for immunofluorescence are listed in Table 1. The cells were imaged under an inverted widefield fluorescence microscope with a 63x oil-immersion objective (DM1-6000-Leica).

qRT-PCRs

RNA was extracted using the TRIzolTM (Life Technologies, 15596026) RNA isolation protocol and precipitated with 100% isopropanol (VWR, 1096341000). cDNA was synthesized from 1 μg of RNA using random hexamers and the SuperScript III reverse transcriptase (InvitrogenTM, 1808005). cDNA was quantified by SYBR green assay (Thermo Fisher Scientific, 4368577) and normalized to actin expression in triplicates. The specific primers used for the amplification of each gene are shown in Table 2.

RNA interference

For standard silencing experiments, HeLa cells were seeded at 150000 cells/ml in a six-wellplate the day before transfection. For transfection, two mixes were prepared. Briefly, for a single well, solution A (5 μl of Lipofectamine RNAiMax transfection reagent (Life Technologies, 13778150) in 200 ul of Optimem medium (Life Technologies, 31985047)) was mixed with solution B (5 ul of siRNA (20 uM) in 200 ul of Optimem medium) and incubated at room temperature (R.T) for 15 minutes. Next, the solution was added dropwise to the cells and the cells were placed in the incubator for 7-8 hours. Then, the media was replaced by fresh DMEM medium and the cells were harvested after 72 h.

For electron tomography experiments, cells were seeded at 150000 cells/ml in 75 cm^2 flasks the day before transfection. The transfection mix was prepared as previously described scaling up the volume 5 times. After for 7-8 hours the medium was exchanged as described above. After 48 hours, the confluent cells were split, diluted and seeded again. At 60 hours, the cells were transfected again following the same protocol as before and collected after 72 hours for the electron tomography protocol.

siRNA were purchased from Dharmacon using the following sequences:

Scrambled: 5'-CGUACGCGGAAUACUUCGAUU-3'
MCRS1: 5′-GGCAUGAGCUCUCCGGAC-3′
MCRS1 siRNA was previously validated [107].

Gel electrophoresis, InstantBlue™ and Western Blot

Protein lysates from mammalian cells were prepared by resupening cell pelles in RIPA bufferBriefly, cell pellets were resuspended in RIPA buffer containing 50 mM Tris-HCl pH 7.4, 150 mM NaCl, 2 mM EGTA, 1% Triton X-100 (Sigma-Aldrich, T8787), 0.5% DOC (Sigma-Aldrich, L4509), 0.1% SDS supplemented with protease inhibitors (Complete™ Mini EDTA-free, Sigma-Aldrich, 11836170001) and incubated on ice for 15 min. Next, the mix was centrifuged during 15 min at 4ºC maximum speed in a table-top centrifuge to retrieve the clarified lysate. Protein quantification was done using the Pierce™ BCA™ kit (Thermo Scientific™, 23225) following manufacturer's instructions with BSA as a standard. In the case of insect cells, the protein analysis was done to determine the expression and quality of the recombinant proteins. For insect cells, cell pellets were resuspended in PBS 1x and sonicated using a Bioruptor® for 30 s. The lysate was centrifuged during 15 min at 4ºC maximum speed in a table-top centrifuge to retrieve the clarified lysate. Protein quantification was done using the Bio-Rad Protein Assay (Bio-Rad, 5000006) (based on the Bradford assay) following manufacturer's instructions with BSA as a standard. Typically, 30-50 μg of protein lysate or around 10 μl of purified protein were diluted in loading buffer 5x (LB), boiled for 10 min and loaded in a 10% SDS-PAGE. The gels were usually run at 200 V during 45 min or at 120 V during 90 min for a better separation when required.

To detect proteins, the gels were stained using Instant*Blue*™ (Sigma-Aldrich, ISB1L) in a shaker for 30 min and washed gently with MiliQWater before scanning.

For WesternBlot, a semi-dry transfer was done to blot the proteins in a 0.45 μm nitrocellulose membrane (GE Healthcare Life Sciences, 10600002). Proteins were transferred for 90 min at 65 mA (the current was set to be equal to the surface of the membrane in cm^2). Next, the membrane was blocked to avoid unspecific antibody binding using 5% milk (Sigma-Aldrich, 70166) in TBS1x at 4ºC overnight. Then, the blot was incubated in a solution of primary antibody in TBS1x and 0.1% Tween20® (Sigma-Aldrich, P1379) (TBS1x-Tween) for 1 h at room temperature (under rotation). Afterwards, to wash-out the excess of primary antibody, the membrane was washed three times with TBS1x-Tween. The secondary antibody was added in TBS1x-Tween for 45 min at room temperature. Again, the blot was washed with TBS1x-Tween. Blots were developed using Alexa Fluor 680 (Invitrogen, A21109) and IRdye 800 (Fisher Scientific, 10733944) at the Odyssey Infrarred Imaging System (Li-cor).

Protein cloning, expression and purification from insect cells

Cell culture

Sf21 (Invitrogen, 11497-013) were grown in suspension in serum-free medium Sf-900^{TM} II (Gibco^{TM}, 10902088) in Erlenmeyer polycarbonate flasks (Thomson and/or Corning) at 27ºC in shaker incubators (Referencia) at 200 rpm. Cell count and viability were monitored regularly on a Countess II FL Automated Cell Counter (Life Technologies). Cells were maintained at a density of 0.25-2 x 10^6 cells/ml.

Cloning

Sequences encoding KANSL3, KANSL1 and MCRS1 proteins (Homo sapiens, accession no. Q9P2N6, Q7Z3B3 and Q96EZ8) were synthesized commercially (Addgene). For individual protein expression, PCR-amplified KANSL3 and KANSL1 were inserted by Gibson assembly® using a commercial Master Mix (New England BioLabs Inc., E2611L) into a pCoofy27 backbone (Addgene, 44003) for fusion of 10xHis-ZZ-TEV and a C-terminal fusion of mGFP. In the case of MCRS1 the backbone was the same but a mCherry C-terminal fusion was PCR-amplified and inserted by Gibson assembly®. All sequences were confirmed by sequencing.

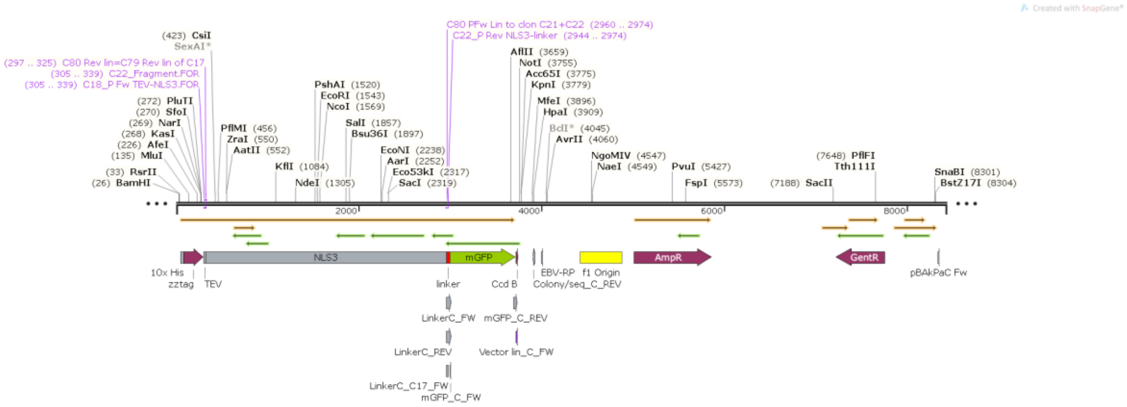
Created with SnapGene®
(423) CsiI
SexAI*
(297 .. 325) C80 Rev lin=C79 Rev lin of C17
(305 .. 339) C22_Fragment.FOR
(305 .. 339) C18_P Fw TEV-NLS3.FOR
(272) PluTI
(270) SfoI
(269) NarI
(268) KasI
(226) AfeI
(135) MluI
(33) RsrII
(26) BamHI
PflMI (456)
ZraI (550)
AatII (552)
KflI (1084)
NdeI (1305)
PshAI (1520)
EcoRI (1543)
NcoI (1569)
SalI (1857)
Bsu36I (1897)
EcoNI (2238)
AarI (2252)
Eco53kI (2317)
SacI (2319)
C80 PFw Lin to clon C21+C22 (2960 .. 2974)
C22_P Rev NLS3-linker (2944 .. 2974)
AflII (3659)
NotI (3755)
Acc65I (3775)
KpnI (3779)
MfeI (3896)
HpaI (3909)
BclI* (4045)
AvrII (4060)
NgoMIV (4547)
NaeI (4549)
PvuI (5427)
FspI (5573)
(7188) SacII
(7648) PflFI
Tth111I
SnaBI (8301)
BstZ17I (8304)
2000
4000
6000
8000
NLS3
mGFP
AmpR
GentR
10x His
zztag
TEV
linker
Ccd B
EBV-RP
Colony/seq_C_REV
f1 Origin
pBAkPaC Fw
LinkerC_FW
mGFP_C_REV
LinkerC_REV
Vector lin_C_FW
LinkerC_C17_FW
mGFP_C_FW

Figure 28. Map of pCoofy27-10xHis-zz-tag-TEV-KANSL3-GFP. All three proteins were cloned into the same backbone for individual expression. MCRS1 with a mCherry at its C-terminus.

For multiple protein expression the MultiBac™ technology[134](Geneva Biotech) for protein complexes was employed. KANSL3-GFP with the 10xHis-ZZ-TEV fusion in N-terminal was PCR-amplified and inserted by Gibson assembly® in a pACEBac1 (Geneva Biotech) acceptor vector. Similarly, KANSL1 with a Flag tag in C-terminal was PCR-amplified and inserted in a pIDK donor vector (Geneva Biotech). To generate a single construct, the acceptor and donor vectors were fused by Cre-LoxP recombination following the MultiBac™ user guide. The correct fusion was confirmed by sequencing.

Baculovirus expression system (BEVS)

Recombinant baculoviruses were generated using the Tn7 transposition based DH10EmBacY virus[134]. Correct gene integration was assessed by blue-white selection and confirmed by PCR using the recombinant bacmid DNA as a template using gene specific primers. Briefly, to prepare recombinant bacmid DNA, 5-10 ng of the construct were incubated on ice (15 min) with 100 μl of electrocompetent DH10EmBacY cells (home-made). Following electroporation (BIORAD, 1.8 – 2 kV), cells were incubated shaking over night at 37ºC in SOC 1x (Super Optimal Broth) medium for recovery. Then, cells were plated on agar containing kanamycin (50 μg/ml), gentamycin (7 μg/ml), tetracyclin (10 μg/ml), Bluo-Gal (100 μg/ml) (Sigma-Aldrich, B2904) and IPTG (40 μg/ml) (Panreac, A4773.0005). To ensure the correct gene integration, white colonies (containing the expression cassette) were streaked on an agar plated containing the compounds mentioned above. Finally, white cells containing the bacmid DNA were harvested over night at 37 ºC in LB (L-Broth) containing kanamycin (50 μg/ml), gentamycin (7 μg/ml) and tetracyclin (10 μg/ml). The bacmid DNA was extracted using the Qiagen miniprep kit (Qiagen, 27106) and precipitated in isopropanol. To verify the presence of the gene of interest in the recombinant DNA, a PCR using the pUC/ M13 Forward and Reverse primers (hybridize to sites flanking the mini-*att*Tn7) using the bacmid DNA as a template was performed. To generate the baculoviruses, the recombinant bacmid DNA was transfected on adherent sf21 cells. 2 ml of sf21 cells with 1 x 10^6 cells in Sf-900^{TM} II medium were seeded per well of a 6-well plate at least 30 min before transfection. 3-5 μl of bacmid DNA, 4 μl of X-tremeGENE^{TM} HP DNA transfection reagent (Sigma-Aldrich, 63666236001) and 200 μl of Sf-900^{TM} II medium were mixed and complex formation was allowed for at least 15 min at room temperature (volume per well). The solution was added dropwise to the insect cells and the cells were kept at 27ºC during 60 h. Then, the supernatant (from now on V_0) was collected. To amplify the baculovirus titer, 4 ml of V_0 were added to 30 ml of cells in suspension diluted at 0.5 x 10^6 cells/ml. The cells were maintained in a shaker for 2-3 days and then, the supernatant containing the amplified virus (from now on V_1) was collected and kept protected from light at 4 ºC. Through all the stages of viral production, the YFP signal of sf21 cells could be assessed using a fluorescence microscope **(**FLoid™ Cell Imaging Station, Life Technologies) as a marker of infection. Protein expression could be also determined by WesternBlot.

Protein expression

For protein expression, sf21 cells were diluted in Sf-900^{TM} II medium to 0.5 x 10^6 cells/ml. Typically, 500 ml of cells were infected with 5 ml of V_1 (1/100 dilution), incubated at 27 ºC at 200 rpm and harvested after 5-6 days. YFP fluorescence was monitored as previously described to determine the maximal infection and increased efficiency of protein production.

Protein purification

KANSL3-GFP was expressed as previously described in insect cells and purified as follows. Cell pellets were resuspended in a buffer containing 25 mM HEPES; 300 mM KCl, 12.5 mM MgCl2, 0.5% Tween supplemented with Arginine and Glutamate and Complete protease inhibitors (Roche) added. The cell lysate was homogeneized by rotation at 4 ºC and sonicated for 2 min at 50% intensity. Then, the lysate was ultracentrifuged at 13000 rpm for 30 min at 4 ºC. The cleared lysate was incubated with pre-washed IgG beads for 2 h at 4 ºC in rotation. Next, the lysate with the beads was centrifuged at 800 rpm at 4 ºC for 5 min to retrieve beads with the affinity bound protein. The beads were washed three times with lysis buffer and then, the TEV protease was added to the beads for cleavage at 22ºC during 2 h. The cleaved protein was further purified by size exclusion chromatography using FPLC with a Superose 6 Increase 10/300 GL size exclusion column (GE) in an Äkta purifier. The buffer for the size exclusion chromatography (SEC) was 25 mM HEPES; 300 mM KCl, 12.5 mM MgCl2 and 5% sucrose. To determine the molecular weight of the proteins, the column was calibrated with commercial protein standards (CYTIVA, 28403842). Proteins were analyzed by SDS-PAGE and InstantBlueTM staining and snap frozen in aliquots in liquid nitrogen. KANSL1-GFP was purified following the same protocol. MCRS1-Cherry was purified using the same protocol.

Insect cell pellets with co-expressed KANSL3-GFP and KANSL1-Flag were co-purified following the same strategy. Cells were resuspended in lysis buffer containing 25 mM HEPES pH 7.0, 150 mM KCl, 12.5 mM $MgCl_2$, 10% glycerol, 0.4% Tween20 and incubated with pre-washed IgG beads for 2 h at 4 ºC. Next, the zz-tag in KANSL3-GFP was cleaved to elute the proteins from the beads and the samples analyzed by WB.

Protein expression and purification from bacteria

GST-MCRS1 was purified from bacteria. GST-MCRS1 was available cloned in a pGEX plasmid. For protein expression, 100 μl of BL21 (DE3) cells were transformed with 1 μl of DNA and plated on agar containing ampicillin overnight. Next, a colony was picked and grown on an LB-medium supplemented with ampicillins at 37ºC overnight. The bacterial culture was diluted 1:50 in 2 L of LB-medium supplemented with ampicillin and let grow until the optical density (OD) at 595 nm reached 0.6. Then, protein expression was induced by adding 0.5 mM IPTG during 4 hours at 37 ºC. Finally the cell culture was harvested by centrifugation during 15 min at 4000 rpm at 4ºC. Cells were frozen in liquid nitrogen and stored at -80ºC until purification. For protein purification, the cell pelled was resuspended in 25 ml ice-cold lysis buffer containing 0.5% Triton X-100 in PBS1x supplemented with protease inhibitors. The lysate was sonicated for 3 min at 50% duty on ice. For clarification, the cell lysate was centrifuged during 30 min at 15000 rpm at 4ºC. The lysate was incubated with 1 ml of pre-washed glutathione beads (VWR, 17513201) for 2 h at 4ºC in rotation under rotation. After that, the beads were retrieved by centrifugation at 600 rpm during 3 min and washed three times with 25 ml PBS1x supplemented with protease inhibitors. Finally the protein was eluted on a column with 4 x 0.5 ml elution buffer (50 mM Tris-HCl pH 8.0, 200 mM KCl, 1 mM DTT and 10 mM reduced glutathione) and dialyzed using a PD-10 column (GE Healthcare, 17085101) in the same buffer without reduced glutathione. Proteins were snap frozen in liquid nitrogen and kept at -80ºC.

In vitro protein pull-downs

For *in vitro* pull-down assays, lysates of KANSL3-GFP and KANSL1-GFP in lysis buffer containing 25 mM HEPES pH 7.0, 150 mM KCl, 12.5 mM $MgCl_2$, 10% glycerol and 0.4% Tween20 (supplemented with protease inhibitors) were incubated with recombinant GST-MCRS1 in presence of glutathione beads (VWR, 17513201) for 1h at 4ºC. After incubation, the beads were centrifuged at 800g for 5 min at 4ºC and washed three times in the same lysis buffer but with increased salt concentration (250 mM KCl). Bound proteins were eluted with LB5x and kept for analysis.

In vitro assays by TIRF microscopy

- Tubulin handling, purification and labelling:

The buffer of choice for tubulin handling is BRB80. A stock of BRB805x was prepared by dissolving 60.48 g of K-PIPES (Sigma-Aldrich, P6757) in ~ 480 ml MiliQH_2O. 5 mM of $MgCl_2$ and 2.5 mM of EGTA were added and the solution was stirred until clear. The pH was adjusted to 6.8 using KOH and MiliQH_2O added to 500 ml. The stock solution was kept at 4ºC and diluted in MiliQH_2O to BRB801X and BRB802x.

Bovine brain was purified as previously described135and kept in liquid nitrogen. For the TIRF experiments that will be described later, recycled tubulin was covalently labelled with ATTO 647-NHS ester (Merck Chemicals, 7376), TAMRA dye (InvitrogenTM, C1171) and NHS-Biotin (ThermoFisher Scientific, 20217) following standard procedures136.

- Coverslip preparation:

Different types of coverslides were prepared for the different experimental set-ups as follows:

Easy-clean coverslips

18 mm x 18 mm coverslips (Thermo Scientific^{TM}, BB01800180AC53MNT0) were loaded onto a porcelain rack. The rack was then immersed in a glass container with a solution of Mucasol^{TM} 5% (Sigma-Aldrich, Z6371818) and sonicated (ultrasonic bath) for 15 min. The rack was rinsed abundantly with deionized water in the container and fully dried. Next, the container was filled with pure ethanol and sonicated for 10 min. The rack was rinsed abundantly with nanopure water in the container. Finally, the rack was taken out of the container and the coverslips fully blew dried using nitrogen gas and further stored in a glass container at R.T.

Silanized coverslips

22 mm x 22 mm coverslips (Thermo Scientific^{TM}, BB02200220AC53MNT0) were loaded onto a porcelain rack. The rack was then immersed in a glass container with a solution of Mucasol^{TM} 5% and sonicated (bath) for 15 min. The rack was rinsed abundantly with deionized water and transferred sequentially to glass containers with acetone (10 min),

ethanol (10 min) and nanopure water (1 min). Next, the coverslips were carefully immersed in a Piranha bath (1 H_2O_2 : 2 H_2SO_4) (Sigma-Aldrich, H1009; Panreac, 4710581611) heated at 60 ºC for 1 hour. The racks were directly transferred from the Piranha solution to three nanopure water baths, for 1 min each. Then, the coverslips were immersed sequentially into a 0.1 M KOH (Merck, 1-05033-1000) bath for 15 min and two nanopure water baths for 1 min. The coverslips were fully blew dried using nitrogen gas. For silanization, the clean coverslips were transferred to a container filled with a solution of 0.05% dichlorodimethylsilane (Sigma-Aldrich, 440272) in trichloroethylene (VWR, 28.735.2929) at room temperature for 1 hour. Next, the glasses were sonicated sequentially in three methanol baths for 5, 15 and 30 min. Finally, the coverslips were fully blew dried with nitrogen gas and stored in a glass container with silica gel desiccation bags until further use.

Biotinylated coverslips

22 mm x 22 mm coverslips with biotin groups tethered to a low-density PEG coating were purchased (MicroSurfaces Inc., Bio_01 2007134-01).

- Tubulin polymerization:

Taxol-stabilized microtubules

Taxol-stabilized MTs (Tx-MTs from now) were prepared by polymerization of a mixture of unlabelled tubulin and labelled-tubulin (rhodamine or Alexa647-tubulin) (concentrations) in a mix of 5 mM $MgCl_2$, 1 mM GTP and DMSO (Sigma-Aldrich, D41639) (1.2 µl) in BRB801x. The polymerization mix was incubated during 30 min in a thermal block at 37ºC. The MTs were stabilized by the addition of 193.75 µl of 10 µM Paclitaxel (Sigma-Aldrich, T7402) in BRB80 (from now on BRB80T) and kept until use at R.T. Before experiments, MTs were spun down in a table-top centrifuge for 5 min at 120000g to remove the free tubulin and resuspended in BRB80T.

GMPCPP microtubule seeds

Short MT seeds for dynamic MTs experiments were prepared using GMPCPP (Guanylyl-(alpha, beta)-methylene-diphosphonate), a slowly hydrolysable analogue of GTP that keeps MTs stable[137] ,to avoid using Paclitaxel. The seeds were prepared by polymerization of a mixture of unlabeled tubulin (stock 200 µM), biotin-tubulin (stock 200 µM), labelled-tubulin (stock 200 µM) and 3 µl of GMPCPP (Jena Biosciences, NU-405L) in BRB801x (50 µl total volume). The mixture was kept at least 5 min on ice for the GMPCPP to replace the GTP in the tubulin and then incubated in a thermal block at 37 ºC for 1 hour. Then, 450 µl of warm BRB801x were added to the solution and the seeds spun-down in a table-top centrifuge at maximum speed for 10 min. The supernatant was removed and 50 µl of warm BRB801x were added to the seeds before centrifuging again. Finally, the seeds were resuspended in 500 µl of BRB801x and kept protected from light until further use.

- Microtubule localization assays using Taxol-stabilized MTs:

To investigate the localization of the different KANSL-complex candidates on MTs, the fluorescent recombinant proteins were incubated with stabilized-MTs in a flow-cell and imaged under the TIRF microscope following a protocol adapted from Stefan Diez's group[122,138]. The experiments were performed in a 2 mm-wide flow-channel made from a 22 mm x 22 mm silanized glass and a 18 mm x 18 mm Easy-clean glass. Two stripes of Parafilm® adhesive tape (Sigma-Aldrich, P7793) were melted in between the two coverslips to glue them and form the channel. Next, a solution of 0.5 mg/ml of anti-β-tubulin antibody in BRB801x (Sigma-Aldrich, T7816) was perfused in the channel and incubated for 5 min. The channels were rinsed twice with 20 μl of BRB801x to remove the excess of antibody. Then, 1% Pluronic® F-127 in BRB801x (prepared by stirring o/n) (Sigma-Aldrich, P2443) was added to block the surface for at least 30 min. The channel was rinsed once with 20 μl of BRB80Tx and the Tx-MTs were flushed into the channel and incubated for approximately 1 min. After the affinity binding of the MTs, the free MTs were washed out twice with 20 μl solution of BRB80T. Before imaging an oxygen scavenger solution containing 20 mM D-glucose (Sigma-Aldrich, 1.08337), 70 μg/ml glucose oxidase (Sigma-Aldrich, G7141) , 10 μg/ml catalase (Sigma-Aldrich, C40) and 20 mM DTT in BRB80T was added to prevent photobleaching. Similarly, the KANSL-complex candidates, namely MCRS1-Cherry and KANSL3-GFP, were added in different concentrations in a solution of BRB80T with the scavengers and incubated with the MTs. Then, their localization on the MT lattice was studied under the TIRF microscope.

- Microtubule dynamics assays using seeds:

To investigate the interaction of MCRS1-Cherry with dynamic MTs a protocol adapted from Thomas Surrey's group[123]. The channels were prepared from a commercial biotinylated coverslip and a 26 mm x 76 mm microscopic slide (Fisher, 11562203). The microscopic slide was treated with 2 mg/ml poly-L-Lysine-Polyethylene glycol (PLL-PEG) solution to avoid unspecific protein binding (SuSoS, PLL(20)-g[3.5]- PEG(2)). The biotinylated coverslip was cut in four squared-pieces with the help of a diamond tip. The flow channel was created by gluing one of the pieces on top of a microscopic slide using two stripes of double-sided sticky tape (Tesa®). Next, a solution of 5% Pluronic® F-127 in BRB801x (prepared by stirring o/n) was added to the chamber for 10 min followed by twice 50 μl of 0.5 mg/ml kappa-casein (Sigma-Aldrich, C0406) dissolved in assay buffer (AB) (20mM BRB80, 0.75 mM EGTA, 1.75 mM $MgCl_2$ (Merck, 63069), 50 mM KCl, 2 mM GTP, 0.1% Methylcellulose, 20 mM D-glucose, 5 mM β-Mercaptoethanol (Sigma-Aldrich, 444203) in water) (casein buffer) to block unspecific binding to the surface. Then, a solution of 0.05 mg/ml of NeutrAvidin™ (ThermoFisher, A2666) in casein buffer was flushed into the channel and incubated for 3 min for the affinity binding between the Biotin and the NeutrAvidin™ to occur. The excess of protein was washed out twice with 50 μl of wash buffer (WB) (1 AB : 1 BRB801x) and then, 50 μl of GMPCPP seeds containing biotin (1 : 50 – 1 : 100 dilution in BRB801x) were added for 5 min to be tethered to the surface. The channel was rinsed twice with 50 μl of WB and twice with 50 μl of AB before adding the final assay mix. The final assay had 12.5 mM of a tubulin mix (1 labeled tubulin : 6 unlabeled tubulin), an oxygen scavenger mix (0.75 mg/ml glucose oxidase and 0.18 mg/ml catalase) and the protein of interest in AB. The chamber was sealed with grease to avoid desiccation.

- TIRF microscopy:

Both type of experiments were performed using total internal reflection fluorescence (TIRF) microscopy but using two different microscopy set-ups. For the microtubule localization assays, a Ground State Depletion (GSD) microscope (Leica) was adapted for TIRF imaging. The flow-cell was inserted in a home-made steel holder (kindly customized by Verena Ruprecht, CRG and Stefan Wieser, ICFO following a design of Stefan Diez's group) specific for the microscope adaptor. The holder allowed for the continuous exchange of solutions on-stage. The samples were imaged with a 100x 1.47 numerical aperture objective lens and TIRF penetration depth of 200 nm. Typically, two-color images were acquired with a 100 ms exposure time for tubulin (647 nm or 532 nm) and GFP (488 nm) or mCherry (532 nm) after protein incubation with the MTs using an EM-CCD camera (Andor iXon 3 897).

For the microtubule dynamics assays, an iMIC microscope (TILL Photonics) was used. The flow-cell was imaged directly up-side down on a 100x 1.49 numerical aperture objective lens. The temperature was kept in the chamber at 31 ºC. Two-color time-lapse imaging was done at time and exposure for tubulin (640 nm) and mCherry (532 nm) using three Evolve 512 EMCCD cameras (Photometrics). After microscopy, acquired images or time-lapses were analyzed using Fiji[139].

Genomics

RNA-seq

RNA-seq data of NSL3-silencing (in *Mus musculus* embryonic stem cells) was analyzed from available datasets in the GEO repository (GSM1386918 siNSL3; GSM1386919 siNSL3; GSM13896820 siNSL3; GSM1386927 Scramble 1; GSM12896928 Scramble 2 (referencia asifa).

The pipeline followed by the Bioinformatics Unit of CRG for the analysis was the following. The quality of the sequencing data was analyzed using the FastQC software v0.11.5 (referencia). An estimation of ribosomal RNA in the raw data was obtained using riboPicker versio 0.4.3 (referencia). The reads were aligned to the GENCODE version of the genome of *Mus musculus* of the release M21 (referencias) and the raw read counts per gene were obtained using STAR and the GENCODE release M21 annotation). The R/Bioconductor package DESeq2 version 1.22.2 (R version 3.5.0) (referencias) was used to assess the differentially epressed genes between the experimental groups, using the Wald statistical test and the False Discovery Rate (FDR) for the p-value correction. Prior to the differential expression analysis, genes with the sum of raw counts across all samples below 10 were discarded, the library sizes were normalized using the default DESeq2 method and the read counts were log2 transformed. The mouse genes were converted to human ortologues using the R package biomaRt version 2.38.0.

ChIP-seq

ChIP-seq data of the NSL complex members NSL3 and MCRS1 (in *Mus Musculus* embryonic stem cells) was analyzed from available datasets in the GEO repository (GSM1251941 Input replicate A; GSM1251942 Input replicate B; GSM1251943 MCRS1 replicate A; GSM1251944 MCRS1 replicate B; GSM1251951 KANSL3 replicate A;

GSM1251952 KANSL3 replicate B) (referencia). The pipeline followed by the Bioinformatics Unit of CRG for the analysis was the following. The quality of the sequencing data was analyzed using the FastQC software v0.11.5 (referencia). Reads were aligned to the GENCODE version of the genome of the *Mus musculus* of the release M21 (Referencia). The quality control of the mapping was done using QualiMap v.2.2.1 (Referencia). Peak calling was done using MACS2 v2.1.1 (referencia). Peaks were annotated using HOMER v4.9.1 (referencia) in which TSS by default is defined from -1kb to +100bp and TTS, from -100 bp to +1kb) against corresponding Ensemble or GENCODE annotations. The mouse genes were converted to human ortologues using the R package biomaRt version 2.38.0.

Electron tomography of mitotic spindles

Electron tomography of mitotic spindles was performed in collaboration with Robert Kiewisz, Müller-Reichert group, TU Dresden. We followed their protocol to select mitotic cell and reconstruct them[118].

Sample preparation for electron tomography

- Sapphire disc coating

For electron tomography, mitotic cells were attached and fixed on sapphire discs (M. Wohlwend GmbH, Art. 500) coated with Poly-L-Lysine and fibronectin prepared as follows. 24 hours prior to sample preparation discs were carefully cleaned in piranha solution (3 H_2SO_4:1 H_2O_2 for 5 minutes. Next, discs were placed onto a wooden stick and allowed to dry. A drop of Poly-L-Lysine 0.1% (w/v) (Sigma-Aldrich, P8920) was added on top of the discs for 5 minutes. After that, the drop was removed and the discs were dried in an oven at 60ºC for 2 hours. Then, a 1:10 solution of fibronectin (Sigma-Aldrich, F4759) in PBS1x was added on top of the Poly-L-Lysine coating and the discs kept in an incubator at 37ºC for 2 hours. Finally, the fibronectin was washed-away and the discs were stored for the experiments.

- Mitotic shake-off and high-pressure freezing

72 hours after the treatment with siRNA, the mitotic cells were collected by “shake-off”. Mitotic cells round up and are less firmly attached to the substrate so upon shaking or

tapping they detach from the flask. In this protocol, two “shake-off” rounds were performed. First each flask was tapped ~10 times on all its sides and the media was removed and trashed. New media was added and the cells were put back to the incubator for 2 hours. The purpose of this first “shake-off” is to get rid of the cells that are not healthy. Next, each flask was tapped again ~10 times at each side and in this occasion the media was collected and centrifuged at 900 rpm for 4 minutes at 37ºC to pellet the mitotic cells. Then, the pellet was resuspended in 1 ml of media supplemented with 10% bovineserum albumin (BSA) acting as a cryo-protectant for the freezing. 500 µl of cell suspension were added on top of the coated sapphire discs and let attach to the coated surface in the incubator at 37ºC for 10 minutes. After that, a sapphire disc was placed with the attached cells facing down on a 95 aluminium planchette with a cavity pre-filled with 5 µl of warm freezing media containing 10% BSA for high-pressure freezing. High-pressure freezing is used to avoid the formation of ice and to preserve the cell ultrastructure (Reference). The sandwich carriers were then placed in the specimen holder (M. Wohlend GmbH, Art. 290) clamped, and immediately cryo-immobilized using a Wohlwend high-pressure freezer (Wohlwend GmbH) under high pressure (~2000 bar) with a cooling rate of ~20000ºC/s. The samples were then stored in liquid nitrogen until further processing.

In parallel, cell flasks were scrapped and the remaining cells resuspended in PBS1x, centrifuged and frozen to later assess the protein levels by western blot as previously described.

- Freeze substitution

Freeze-substitution consists on the replacement of the water in the sample (in this case ice) with stain in preparation for the embedding of the cells. For the freeze-substitution the samples were transferred to cryo-vials filled with a cocktail of anhydrous acetone containing 1% osmium tetroxide (OsO_4) and 0.1% uranyl acetate (UA) ($UO_2(CH_3COO)_2.2H_2O$) (Polysciences, 21447-25). Freeze-substitution was done using an automatic freeze-substitution machine (EM AFS, Leica Microsystems). The freezing parameters were the following: samples were kept at -90ºC for 1 hour, then warmed up to -30ºC in steps of 5ºC per hour and maintained at -30ºC for 5 hours. Next, the temperature was increased to 0ºC in steps of 5ºC per hour. Finally, samples were washed once with pure acetone at room temperature and transferred to the plastic mold for the embedding.

- Embedding, pre-selection and cutting

For the embedding the samples were placed on a round plastic cylinder 10 mm x 3 mm (Reference), in this case with the cells facing upwards. Samples were infiltrated with a mixture of resin (epon/araldite) and acetone in three steps: 1:3, 1:1 and 3:1 (resin:acetone w/v). In each step, the samples were incubated during 1 hour with the mixture. Next, the samples were embedded purely in resin and incubated overnight at room temperature. For polymerization, the samples were kept at 60ºC for 48 hours in an oven. After polymerization the plastic mold containing the samples was cut with a scalpel and all the individual molds separated with the help of a small surgical chisel and a hammer. In a first step of polishing, the resin around the sapphire discs was removed using a razor blade. Next, the resin on top and around the disc was removed. Finally, the sapphire disc was detached from the resin.

In order to select the cells in metaphase, the top of the resin block was screened using an upright brightfield microscope. The two main characteristics to select a metaphase cell were a rounded shape and a distinguishable metaphase plate. After choosing the cell of interest, the resin was further trimmed and finally the block was placed in the holder of an Ultracut UCT Microtome (Leica Microsystems). Serial semi-thick (300 nm) sections were cut and mounted on a grid holder. Post-staining was done in 2% UA for 10 min followed by a 0.4% of Reynold's lead citrate solution. 15-nm colloidal gold particles were attached to both sides of the sections to serve as fiducial markers for the tomographic reconstruction.

- Pre-selection of mitotic spindles

Before the acquisition of the data with electron tomography, the sections were screened with a TECANAI T12 Biotwin TEM (ThermoFisher Scientific) operated at 120kV and equipped with an F214 CCD camera (TVIPS GmbH). Images of the region of interest were acquired at 1200x magnification with 1 s exposure time. The electron micrographs were obtained using the EMMenu Software (TVIPS GmbH) and analyzed using[139]. To choose a cell for ET, the metaphase plate had to be correctly formed when looking at the chromosome area in 3D. Additionally, in the case of MCRS1-silenced cells, the spindle had to present the specific features described for this phenotype: narrower spindle angle and MTs splayed out.

Electron tomography

- Acquisition

ET was performed on the selected metaphase cells. Series of tilted views were recorded using a TECNAI F30 transmission electron microscope (FEI Company) operated at 300 kV. For dual-axis ET, images were captured every 1.0° over a ± 60° range at a pixel size of 2.3 nm (a-axis) using a Gatan US1000 2K x 2K CCD camera. For the acquisition of the second axis, the grid was rotated 90º and another series of tilted views was acquired likewise (b-axis). In order for the reconstruction not the be extremely long but at the same time obtaining enough information, a quarter of volume of the mitotic spindle was acquired for this project.

- Three-dimensional reconstruction, automatic segmentation of microtubules and post-inspection of the segmented microtubules

For the tomogram reconstruction, the IMOD software package was used[140,141]. For image processing the tilted views were aligned using the positions of the fiducials. Tomograms were computed for each tilt axis (a and b) using the R-weighted back-projection algorithm. The tomograms were flattened using the “Flatten Volume” algorithm from the Etomo package.

For further processing of the 3D reconstructed electron tomograms, the ZIB Amira software was used[142]. The microtubules were tracked automatically (segmentation) using the “Trace Correlation Lines” and the “Cylinder Correlation” modules from the Amira package. Then, a manual correction was done to determine the false-positive and false-negative MT segmentations. This correction included the extension, shortening, or fusion of segmented MTs, splitting wrongly connected MTs, or tracing of MTs which could not be identified automatically by the software.

- Data analysis and statistics:

After 3D reconstruction, the data was analyzed with the ZIB Amira Software to obtain the different parameters of interest: number of microtubules per k-fiber, interkinetochore distance, minus-end distribution or end morphology. Afterwards, the spatial analysis was done using the tool ASGA: automatic spatial-graph analysis developed by Robert Kiewisz (https://zenodo.org/record/3834102)[143].

Analysis of the number of microtubules per k-fiber was done using a Generalized Linear Model (GLM) in R using Poisson likelihood function and log link function. The Poisson distribution is generally used to model discrete positive outcomes such as the number of microtubules, when the numbers are small and cannot be approximated by a normal distribution ($n < 20$).

Analysis of the MT end morphology was modelled as a binary outcome (open vs closed), such that the number of open ends is naturally drawn from a binomial distribution depending on the true unobserved proportion of open ends. To model the dependency of the proportion of open ends on the distance to the spindle pole, we discretize the data into 16 different intervals, and counted the number of open ends called by each observer. We used a 3rd order b-splines on the underlying logit transformation of the proportion of open ends to jointly infer the proportion of open ends at each possible distance from the pole. We added the observer as a random effect to take into account the differences in the classification made by the two independent observerse. Data and code to reproduce these analysis can be found at https://bitbucket.org/cmartiga/kfibers/src/master/.

Materials

Antibody	Produced in	IF dilution	WB dilution	Company
MCRS1	Rabbit	----------------	1 µg/ml	Merck - HPA039057
MCRS1	Rabbit	5 µg/ml	----------------	Home-made
GFP	Rabbit	----------------	1:300	Home-made
Flag	Mouse	----------------	1 µg/ml	Sigma-Aldrich -F1804
DM1A (tubulin)	Mouse	1 µg/ml	0.1 µg/ml	Sigma-Aldrich T6199

Table 1. Antibodies used in immunofluorescence and Western Blot.

Oligonucleotide		Sequence (5’-3’)	Application
Actin	Forward	CGAGAAGATGACCCAGATCATG	qRT-PCR
	Reverse	CCACAGGACTCCATGCCCAGG	qRT-PCR
MCRS1	Forward	GTTCGGGGAGTGAACCCTC	qRT-PCR
	Reverse	CACGCTTGGTGAGTCCAGG	qRT-PCR
KANSL3	Forward	GCATGAACGGGAGCTGGACC	qRT-PCR
	Reverse	ACATGCCGTTCACACTCATT	qRT-PCR
KATNAL1	Forward	AGCTCCACCTCAGATCAGGC	qRT-PCR
	Reverse	CTTGTCATCTCTCCCTCTTGCTC	qRT-PCR
GTSE1	Forward	ACGTGAACATGGATGACCCTA	qRT-PCR
	Reverse	TCATCATCTTCATTTGCACTCG	qRT-PCR
Clasp2	Forward	TTCGATCTCGAGAAGGCGTG	qRT-PCR
	Reverse	CCGCCTGAACTTTGCACTTC	qRT-PCR
Nuf2	Forward	TACCATTCAGCAATTTAGTTACT	qRT-PCR
	Reverse	TAGAATATCAGCAGTCTCAAAG	qRT-PCR
pUC/M13	Forward	CCCAGTCACGACGTTGTAAAACG	PCR
	Reverse	AGCGGATAACAATTTCACACAGG	PCR
mCherry	Forward	GCGGGCAGCGGCGAATTTGTGAGCAAGGGCGAGGAG	Gibson Assembly
	Reverse	AACATCAGGTTAATGGCGCTACTTGTACAGCTCGTCCATGC	Gibson Assembly
MCRS1-p-Coofy27	Forward	AACATCAGGTTAATGGCGCTACTTGTACAGCTCGTCCATGC	Gibson Assembly
	Reverse	GCATGGACGAGCTGTACAAGTAGCGCCATTAACCTGATGTT	Gibson Assembly
KANSL1-pcDNA3.1+/C-(K)-DYK	Forward	GGATCTCGAGCCATGGTGATGGCTGCGATGGCGCCCGCT	Gibson Assembly
	Reverse	CGCATGCTATGCATCAGCTGTCACTTATCGTCGTCATCCTTGTA	Gibson Assembly
	Forward	GGCAGCGCGGGCAGC	Gibson Assembly

10xHis-ZZ-TEV-linker-GFP-pCoofy27	Reverse	GCCCTGAAAATAAAGATTCTCAGAACCAC	Gibson Assembly
TEV-KANSL3-linker	Forward	GAGAATCTTTATTTTCAGGGCATGGCCCACCGGGG	Gibson Assembly
	Reverse	GCTGCCCGCGCTGCCGGGTGCTGGAGGCAGG	Gibson Assembly

Table 2. Oligonucleotides for qRT-PCR and Gibson Assembly

Bibliography

7. Bibliography

1. Alberts, B. *et al. Molecular Biology of the Cell*. 5th edition; vol. 43 (2007).

2. Cooper, G. M. *The Cell: A Molecular Approach*. 2nd edition (2000).

3. Chaaban, S. & Brouhard, G. J. A microtubule bestiary: Structural diversity in tubulin polymers. *Molecular Biology of the Cell* vol. 28 2924–2931 (2018).

4. Horio, T. & Hotani, H. Visualization of the dynamic instability of individual microtubules by dark-field microscopy. *Nature* 321, 605-607 (1986).

5. Mitchison, T. & Kirschner, M. Dynamic instability of microtubule growth. *Nature* 312, 237–242 (1984).

6. Richard McIntosh, J. *et al.* Microtubules grow by the addition of bent guanosine triphosphate tubulin to the tips of curved protofilaments. *J. Cell Biol.* 217 (8): 2691-2708 (2018).

7. Weisenberg, R. & Taylor, E. W. Studies on ATPase activity of sea urchin eggs and the isolated mitotic apparatus. *Exp. Cell Res.* 53 (2-3), 372-384 (1968).

8. Weisenberg, R. C. Changes in the organization of tubulin during meiosis in the eggs of the surf clam, Spisula Solidissima. *J. Cell Biol.* 54 (2): 266-278 (1972).

9. Brouhard, G. J. Dynamic instability 30 years later: Complexities in microtubule growth and catastrophe. *Molecular Biology of the Cell*. 26 (7): 1207-1210.

10. Kirschner, M. W., Kirschner, M. W., Mitchison, T. & Mitchison, T. Microtubule dynamics. *Nature* 324, 621 (1986).

11. Mitchison, T. J. The engine of microtubule dynamics comes into focus. *Cell* 157, 1008–1010 (2014).

12. Alushin, G. M. *et al.* High-Resolution microtubule structures reveal the structural transitions in αβ-tubulin upon GTP hydrolysis. *Cell* 157, 1117–1129 (2014).

13. Brouhard, G. J. & Rice, L. M. Microtubule dynamics: An interplay of biochemistry and mechanics. *Nature Reviews Molecular Cell Biology*. 19 (7): 451-463 (2018).

14. Akhmanova, A. & Steinmetz, M. O. Control of microtubule organization and dynamics: Two ends in the limelight. *Nature Reviews Molecular Cell Biology*. 16, 711-726 (2015).

15. Chrétien, D., Fuller, S. D. & Karsenti, E. Structure of growing microtubule ends: Two-dimensional sheets close into tubes at variable rates. *J. Cell Biol.* 129 (5):1311-1328 (1995).

16. Müller-Reichert, T., Chrétien, D., Severin, F. & Hyman, A. A. Structural changes at microtubule ends accompanying GTP hydrolysis: Information from a slowly hydrolyzable analogue of GTP, guanylyl (α,β)methylenediphosphonate. *Proc. Natl. Acad. Sci. U. S. A.* 95 (7): 3661-3666 (1998).

17. Höög, J. L. *et al.* Electron tomography reveals a flared morphology on growing microtubule ends. *J. Cell Sci.* 124: 693-698 (2011).

18. McIntosh, J. R. *et al.* Fibrils Connect Microtubule Tips with Kinetochores: A Mechanism to Couple Tubulin Dynamics to Chromosome Motion. *Cell* 135 (2): 322-333 (2008).

19. Kollman, J. M., Polka, J. K., Zelter, A., Davis, T. N. & Agard, D. A. Microtubule nucleating γ 3-TuSC assembles structures with 13-fold microtubule-like symmetry. *Nature* 466, 879-882 (2010).

20. O'Toole, E. T. *et al.* Morphologically distinct microtubule ends in the mitotic centrosome of Caenorhabditis elegans. *J. Cell Biol.* 163 (3): 451-456 (2003).

21. Simon, J. R. & Salmon, E. D. The structure of microtubule ends during the elongation and shortening phases of dynamic instability examined by negative-stain electron microscopy. *J. Cell Sci.* 96 (Pt 4): 571-582 (1990).

22. Mandelkow, E. M., Mandelkow, E. & Milligan, R. A. Microtubule dynamics and microtubule caps: A time-resolved cryo-electron microscopy study. *J. Cell Biol.* 114 (5): 977-991 (1991).

23. Rice, L. M. A new look for the growing microtubule end? *J. Cell Biol.* 217 (8): 2609-2611 (2018).

24. VandenBeldt, K. J. *et al.* Kinetochores Use a Novel Mechanism for Coordinating the Dynamics of Individual Microtubules. *Curr. Biol.* 16 (12): 1217-1223 (2006).

25. Paz, J. & Lüders, J. Microtubule-Organizing Centers: Towards a Minimal Parts List. *Trends Cell Biol* 28 (3): 176-187 (2018).

26. Zheng, Y., Wong, M. L., Alberts, B. & Mitchison, T. Nucleation of microtubule assembly by a γ-tubulin-containing ring complex. *Nature* 378 (6557): 578-583 (1995).

27. O'Toole, E. T., Winey, M. & McIntosh, J. R. High-voltage electron tomography of spindle pole bodies and early mitotic spindles in the yeast Saccharomyces cerevisiae. *Mol. Biol. Cell* 10 (6): 2017-2031 (1999).

28. Wieczorek, M. *et al.* Asymmetric Molecular Architecture of the Human γ-Tubulin Ring Complex. *Cell* 180 (1):165-175 (2020).

29. Consolati, T. *et al.* Microtubule Nucleation Properties of Single Human γTuRCs Explained by Their Cryo-EM Structure. *Dev. Cell* 53 (5) 603-617 (2020).

30. Roostalu, J. & Surrey, T. Microtubule nucleation: Beyond the template. *Nat Rev Mol Cell Biol* 18: 702-710.

31. Tovey, C. A. & Conduit, P. T. Microtubule nucleation by γ-tubulin complexes and beyond. *Essays Biochem* 62 (6): 765-780.

32. Lüders, J. *The microtubule cytoskeleton: Organisation, function and role in disease*. 1st edition (2016).

33. Meunier, S. & Vernos, I. Microtubule assembly during mitosis - from distinct origins to distinct functions? *J. Cell Sci.* 125, 2805–2814 (2012).

34. Gadde, S. & Heald, R. Mechanisms and molecules of the mitotic spindle. *Curr Biol* 14 (18): 797-805 (2004).

35. Petry, S. Mechanisms of Mitotic Spindle Assembly. *Annu. Rev. Biochem.* 2 (85): 659-683 (2016).

36. Rosenblatt, J. Spindle assembly: Asters part their separate ways. *Nat. Cell Biol.* 7 (3): 219-222 (2005).

37. Zhai, Y., Kronebusch, P. J. & Borisy, G. G. Kinetochore microtubule dynamics and the metaphase-anaphase transition. *J. Cell Biol.* 131 (3): 721-734 (1995).

38. Teixidó-Travesa, N., Roig, J. & Lüders, J. The where, when and how of microtubule nucleation - one ring to rule them all. *J. Cell Sci.* 125: 4445-4456 (2012).

39. Toso, A. *et al.* Kinetochore-generated pushing forces separate centrosomes during bipolar spindle assembly. *J. Cell Biol.* 184 (3): 365-372 (2009).

40. Bettencourt-Dias, M. & Glover, D. M. Centrosome biogenesis and function: Centrosomics brings new understanding. *Nat Rev Mol Cell Biol*. 8 (6): 451-463.

41. Lecland, N. & Lüders, J. The dynamics of microtubule minus ends in the human mitotic spindle. *Nat. Cell Biol.* 16 (8): 770-800 (2014).

42. Bettencourt-Dias, M. Q&A: Who needs a centrosome? *BMC Biol.* 11 (28) (2013).

43. Caudron, M., Bunt, G., Bastiaens, P. & Karsenti, E. Cell Biology: Spatial coordination of spindle assembly by chromosome-mediated signaling gradients. *Science* 309 (5739): 1373-1376 (2005).

44. Scrofani, J., Sardon, T., Meunier, S. & Vernos, I. Microtubule nucleation in mitosis by a RanGTP-dependent protein complex. *Curr. Biol.* 25 (2): 131-140 (2015).

45. Meunier, S. & Vernos, I. Acentrosomal Microtubule Assembly in Mitosis: The Where, When, and How. *Trends in Cell Biol*. 26 (2): 80-87 (2015).

46. Cavazza, T. & Vernos, I. The RanGTP pathway: From nucleo-cytoplasmic transport to spindle assembly and beyond. *Front. Cell Dev Biol.* 3 (2016).

47. O'Connell, C. B., Lončarek, J., Kaláb, P. & Khodjakov, A. Relative contributions of chromatin and kinetochores to mitotic spindle assembly. *J. Cell Biol.* 187 (1): 43-51 (2009).

48. Maresca, T. J. *et al.* Spindle Assembly in the Absence of a RanGTP Gradient Requires Localized CPC Activity. *Curr. Biol.* 19 (14): 1210-1215 (2009).

49. Trivedi, P. *et al.* The binding of Borealin to microtubules underlies a tension independent kinetochore-microtubule error correction pathway. *Nat. Commun.* 10, 682 (2019).

50. Sánchez-Huertas, C. & Lüders, J. The augmin connection in the geometry of microtubule networks. *Current Biology*. 25 (7): R294-299.

51. Petry, S., Groen, A. C., Ishihara, K., Mitchison, T. J. & Vale, R. D. Branching microtubule nucleation in xenopus egg extracts mediated by augmin and TPX2. *Cell* 152 (4): 768-777 (2013).

52. Alfaro-Aco, R., Thawani, A. & Petry, S. Structural analysis of the role of TPX2 in branching microtubule nucleation. *J. Cell Biol.* 216 (4): 983-997 (2017).

53. Alfaro-Aco, R., Thawani, A. & Petry, S. Biochemical reconstitution of branching microtubule nucleation. *Elife* 9: e49797(2020).

54. Verma, V. & Maresca, T. J. Direct observation of branching MT nucleation in living animal cells. *J. Cell Biol.* 218 (9): 2829-2840 (2019).

55. Tariq, A., Green, L., Jeynes, J. C. G., Soeller, C. & Wakefield, J. G. In vitro reconstitution of branching microtubule nucleation. *Elife* 9: e49769 (2020).

56. Goshima, G., Mayer, M., Zhang, N., Stuurman, N. & Vale, R. D. Augmin: A protein complex required for centrosome-independent microtubule generation within the spindle. *J. Cell Biol.* 181 (3): 421-429 (2008).

57. Zhu, H., Coppinger, J. A., Jang, C. Y., Yates, J. R. & Fang, G. MFAM29A promotes microtubule amplification via recruitment of the NEDDI-γ-tubulin complex to the mitotic spindle. *J. Cell Biol.* 122 (15): 2750-2759 (2008).

58. Horio, T., Murata, T. & Murata, T. The role of dynamic instability in microtubule organization. *Front. Plant Sci.* 5: 511 (2014).

59. Nixon, F. M. *et al.* The mesh is a network of microtubule connectors that stabilizes individual kinetochore fibers of the mitotic spindle. *Elife*. 4: e07635 (2015).

60. Booth, D. G., Hood, F. E., Prior, I. A. & Royle, S. J. A TACC3/ch-TOG/clathrin complex stabilises kinetochore fibres by inter-microtubule bridging. *EMBO J.* 30 (5): 906-919 (2011).

61. Wilde, A. 'HURP on' we're off to the kinetochore! *Journal of Cell Biology*.173 (6): 829-831 (2006).

62. International Review of Cell and Molecular Biology (2008)

63. Elting, M. W., Hueschen, C. L., Udy, D. B. & Dumont, S. Force on spindle microtubule minus ends moves chromosomes. *J. Cell Biol.* 206, 245–256 (2014).

64. Dudka, D. *et al.* Complete microtubule-kinetochore occupancy favours the segregation of merotelic attachments. *Nat. Commun.* 9, 2042 (2018).

65. Sawin, K. E. & Mitchison, T. J. Poleward microtubule flux in mitotic spindles assembled in vitro. *J. Cell Biol.* 112 (5): 941-54 (1991).

66. Buster, D. W., Zhang, D. & Sharp, D. J. Poleward tubulin flux in spindles: Regulation and function in mitotic cells. *Mol. Biol. Cell* 18 (8): (2007).

67. Ganem, N. J. & Compton, D. A. Functional roles of poleward microtubule flux during mitosis. *Cell Cycle*. 5 (5): 481-485 (2006).

68. Manning, A. L. *et al.* The kinesin-13 proteins Kif2a, Kif2b, and Kif2c/MCAK have distinct roles during mitosis in human cells. *Mol. Biol. Cell* 18, 2970–2979 (2007).

69. Grishchuk, E. L., Molodtsov, M. I., Ataullakhanov, F. I. & McIntosh, J. R. Force production by disassembling microtubules. *Nature* 438 (7066): 384-388 (2005).

70. Mitchison, T. J. Polewards microtubule flux in the mitotic spindle: Evidence from photoactivation of fluorescence. *J. Cell Biol.* 109 (2): 637-652 (1989).

71. Musacchio, A. & Desai, A. A molecular view of kinetochore assembly and function. *Biology*. 6 (1): 5 (2017).

72. Sikirzhytski, V. *et al.* Direct kinetochore-spindle pole connections are not required for chromosome segregation. *J. Cell Biol.* 206, 231–243 (2014).

73. Monda, J. K. *et al.* Microtubule Tip Tracking by the Spindle and Report Microtubule Tip Tracking by the Spindle and Kinetochore Protein Ska1 Requires Diverse Tubulin-Interacting Surfaces. *Curr. Biol.* 27 (23): 3666-3675.e6 (2017).

74. Gudimchuk, N. *et al.* Kinetochore kinesin CENP-E is a processive bi-directional tracker of dynamic microtubule tips. *Nat. Cell Biol.* 15(9):1079-1088 (2013).

75. Monda, J. K. & Cheeseman, I. M. The kinetochore-microtubule interface at a glance. *J. Cell Sci.* 131 (2018).

76. Musacchio, A. & Salmon, E. D. The spindle-assembly checkpoint in space and time. *Nat Rev Mol Cell Biol.* 8 (5): 379-93 (2007).

77. Dudka, D., Castrogiovanni, C., Liaudet, N., Vassal, H. & Meraldi, P. Spindle-Length-Dependent HURP Localization Allows Centrosomes to Control Kinetochore-Fiber Plus-End Dynamics. *Curr. Biol.* 29 (21): 3563-3578.e6 (2019).

78. DeLuca, J. G. *et al.* Kinetochore Microtubule Dynamics and Attachment Stability Are Regulated by Hec1. *Cell* 127 (5): 969-982 (2006).

79. Long, A. F., Suresh, P. & Dumont, S. Individual kinetochore-fibers locally dissipate force to maintain robust mammalian spindle structure. *J Cell Biol* 219 (8): e201911090 (2020)

80. Hueschen, C. L., Galstyan, V., Amouzgar, M., Phillips, R. & Dumont, S. Microtubule End-Clustering Maintains a Steady-State Spindle Shape. *Curr. Biol* 29 (4): 700-708.e5. (2019).

81. Meunier, S. & Vernos, I. K-fibre minus ends are stabilized by a RanGTP-dependent mechanism essential for functional spindle assembly. *Nat. Cell Biol.* 13, 1406–14 (2011).

82. Meunier, S. *et al.* An epigenetic regulator emerges as microtubule minus-end binding and stabilizing factor in mitosis. *Nat. Commun.* 6: 7889 (2015).

83. Atherton, J. *et al.* A structural model for microtubule minus-end recognition and protection by CAMSAP proteins. *Nat. Struct. Mol. Biol.* 24, 931–943 (2017).

84. Akhmanova, A. & Steinmetz, M. O. Microtubule minus-end regulation at a glance. *Journal Cell Sci.* 132 (2019).

85. Goodwin, S. S. & Vale, R. D. Patronin Regulates the Microtubule Network by Protecting Microtubule Minus Ends. *Cell* 143, 263–274 (2010).

86. Hendershott, M. C. & Vale, R. D. Regulation of microtubule minus-end dynamics by CAMSAPs and Patronin. *Proc. Natl. Acad. Sci. U. S. A.* 111 (16): 5860-5865 (2014).

.

87. Pavlova, G. A. *et al.* The role of Patronin in Drosophila mitosis. *BMC Mol. Cell Biol.* 20, 7 (2019).

88. Jiang, K. *et al.* Microtubule Minus-End Stabilization by Polymerization-Driven CAMSAP Deposition. *Dev. Cell* 28 (3): 295-309 (2014).

89. Hendershott, M. C. & Vale, R. D. Regulation of microtubule minus-end dynamics by CAMSAPs and Patronin. *Proc. Natl. Acad. Sci. U. S. A.* 111, 5860–5865 (2014).

90. Higgins, J. *et al.* Human ASPM participates in spindle organisation, spindle orientation and cytokinesis. *BMC Cell Biol.* 11, 85 (2010).

91. Ito, A. & Goshima, G. Microcephaly protein Asp focuses the minus ends of spindle microtubules at the pole and within the spindle. *J. Cell Biol.* 211, 999–1009 (2015).

92. Jiang, K. *et al.* Microtubule minus-end regulation at spindle poles by an ASPM-katanin complex. *Nat. Cell Biol.* 19(5):480-492 (2017).

93. Kuo, Y. W., Trottier, O., Mahamdeh, M. & Howard, J. Spastin is a dual-function enzyme that severs microtubules and promotes their regrowth to increase the number and mass of microtubules. *Proc. Natl. Acad. Sci. U. S. A.* 116, 5533–5541 (2019).

94. Chang, C. C., Huang, T. L., Shimamoto, Y., Tsai, S. Y. & Hsia, K. C. Regulation of mitotic spindle assembly factor NuMA by Importin-β. *J. Cell Biol.* 216: 3453–3462 (2017).

95. Chinen, T. *et al.* Nu <scp>MA</scp> assemblies organize microtubule asters to establish spindle bipolarity in acentrosomal human cells. *EMBO J.* 39, (2020).

96. Taulet, N. *et al.* IFT88 controls NuMA enrichment at k-fibers minus-ends to facilitate their re-anchoring into mitotic spindles. *Sci. Rep.* 9, 10311 (2019).

97. Cai, Y. *et al.* Subunit composition and substrate specificity of a MOF-containing histone acetyltransferase distinct from the Male-specific Lethal (MSL) complex. *J. Biol. Chem.* 285, 4268–4272 (2010).

98. Wu, D. *et al.* O-Linked N-acetylglucosamine transferase 1 regulates global histone H4 acetylation via stabilization of the nonspecific lethal protein NSL3. *J. Biol. Chem.* 292, 10014–10025 (2017).

99. Sheikh, B. N., Guhathakurta, S. & Akhtar, A. The non-specific lethal (NSL) complex at the crossroads of transcriptional control and cellular homeostasis . *EMBO Rep.* 20 (7): e47630 (2019).

100. Raja, S. J. *et al.* The nonspecific lethal complex is a transcriptional regulator in Drosophila. *Mol. Cell* 38 (6): 827-841 (2010).

101. Feller, C. *et al.* The MOF-containing NSL complex associates globally with housekeeping genes, but activates only a defined subset. *Nucleic Acids Res.* 40 (4): 1509-1522 (2012).

102. Chelmicki, T. *et al.* MOF-associated complexes ensure stem cell identity and Xist repression. *Elife* 3: e02024 (2014).

103. Klein, B. J. *et al.* PHF20 Readers Link Methylation of Histone H3K4 and p53 with H4K16 Acetylation. *Cell Rep.* 17, 1158–1170 (2016).

104. Chatterjee, A. *et al.* MOF Acetyl Transferase Regulates Transcription and Respiration in Mitochondria. *Cell* 167, 722-738.e23 (2016).

105. Karoutas, A. *et al.* The NSL complex maintains nuclear architecture stability via lamin A/C acetylation. *Nat. Cell Biol.* 21, 1248–1260 (2019).

106. Fawal, M. A., Brandt, M. & Djouder, N. MCRS1 binds and couples rheb to amino acid-dependent mTORC1 activation. *Dev. Cell* 33, 67–81 (2015).

107. Lee, SH., Lee, MS., Choi, TI. *et al.* MCRS1 associates with cytoplasmic dynein and mediates pericentrosomal material recruitment. *Sci Rep* 6, 27284 (2016).

108. Ali, A., Veeranki, S. N., Chinchole, A. & Tyagi, S. MLL/WDR5 Complex Regulates Kif2A Localization to Ensure Chromosome Congression and Proper Spindle Assembly during Mitosis. in *Developmental Cell* 41 (6): 605-622.e7 (2017).

109. Pavlova, G. A. *et al.* RNAi-mediated depletion of the NSL complex subunits leads to abnormal chromosome segregation and defective centrosome duplication in Drosophila mitosis. *PLoS Genet.* 15, (2019).

110. Goshima, G. *et al.* Genes required for mitotic spindle assembly in Drosophila S2 cells. *Science (80-.).* 316, 417–421 (2007).

111. Petry, S. & Vale, R. D. A new cap for kinetochore fibre minus ends. *Nat. Cell Biol.* 13, 1389–1391 (2011).

112. Yang, H. *et al.* Mps1 regulates spindle morphology through MCRS1 to promote chromosome alignment. *Mol. Biol. Cell* 30, 1060–1068 (2019).

113. Meunier, S., Timón, K. & Vernos, I. Aurora-A regulates MCRS1 function during mitosis. *Cell Cycle* 15, 1779–1786 (2016).

114. Eibes, S. & Roig, J. MCRS1: Not only ran. *Cell Cycle* 15, 2693–4 (2016).

115. Hutchins, J. R. a *et al.* Systematic Characterization of Human Protein Complexes Identifies Chromosome Segregation Proteins. *Science (80-.).* 328, 593–599 (2010).
116. So, C. *et al.* A liquid-like spindle domain promotes acentrosomal spindle assembly in mammalian oocytes. *Science (80-.).* 364, (2019).

117. Richard McIntosh, J., O'Toole, E., Page, C. & Morgan, G. Ultrastructural analysis of microtubule ends. in *Methods Mol Biol* 2101:191-209 (2020).

118. Kiewisz, R., Müller-Reichert, T. & Fabig, G. High-throughput screening of mitotic mammalian cells for electron microscopy using classic histological dyes. in *Meth Cell Biol* (2020).

119. Maresca, T. J. & Salmon, E. D. Intrakinetochore stretch is associated with changes in kinetochore phosphorylation and spindle assembly checkpoint activity. *J. Cell Biol.* 184 (3): 373-381 (2009).

120. Uchida, K. S. K. *et al.* Kinetochore stretching inactivates the spindle assembly checkpoint. *J. Cell Biol.* 184 (3): 383-390 (2009).

121. Herter, F. Supervised Classification of Microtubule Ends : An Evaluation of Machine Learning Approaches. *Master thesis* (2018).

122. Gell, C. *et al.* Microtubule dynamics reconstituted in vitro and imaged by single-molecule fluorescence microscopy. *Methods Cell Biol* 95:221-45 (2010).

123. Bieling, P., Telley, I. A., Hentrich, C., Piehler, J. & Surrey, T. Fluorescence microscopy assays on chemically functionalized surfaces for quantitative imaging of microtubule, motor, and +tip dynamics. *Methods Cell Biol* 95:555-80 (2010).

124. DeLuca, K. F., Lens, S. M. A. & DeLuca, J. G. Temporal changes in Hec1 phosphorylation control kinetochore - Microtubule attachment stability during mitosis. *J. Cell Sci.* 124(Pt 4):622-34 (2011).

125. Chen, X. *et al.* Remote control of microtubule plus-end dynamics and function from the minus-end. *Elife* 8, e48627 (2019).

126. Yokoyama, H. Chromatin-Binding Proteins Moonlight as Mitotic Microtubule Regulators. *Trends Cell Biol* 26: 161–164.

127. Somma, M. P. *et al.* Moonlighting in Mitosis: Analysis of the Mitotic Functions of Transcription and Splicing Factors. *Cells* 9, 1–27 (2020).

128. Suresh, P., Long, A. F. & Dumont, S. Microneedle manipulation of the mammalian spindle reveals specialized, short-lived reinforcement near chromosomes. *Elife* 9: e53807 (2020).

129. Lecland, N. *et al.* Establishment and mitotic characterization of new Drosophila acentriolar cell lines from DSas-4 mutant. *Biol. Open* 2: 314-323 (2013).

130. Cuveillier, C. *et al.* MAP6 is an intraluminal protein that induces neuronal microtubules to coil. *Sci. Adv.* 6(14): eaaz4344 (2020).

131. Nehlig, A., Molina, A., Rodrigues-Ferreira, S., Honoré, S. & Nahmias, C. Regulation of end-binding protein EB1 in the control of microtubule dynamics. *Cell*

MolLife Sci 74 (13): 2381-2393 (2017).

132. Jiang, K. *et al.* A proteome-wide screen for mammalian SxIP motif-containing microtubule plus-end tracking proteins. *Curr. Biol.* 22(19):1800-7 (2012).

133. Barr, A. R. & Gergely, F. Aurora-A: The maker and breaker of spindle poles. *Journal Cell Sci* 120: 2987-2996 (2007).

134. Bieniossek, C., Imasaki, T., Takagi, Y. & Berger, I. MultiBac: Expanding the research toolbox for multiprotein complexes. *Trends in Biochem Sci*. 37(2):49-57 (2012).

135. Castoldi, M. & Popov, A. V. Purification of brain tubulin through two cycles of polymerization- depolymerization in a high-molarity buffer. *Protein Expr. Purif.* 32 (1): 83-88 (2003).

136. Hyman, A. *et al.* Preparation of modified tubulins. *Methods Enzymol.* 196: 478-485 (1991).

137. Hyman, A. A., Salser, S., Drechsel, D. N., Unwin, N. & Mitchison, T. J. Role of GTP hydrolysis in microtubule dynamics: Information from a slowly hydrolyzable analogue, GMPCPP. *Mol. Biol. Cell* 3 (10): 1155-1167 (1992).

138. Reuther, C., Diego, A. L. & Diez, S. Kinesin-1 motors can increase the lifetime of taxol-stabilized microtubules. *Nature Nanotech* 11, 914-915 (2016).

139. Schindelin, J. *et al.* Fiji: An open-source platform for biological-image analysis. *Nat Methods*. 9(7):676-82 (2012).

140. Kremer, J. R., Mastronarde, D. N. & McIntosh, J. R. Computer visualization of three-dimensional image data using IMOD. *J. Struct. Biol.* 116 (1): 71-6 (1996).

141. Mastronarde, D. N. & Held, S. R. Automated tilt series alignment and tomographic reconstruction in IMOD. *J. Struct. Biol.* 197 (2): 102-113 (2017).

142. Stalling, D., Westerhoff, M. & Hege, H. C. Amira: A highly interactive system for visual data analysis. in *Visualization Handbook* (2005).

143. Robert Kiewisz. ASGA: Automatic Spatial-Graph Analysis (ASGA) (Version v0.3). (2020).

Annex

8. Annex

8.1. ¼ of a full spindle displays the same characteristics of the full volume of the spindle

Before doing ET of a ¼ of HeLa-Kyoto spindle, we verified that ¼ of volume was representative of a full spindle. In order to do so, we splitted the full reconstructed spindle in quarters and compared the interkinetochore distance and number of KMT per k-fiber of those quarters to that of the full volume (Figure A A) and A B)). We did not find significant differences among the means in both measurements after ANOVA analysis. Therefore, we can conclude that a quarter of a spindle displays the same features as a full spindle.

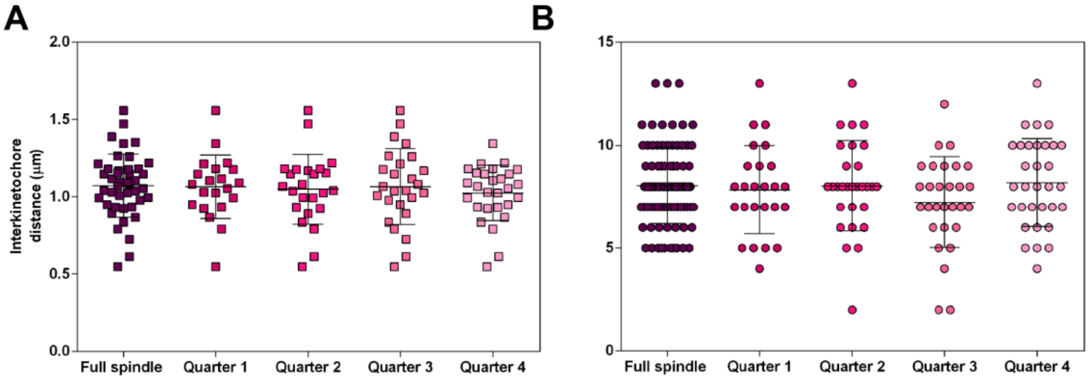

Figure A. Comparison of the characteristics of a full spindle versus its versus three quarters. A) Interkinetochore distance. Scatter plot of the interkinetochore distance of a full spindle and the same spindle divided in quarters. The mean interkinetochore distance is 1.07±0.20 µm for the full spindle, 1.06±0.20 µm for quarter 1, 1.05±0.23 µm for quarter 2, 1.06±0.24 µm for quarter 3 and 1.03±0.18 µm for quarter 4. There are no significant differences among the means after ANOVA analysis p-value = 0.9192 (p-value > 0.05). Number of kinetochore pairs: full spindle N= 43; Quarter 1= 21; Quarter 2= 24; Quarter 3= 26; Quarter 4= 28. B) Number of KMTs per k-fiber. Scatter plot of the number of KMTs per k-fiber of a full spindle and three of its quarters. The mean number of KMTs for the full spindle is 7.97±2.03, for the quarter 1 8.33±1.93, for the quarter 2 8.24±1.83 and for the quarter 3 7.44±2.23. There are no significant differences among the means after ANOVA analysis p-value = 0.3791 (p-value > 0.05). Number KMTs: Full spindle N= 93; Quarter 1= 25; Quarter 2= 29; Quarter 3= 29; Quarter 4= 32.

8.2. Proportion of open minus-ends matching for both classifiers

For the HeLa-Kyoto cell in Figure XXX, 116 MT minus-ends were classified equally by both classifiers. 77 were labelled as open and 34 were labelled as closed. When calculating the proportion of open ends from the total of open and closed ends, 75% of ends are open at position 0.0 whereas 25% of ends are closed for both observers (Figure B).

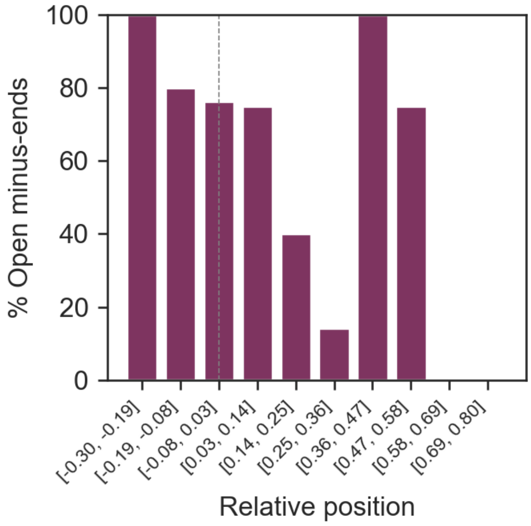

Figure B. Proportion of open minus-ends in a ¼ of spindle taking into account only the matching ends for both classifiers. Bar chart of the proportion of open minus-ends at different relative positions (being 0.0 the location of the centrioles). In this analysis, only the ends assigned the same morphology by both classifiers are considered.

8.3. Analysis of protein levels after silencing MCRS1

Protein levels after MCRS1-silencing were analyzed by Western Blot (Figure C). The protein levels after the double transfection (Figure AB) used for the acquisition of the tomographic data were significantly higher than those achieved with a single transfection.

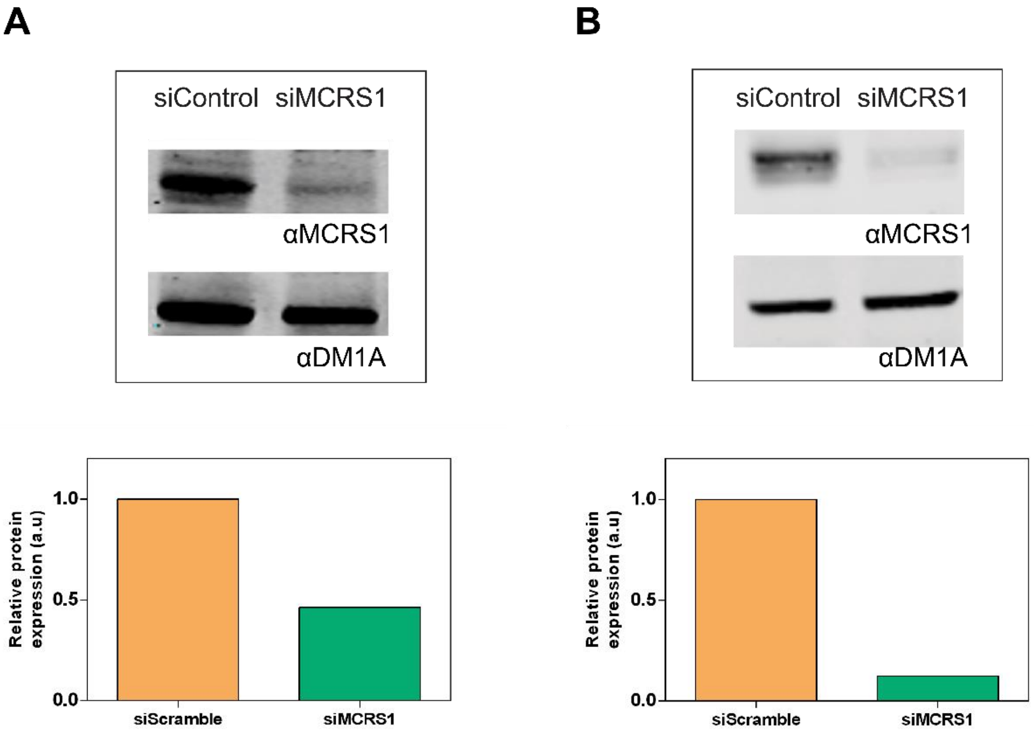

Figure C. Analysis of the protein levels after MCRS1-silencing. A) Western Blot analysis of a silencing experiment for immunofluorescence characterisation of the morphological features in MCRS1-silenced cells. The relative expression of MCRS1 versus tubulin (DM1A) was normalized to the value of siControl. siMCRS1 relative expression is 0.46. B) Western Blot analysis of the MCRS1-silencing for ET The relative expression of MCRS1 versus tubulin (DM1A) was normalized to the value of siControl. siMCRS1 relative expression is 0.12.

8.4. All three control, siScramble and siMCRS1 cells are in metaphase

Interkinetochore distances were used as a marker of the mitotic stage. The three cells employed for the reconstructions of the quarters were determined to be in metaphase after those measurements (Figure D).

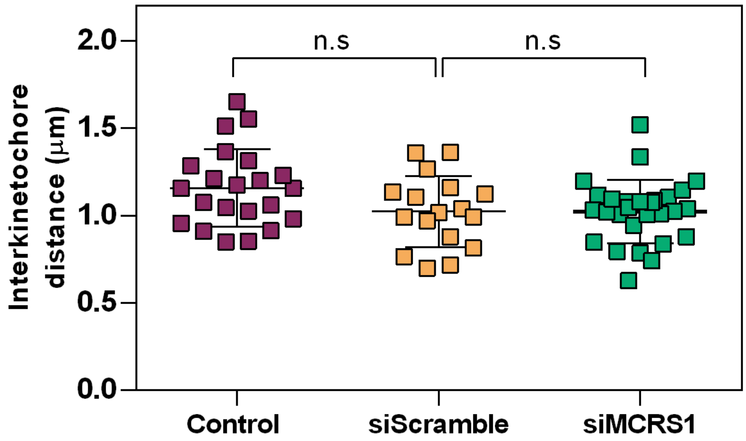

Figure D. Determination of the interkinetochore distance for the WT, siControl and siMCRS1. Scatter plot of the interkinetochore distance measured for the three conditions. The mean interkinetochore distance for the control is 1,158 ± 0,04761 (N=22), for the siScramble 1,023 ± 0,04965 (N=17) and for the siMCRS1 1.024±0.03432 (N=28). Significant differences between WT and siControl (p-value= 0,0598) and between siControl and siMCRS1 (p-value= 0.9885) were not found. All mean values are in the range of what is expected for a metaphase cell.

8.5. Analysis of mitotic transcripts levels after MCRS1-silencing

To analyze the posible moonlighting effect of the KANSL-complex in mitosis we looked into available transcriptomics data on the GEO repositoires. We selected data from mouse embryonic stem cells (GSE57701) including both expression and binding profiling. We performed a transcriptomicc analysis of KANSL3-silencing and scramble control mouse ES cells. Differential expression analysis showed changes in the expression of 9160 genes (adjusted p-value <0.05), 4671 of them have higher expression and 4489 were downregulated in KANSL3 depleted cells (Figure E.A). To try to find out which of those genes were directly regulated by the KANSL-complex, we looked at the ChIP-seq data of MCRS1 and KANSL3.As KANSL3 is only present in the KANSL-complex, we crossed both profiling data and RNA-seq data assuming that the candidate genes would be regulated by the KANSL-complex. By determining the overlap between the promoter regions of the genes bound by the KANSL-complex and the genes that change their expression after KANSL3-silencing, we obtained a list of 1106 downregulated and 816 upregulated target genes (Figure EB).

From this list, we manually selected some mitotic targets that could play a role on the k-fiber dynamics regulation (Figure EC). Nuf2, Clasp2 and Katnal1 appeared as downregulated whereas Gtse1 was upregulated. MCRS1 is also shown in Figure EC as it is the protein we silenced in our experiments. Bearing in mind that this data was obtained from KANSL3-silenced cells, we reasoned that if both proteins would be forming a complex, as suggested also by the ChIP-seq profiles (Figure EB), they could be regulating the same genes. Therefore, we silenced MCRS1 in HeLa cells during 72 h and analyzed the transcript levels for the different candidates by qRT-PCR. As depicted in Figure ED, MCRS1 expression is significantly downregulated in the silenced cells (p-value < 0.00001; ****). However, we could not detect significant differences in expression levels among the control and MCRS1-silenced cells for the candidate targets.

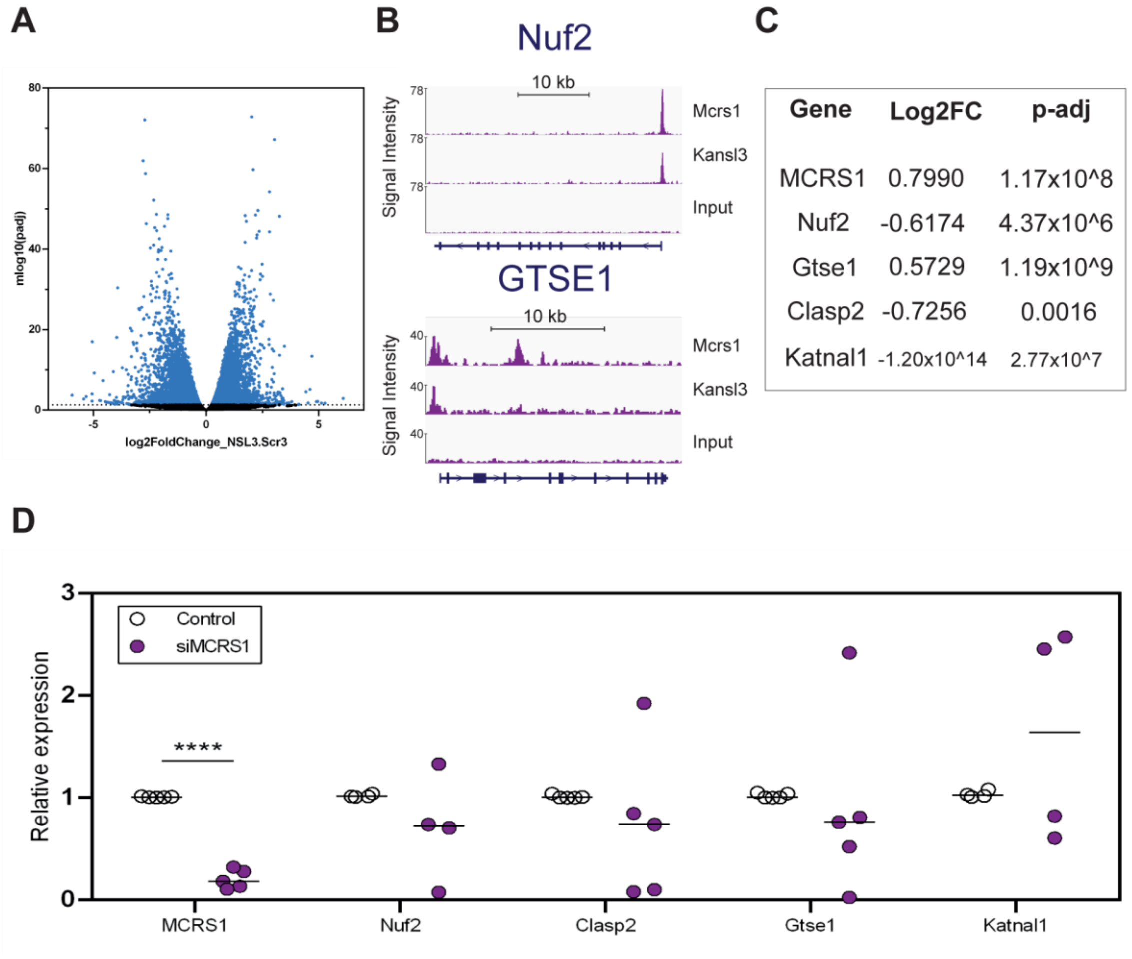

Gene	Log2FC	p-adj
MCRS1	0.7990	1.17x10^8
Nuf2	-0.6174	4.37x10^6
Gtse1	0.5729	1.19x10^9
Clasp2	-0.7256	0.0016
Katnal1	-1.20x10^14	2.77x10^7

Figure E. Analysis of the mitotic transcripts levels after MCRS1-silencing in HeLa cells. The RNA-seq data was obtained from KANSL3-silenced mouse embryonic stem cells (MES). ChIP-seq data was obtained from the same cell for promoters of genes to which MCRS1 and KANSL3 were bound. A) Volcano plot showing differentially expressed genes between KANSL3-silenced cells and scramble-transfected cells. Light blue dots represent differentially expressed genes with a p-value <0,01 and dark blue dots with and adjusted p-value <0,05. B) ChIP-seq data of KANSL3 and MCRS1 binding to promoters of Nuf2 and GTSE1. C) Table with the selected genes after the overlap between A) and B). Expression levels are shown as Log2FC of KANSL3-silenced versus scramble. Negative values indicate downregulation. P-adjusted values are depicted. C) Scatter plot of the relative expression of different mitotic genes (horizontal axis) in control and MCRS1-silenced cells. Expression levels are relative to the actin levels.

For on the future it would be interesting to assess the protein levels of these candidates by WB and immunfluorescence to confirm these results. Additionally, different mitotic factors could be investigated in the same way to investigate the possible moonlighting role of the KANSL-complex in the mitotic mammalian cells.